

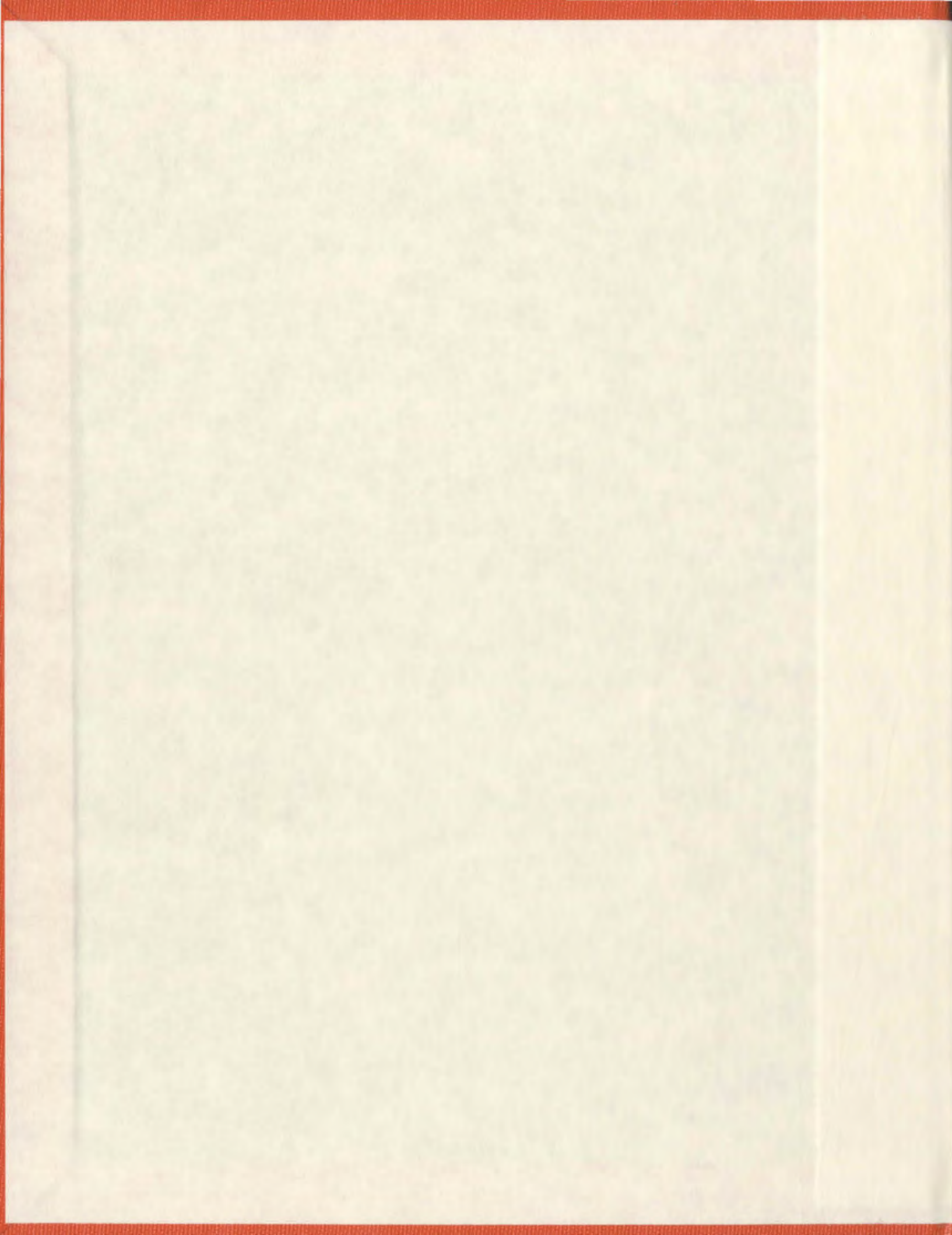
RELIABILITY ANALYSIS AND CONDITION
MONITORING OF A HORIZONTAL AXIS WIND TURBINE

CENTRE FOR NEWFOUNDLAND STUDIES

**TOTAL OF 10 PAGES ONLY
MAY BE XEROXED**

(Without Author's Permission)

MUHAMMAD MOHSIN K KHAN



RELIABILITY ANALYSIS AND CONDITION MONITORING OF A HORIZONTAL AXIS WIND TURBINE

by

© **Muhammad Mohsin K Khan**

A Thesis submitted to School of Graduate Studies
In partial fulfillment of requirement for the Degree of
Masters of Engineering

Faculty of Engineering and Applies Sciences
Memorial University of Newfoundland

October 11, 2005

St.John's

Newfoundland

Canada



Abstract

Wind is one of the cheapest and cleanest sources of energy. However, large and frequent fluctuations in wind intensity and directions cause serious problems in harvesting this energy. Wind turbines are subjected to many harsh environmental conditions, which lead to their failure or degraded performance. Hence an assessment of total lifetime and reliability of wind turbine components is required. Moreover a condition monitoring system is also needed to keep an eye on ever changing effects of environment on different components. This thesis comprises of two main objectives.

First objective of research deals with component based reliability analysis, which involves four steps. To accomplish first objective an assessment of failure modes using Failure Mode and Effect Analysis (FMEA) approach is first conducted. Subsequently, based on working and environmental conditions and failure characteristics, the reliability of each individual component is computed. Standard procedures like fault tree and markov analysis are also carried out.

The second goal of research makes use of the results of reliability analysis, to design a safety system for wind turbines. Based on sensitivity of all the components, a number of parameters are selected for monitoring the most venerable components. A monitoring system is suggested using a single board computer (SBC), signal conditioning electronics and sensors. This SBC is responsible for monitoring of selected parameters. This

computer as proposed in thesis will interact with system's built in PLC to initiate shutdown of the system if an alarming changes in parameters are detected.

This research brings in to focus the need for a component based reliability analysis of small wind turbine systems. These systems appear to be reliable for some portion of the year and remain in stand by or for maintenance rest of the time. The need for condition monitoring system is also proved by lower reliability of specific components that require constant monitoring.

Keywords: Wind turbine reliability, Condition monitoring, Renewable energy, Reliability engineering, Fault prediction, Instrumentation and measurements.

Acknowledgements

First of All I would like to Thank God Almighty for this accomplishment and making me strong and keeping me steadfast in the ways of trials and tribulations that have come during the completion of thesis.

I would like to extend my deepest gratitude toward my both supervisors Drs. Tariq Iqbal and Faisal Khan for providing me with this unique research opportunity. I would like to thank them for supporting me financially and guiding me through my Masters of Engineering Degree. Without their proper guidance and timely advice I would not have been able to accomplish the deadlines and quality in my work that was expected from me.

I would like to thank all the Professors at the faculty who have imparted knowledge on me in one way or the other through different courses, which will be a permanent contribution in my grooming as a research engineer.

Finally I would like to thank my parents for their understanding, overwhelming moral support, encouragement and blessings. I would like to thank my sisters for being supportive in the whole process. I would also like to thank all my friends and colleagues at the faculty who have helped me during my research for Masters of Engineering degree at Memorial University of Newfoundland.

Table of Contents

Abstract	i
Acknowledgements	iii
Table of Contents	iv
List of Tables	ix
List of Figures	x
List of Symbols and Abbreviations	xii
Chapter 1. Introduction	
1.1 Wind Turbines – History and Development	1
1.2 Modern Wind Turbine Components	4
1.3 AOC-15/50 – System Description	7
1.4 Scope and Purpose of research	8
1.5 Outline of Thesis	10
Chapter 2. Literature Review	
2.1 Introduction	11
2.2 Reliability Analysis in Wind Engineering	12
2.3 Condition Monitoring (CM) techniques in Modern Wind Turbines	18
2.4 Significance of Current Research	25
Chapter 3. Reliability Analysis of AOC-15/50	
3.1 Introduction	28
3.2 Methodology and Component Identification	29
3.3 Failure Mode and Effect Analysis	31

3.4	Failure and Reliability Models	34
3.4.1	Significance of Bath tub Curve	36
3.4.2	Defining Reliability	37
3.5	Reliability Modeling	39
3.5.1	Reliability Model Block Diagram	39
	(i) Blade Assembly	39
	(ii) Drive Train	40
	(iii) Tower and Support	41
3.6	Random failure Models	42
3.6.1	Generator	42
3.6.2	Gearbox	42
3.6.3	Programmable Logic Controller	43
3.7	Time Dependant Reliability Models	43
3.7.1	Yaw Bearing	43
3.7.2	Aerodynamic Tip Brakes	44
3.7.3	Parking Brakes	45
3.8	Physical Reliability Models	46
3.8.1	Blades	48
	3.8.1.1 Static Reliability computation	50
	3.8.1.2 Dynamic Reliability Model (Periodic loading)	51
3.8.2	Bolts	52
	3.8.2.1 Static and Dynamic reliability Models	54
3.8.3	Hub	54

3.8.3.1	Static and Dynamic Reliability Models	55
3.8.4	Anchor Bolts and Tower	56
3.8.4.1	Area of Projected Tower Face	57
3.9	Markov Analysis	58
3.9.1	Conditions	59
3.9.2	Yaw Failure Scenario	60
3.9.3	Transition Rates for state and State Probabilities	60
3.10	Fault Tree Analysis	63
3.11	Summary	65
Chapter 4. Proposed Condition Monitoring System		
4.1	Introduction	66
4.2	Components reliability and parameter selection	67
4.2.1	Methodology adopted for CM system Development	68
4.2.2	Parameter selection	69
4.3	Monitoring of Tip Brake	71
4.4	Monitoring of Yaw Bearing	72
4.5	Vibration Monitoring for Derive Train	76
4.6	Proposed System – Block Diagram	79
Chapter 5. Condition Monitoring System - Implementation		
5.1	Introduction	80
5.2	Sensors and Instrumentation Board Layout	80
5.2.1	Current Sensor	81

5.2.2	Strain Sensor	82
5.2.3	Vibration Sensor	83
5.2.4	Instrumentation board layout	85
5.3	Single Board Computer (SBC)	86
5.4	Test bench setup	87
5.5	Signal conditioning	90
5.5.1	Strain instrumentation circuit	90
5.5.2	Current instrumentation circuit	91
5.5.3	Vibration sensor instrumentation	93
5.6	Signal Calibration	95
5.7	Monitoring Scheme and Results	98
5.7.1	Smart FFT computation routine	100
5.7.2	Results of FFT computation and Frequency spectrum	105
5.8	Summary	106

Chapter 6. Conclusions and Recommendations

6.1	Introduction	107
6.2	Conclusions of Research	107
6.3	Recommendations for improvement	109

References	112
-------------------	-----

Appendix 1 Condition Monitoring Routine- C++ Code	117
--	-----

Appendix 2 Vibration signatures at different input voltages	125
--	-----

Appendix 3	Data Sets – Observation used in current and strain calibration	127
Appendix 4	Further subdivision of sample array to compute FFT	130
Appendix 5	Output screen for SBC connection through HyperTerminal	131

List of Tables

Table 3.1	Failure Mode and Effect Analysis Table.....	32
Table 3.2	Wiebull Shape parameter.....	35
Table 3.3	Reliability models used for components.....	37
Table 3.4	Reliability of yaw bearing $R(t)$	44
Table 3.5	Transition Failure rates for Markov Analysis.....	62
Table 3.6	Markov Analysis results for state 1 – 5.....	63
Table 4.1	Component reliability and Failure Rates.....	67
Table 4.2	Component and selected parameters.....	70

List of Figures

Figure 1.1:	Different sizes of wind turbines.....	04
Figure 1.2:	Technical Drawing – illustration of major components.....	06
Figure 1.3:	AOC-15/50 – Specification diagram	08
Figure 2.1:	Standardized Object Model for WEC Monitoring	19
Figure 2.2:	Scenarios of resistive/inductive imbalance	21
Figure 2.3:	Inductive imbalance using inductor in series.....	22
Figure 3.1:	Flow Chart of tasks for reliability analysis.....	29
Figure 3.2:	System block diagram.....	31
Figure 3.3:	Bathtub Curve and failure regions.....	36
Figure 3.4:	Rotor components in series.....	40
Figure 3.5:	Drive Train in series.....	40
Figure 3.6:	Tower and Support components in series.....	41
Figure 3.7:	Reliability of component with fixed strength - under random load.....	46
Figure 3.8:	5- state Markov Model – Rate diagram.....	60
Figure 3.9:	Fault tree representation.....	64
Figure 4.1:	Flow chart of methodology adopted in CM system development.....	68
Figure 4.2:	Expected variation in current supply to Tip Brake.....	72
Figure 4.3:	Drive Train and yaw support with Tower top.....	74

Figure 4.4:	Proposed System – Block Diagram.....	79
Figure 5.1:	Current Sensor SCD05PUN and Pin configuration.....	82
Figure 5.2:	A typical Metal strain gauge.....	83
Figure 5.3:	ACH-01 diagram adopted from product datasheet.....	84
Figure 5.4:	Instrumentation board layout	85
Figure 5.5:	Pico Flash with Pico I/O mounted and the interrupt LED.....	87
Figure 5.6:	Strain Variation setup	88
Figure 5.7:	Current Variation setup with Ampere meter	88
Figure 5.8:	Motor with Accelerometer mounted on Motor body	89
Figure 5.9:	Vibration Signature at 1.77 volts.....	89
Figure 5.10:	Strain instrumentation circuit.....	91
Figure 5.11:	Current instrumentation circuit.....	93
Figure 5.12:	Vibration interface for ACH-01 and shift stage.....	94
Figure 5.13:	Instrumentation Board.....	94
Figure 5.14:	Current calibration graph- curve fitting using MATLAB.....	96
Figure 5.15:	Strain calibration graph- curve fitting using MATLAB.....	97
Figure 5.16:	CM routine – The Flow chart representation.....	99
Figure 5.17(a):	2-point DFT flow graph	102
Figure 5.17(b):	Flow of complete decimation in time of an 8-point DFT computation.....	102
Figure 5.18:	Mapping process implemented in computation of Frequency coefficients....	104
Figure 5.19:	FFT spectrum for 20 harmonics.....	105

List of Symbols and Abbreviations*

β	Wiebull Distribution Shape parameter
θ	Wiebull Distribution Scale parameter
$\lambda(t)$	Failure Rate as function of time
T	Time to Failure of System
R(t)	Reliability
Pr(x)	Probability of given quantity x
F(t)	Cumulative Probability of Failure
$f(t)$	Failure Probability density Function
$R_{[NAME]}$	Reliability of mentioned component
$R_{D-train}$	Reliability of turbine Drive Train
$R_{Support}$	Reliability of Tower and Support
R_{SYS}	Reliability of System
t	Time as Running Variable
λ	Failure Rate – Numeric Value
s	Shape parameter for Log-normal distribution
x_{med}	Median value of load
x_{mode}	Mode value of Load acting most of time
T	Thrust on Rotor Disk
C_T	Thrust coefficient
ρ	Density of Air

* If the above illustration of any symbols conflicts with the illustration of that symbol given in the following literature, then the preference should be given to the illustration, provided in following chapters.

R	Radius of Rotor
U	Free Stream Wind Speed
M_{β}	Flap wise bending moment on Blade root
r	Instantaneous Radius of blade
B	Number of Blades
R	Radius of Blade
σ_{max}	Maximum Stress
C	Distance to neutral axis of force
I_b	Blade root moment of inertia
k	Strength of Material
α	Load Cycles
η_L	Load Cycles for Blade Model
K	Bending Events per Cycle
n_{rotor}	Rotational Speed of Rotor
H_{op}	Hours of Operation round the year
Y	Number of Years
W	Weight of one Blade
M_w	Moment Due to Blade(s) weight
r_{cg}	Center of gravity Distance of Blade
σ_g	Stress Due to Weight of blade
σ_{gb}	Stress on One Bolt due to Blade Weight
F_c	Centrifugal Force on One Blade

F_{cb}	Centrifugal Force on One bolt
σ_{cb}	Stress Due to F_{cb}
r_b	Radius of one Bolt
T'	Torque
Ω_s	Speed of rotor Revolutions Per Minutes
P	Power
R'	Reliability of One Bolt
R''	Reliability of one HUB Branch
Q	Air density factor
Z_v	Terrain factor
V	Wind speed
$G = G_t$	Gust response factor for tower only
C_f	Force coefficient value
A'	Projected Area
F	Force on One Tower face
λ_N	Transition Failure rates for Markov Analysis
$P_N(t)$	Probability of Being in a given State N
$P(T)$	Probability of Top Event
$F_{[NAME]}$	Cumulative Failure prob. of mentioned component
m_1	Mass of Generator
m_2	Combined mass of Three blades
F_1 and F_2	Forces due to m_1 and m_2

L_1 and L_2	Moment Arm for F_1 & F_2
M_1 and M_2	Moments on Yaw Bearing
M_T	Moment due to Thrust T'
E	Young's Modulus
ϵ	Strain on Yaw Bearing
ϕ	Stress on Yaw Bearing
∇V	Change in Voltage from Bridge circuit
∇R	Change in Resistance of Strain Gauge
MTTF	Mean Time to Failure
AOC	Atlantic Orient Corporation Canada
DFT	Discrete Fourier Transform
FFT	Fast Fourier Transform
GF	Gauge Factor
PLC	Programmable Logic Controller
SBC	Single Board Computer
LED	Light Emitting Diode
FMEA	Failure Mode and Effect Analysis
CM	Condition Monitoring
WEC	Wind Energy Converter
NREL	National Renewable Energy Laboratory

Chapter 1

Introduction

1.1 Wind Turbines – History and Development

Wind is one of the cleanest and inexhaustible energy source. It has been benefiting mankind for a long time in sailing, grinding food and pumping water out of wells. The wind turbines are not new inventions; historically they were invented in earlier B.C times and were not for producing electricity. They were used for taking water out of the well or to do some useful work like grinding grain. Later they were put to use for some other purposes. These early machines were undoubtedly crude and mechanically inefficient, but they served their purpose well for many centuries. They were made from local materials by cheap labor. Maintenance was a problem, which served to keep many people at work. The available materials determined their size. A need for more work was met by building more wind turbines rather than larger ones.

The earliest recorded European wind turbine is dated at 1191. The first corn-grinding wind turbine was built in Holland in 1439. There were a number of technological

developments through the centuries, and by 1600 the most common wind turbine was the tower mill. The word '*mill*' refers to the operation of grinding or milling grain. This application was so common that all wind turbines were often called windmills even when they actually pumped water or performed some other function.

By 1925, commercial wind-electric plants using two- and three-bladed propellers started appearing in the American markets. The most common brands were Wincharger (200 to 1200 W) and Jacobs (1.5 to 3 kW). These were used on farms to charge storage batteries, which were then used to operate radios, lights, and small appliances with voltage ratings of 12, 32, or 110 volts. A good selection of 32 V DC appliances was developed by industry to meet this demand. Then the United States Congress established the Rural Electric Administration (REA) in 1936. Low interest loans were provided so that the necessary transmission and distribution lines could be constructed to supply farmers with electricity. In the early days of the REA, around 1940, electricity could be supplied to the rural customer at a cost of 3 to 6 cents per kWh. The corresponding cost of wind-generated electricity was 12 to 30 cents per kWh when interest, depreciation, and maintenance were included. The lower cost of electricity produced by a central utility, plus the greater reliability, led to the rapid demise of the home wind electric generator (Johnson et. al. 2004).

After 1940, the cost of utility-generated electricity continued to decline slowly, dipping under 3 cents per kWh in the early 1970s. The use of larger and more efficient generating plants accomplished this requirement. A trend of decreasing cost for electricity while

other costs are increasing could not be continued forever, and utility-generated electricity started increasing in cost in the early 1970s reaching the 1940 cost of 6 cents per kWh around 1976. This was accompanied by many consumer complaints, of course, which were largely unjustified when the long-term performance of the utilities in providing low cost, reliable electricity is considered. In addition to home wind electric generation, a number of power companies around the world have built larger wind turbines to supply power to their customers. The largest wind turbine built before the late 1970s was a 1250 kW machine built on Grandpa's Knob, near Rutland, Vermont, in 1941. The modern Wind turbines have passed through a lot of development and research until now. A small glimpse of the development was discussed in above paragraphs. (Johnson et. al. 2004)

There is still a need to emphasize the different sizes of wind turbine systems. A smaller wind turbine unit is comprised of almost the same components as a larger unit, however it has structural and operational limitations in many aspects. On the other hand a smaller wind turbine can be more flexible in installation and have a longer life due to its compact size. Power ratings are also different; a smaller wind turbine may range in the ratings up to 150 kW. A 200 kW unit may qualify as a larger unit if it has the same operational characteristics as 750 kW units or any other larger unit. The operational characteristics for a larger wind turbine system pertain to integrated drive train with coupling between Generator and Gearbox, well-defined yaw control mechanism and pitch control for blades. Smaller units tend to avoid the gearbox-generator coupling and mostly have a custom-built single assembly. The difference is also evident from the tower height and

disk radius, which dictates the operational characteristics of any system. Figure 1.1 gives a better idea to the reader about the different sizes of wind turbines:

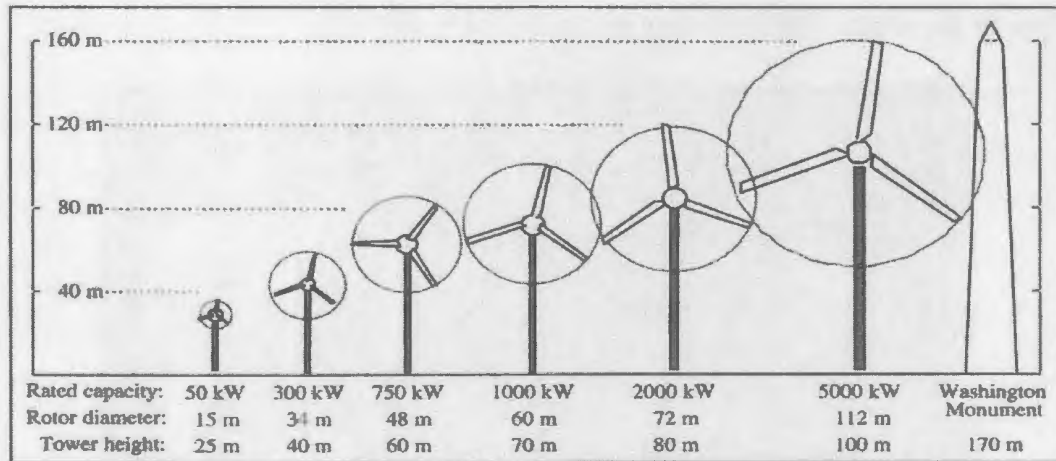


Figure 1.1 Different sizes of wind turbine (Manwell, McGowan and Rogers 2002)

The most common parts/components of a modern wind turbine are discussed in the next section.

1.2 Modern Wind Turbine Components

With recent developments in wind turbine technology, efforts have been made to reduce the additional components and to make the system more efficient, reliable and economical for the manufacturers. A modern wind turbine unit (irrespective of the manufacturer) can be composed of the following basic components.

- Nacelle
- Rotor Blades
- Individual Pitch Mechanism for blades
- Low Speed shaft

- Gear Box
- High Speed shaft
- Generator
- Electronic Controller
- Yaw Mechanism
- Tower
- Hydraulic Brakes

Note: High-speed shaft and low speed shaft are sometime included in the Gearbox assembly. Moreover Yaw mechanism beside the yaw motors (4 motors typically) includes the wind wane and anemometer on the top of nacelle for wind speed and direction measurements.

The tower raises the turbine's assembly above the turbulent air currents close to the ground. Innovative tower designs allow towers to be built at a reduced cost with an increase in height to more than 300 feet. The blades, which spin in the wind to drive the turbine generator, along with the hub are called the rotor. A turbine with a 600 kW electrical generator will typically have a rotor diameter of 44 meters (144 feet) but newer designs have blades spanning 75 meters. Hub houses the blade pitch motors that are used for aerodynamic breaking. Blades and Nacelle are mostly made of reinforced plastic or fiberglass to reduce the weight; in some cases it has a metal frame in nacelle to provide firm support to the structure.

The rotor is attached to the nacelle, which sits atop the tower and includes the gearbox, generator, controller and brakes. A cover protects the components inside the nacelle. The entire nacelle pivots to maintain a point-contact with the shifting wind. The yaw motors/drives, with the help of computer controls, keeps the nacelle pointed into the wind. Blades are turned, or pitched, out of the wind to keep the rotor from turning in winds that are too high or too low to produce electricity. The yaw angle varies from 60 to 95 degrees.

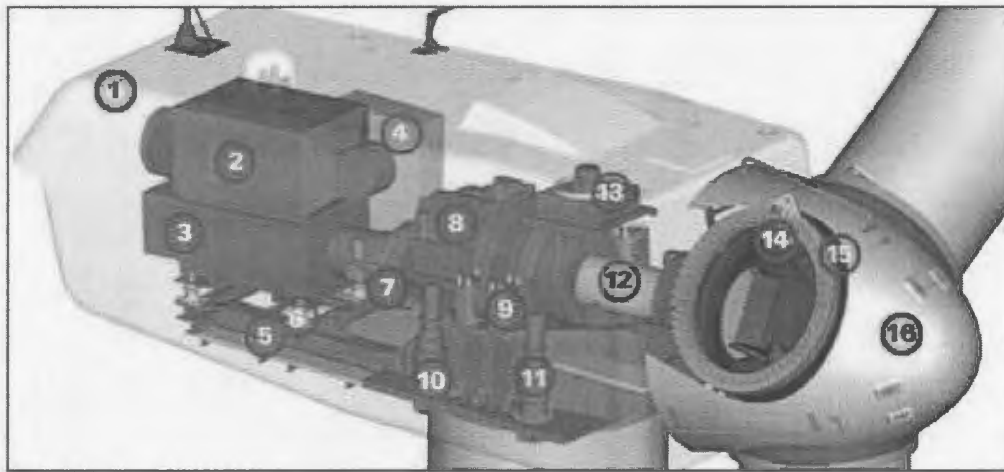


Figure 1.2 *Technical Drawing- Illustration of major components

The size, shape and the number of components vary depending upon the size of unit. A typical unit with ratings 500kW or greater will have all the above components. Smaller turbine systems may have a fewer components depending upon their power ratings, and size. In the following section the system selected for this research is discussed.

* (1) Nacelle, (2) Heat Exchanger, (3) Generator, (4) Control Panel, (5) Main Frame, (6)&(9) Impact Noise insulation, (7) Hydraulic Brakes, (8) Gearbox, (10)&(11) Yaw Drive (12) Rotor Shaft, (13) Oil Cooler (14) Pitch Mechanism (15) Rotor Hub (16) Nose Cone
(www.gepower.com/businesses/ge_wind_energy/en/index.htm)

1.3 AOC-15/50's System Description

The current study is focused on a smaller wind turbine system manufactured locally in Canada by Atlantic Orient Corporation (AOC). The 50-kW AOC-15/50 is an improved and simplified version of the Enertech- 44/60 wind turbine, which was developed in the United States in the early 1980s. The downwind, stall-regulated, three-bladed turbine features passive yaw control, wood epoxy composite blades incorporating NREL-designed airfoils, aerodynamic tip brakes, an electrodynamic brake, and an integrated drive train. This turbine is well suited for remote, stand-alone applications, village power systems, and small wind power plants. The system diagram is given in Figure 1.3.

The AOC-15/50's integrated drive train eliminates many critical bolted joints found in conventional turbine designs and creates an efficient load path from the rotor to the tower top. A cast-steel tower-top plate further improves the efficiency of the load path. The custom-made drive train designed by AOC weighs less than conventional drive trains and eliminates maintenance-prone couplings between the gearbox and the generator. Other design features include tip brakes and an optional yaw damper. The optional yaw damper is a passive hydraulic system that limits yaw rates (and gyroscopic loads) and is available for turbulent wind sites as an optional feature.

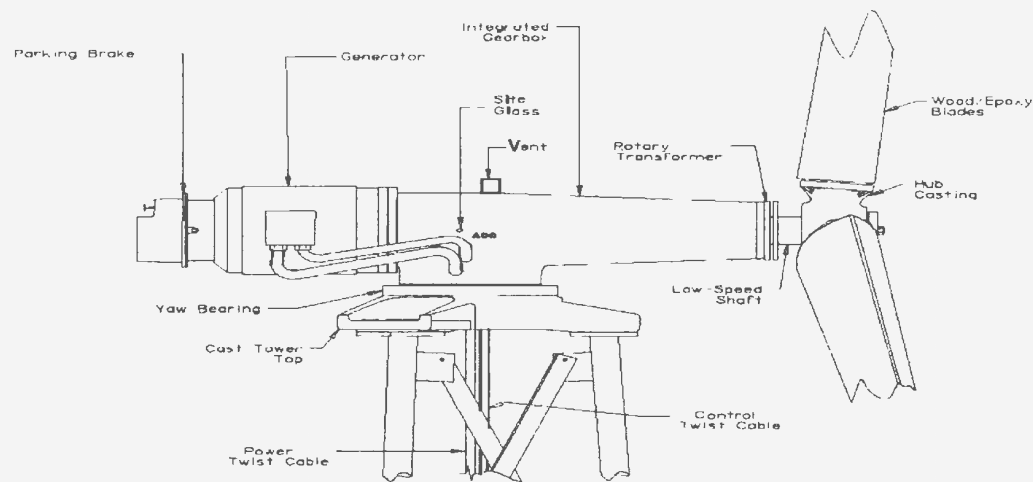


Figure 1.3 AOC 15/50 –Specification Diagram: AOC-15/50 Manual (2002)

1.4 Scope and Purpose of Research

Wind turbine Systems with higher power ratings (greater than 200kW) often have a built in protection system. This type of mechanism protects the unit from a catastrophe. A smaller system has greater pricing constraints than a larger one. AOC-15/50 is a much smaller system with 50 kW rating and has a built in Programmable Logic Controller (PLC) that controls the basic operations of the system and also performs some monitoring tasks. However an independent monitoring system is still needed which is responsible for monitoring the most frequently failing components. In order to proceed with the proposal of such a system, an in-depth component based reliability analysis is deemed necessary.

The first component of this research is to perform a detailed component based reliability analysis of AOC-15/50, which is based on the currently available reliability data. *Failure Mode and Effect Analysis* (FMEA) is the first step in the analysis in which failure modes are identified for all components. Based on failure modes the failure models are selected and the reliability for every component is computed depending upon its working conditions and environmental loads. Fault tree analysis and Markov analysis are performed to understand the failure mechanics and degraded performance scenarios under certain conditions. These analyses also help in determining the overall reliability of the system. As a result of this analysis the most sensitive components come forth.

Second aspect of the research uses the analysis performed in the first component of the research in which the most sensitive components were identified. For every component a measurable parameter is specified, which will help in determining the health of the components. Sensors are selected for monitoring the most sensitive components and electronic interfaces are designed and built. A single board computer is selected to perform the monitoring task, which is interfaced with signal conditioning electronic circuit interface. In event of detecting an alarming change in parameters through the electronic circuits, single board computer will interrupt the PLC to initiate a safe shutdown of the system.

A simulation test bench is also developed in the end to perform experiments and create similar environments for sensors to acquire data for monitoring and analysis.

1.5 Outline of Thesis

After establishing a general idea about wind turbines in this chapter, of the main topics of this thesis are outlined. The second chapter is about the review of literature. In this chapter the scope of research for previous studies is discussed with regards to reliability analysis and condition monitoring keeping in view their applications in wind turbine industry. The formulation of problem by different authors and the problem itself is also discussed along with the significance of this study. After doing the groundwork in two chapters, a detailed component based reliability analysis is performed for the selected system AOC-15/50. The analysis is performed for all selected components listed in chapter 3. In the end of chapter 3, markov analysis also performed. Once the failure prone components are identified a condition-monitoring proposal is prepared in chapter 4, which discusses the basic analysis required for the design of the condition monitoring system. The parameters are identified for every component and the sensitivity of every parameter is determined mathematically. The model and the concept discussed in chapter 4 are put into implementation in chapter 5. Besides discussing system implementation, data acquisition board layout, board setup, instrumentation and single board computer in detail, this chapter also discusses the development of test bench for real time simulation and tuning of the system. The conclusion and recommendations are listed in the last chapter.

Chapter 2

Literature Review

2.1 Introduction

Reliability estimation and Condition Monitoring (CM) have always been a priority method for online inspection of equipment in industries. Reliability analysis helps in making useful predictions about the state of machinery based on previous experience, while CM provides real time data from all or selected components depicting their present condition. Like other industries, the wind power industry is also trying to combine both of the above-mentioned methodologies to existing systems as well as in the other systems under development. By indicating faults while in operation, condition monitoring in machinery like generators and gearboxes can save a wind turbine unit from a catastrophic failure and hence save a lot of money and time. Similarly reliability analysis is deemed mandatory during and after the design for prediction of failure time and reliability of vulnerable components when the system is installed. A number of research papers and reports were published in the past 20 years regarding these issues. Europe has already

adopted this technology and a lot of work has been done in this area. In North America it is still in the stage of development. However, power companies are willing to invest in this area due to greater wind availability, especially in Canada. Some work relevant to present research is highlighted in the following section.

2.2 Reliability Analysis in Wind Engineering

In past 10 years different studies have been conducted stating a number of ways to predict reliability in wind turbines. Reliability analysis is now becoming a requirement in almost all aspects of engineering for asset management purposes and for the estimation of total lifetime of equipment. The work conducted by different authors is discussed briefly.

Seebregts et. al. (1995) tried to put things in perspective for reliability analysis of Lagerwey-15/75 wind turbine while working with the Netherlands Energy Research Foundation. They have introduced the approach of Probabilistic Risk assessment, which incorporates the reliability analysis methods into wind turbine engineering. Lagerwey-15/75 is equipped with an upwind two-bladed rotor that has a diameter of 15.6m and was mass-produced during the 1990s with a rated power of 75kW. This research is crucial to current study as it outlines the generic components for a wind turbine system. The main aim was to study the reliability in a more integrated manner so as to emphasize the areas that required more research. FMEA was implemented at first to check the measures that manufacturers had taken to prevent the failures. Event sequence analysis was performed

for finding the events leading to a complete or partial failure of the system. A block diagram for different states is provided, which outlines different states pertaining to LW15/75 design only. Data collection is done for the parameters of components from 11 turbines representing a 26-year operational period. A reliability qualification was performed using fault tree and event tree methodologies, which were discussed but not illustrated in the paper. Structural reliability analysis was performed for crucial components only. For the stochastic variables a normal distribution was used. A failure integral was developed using Mean Value Approach (MVA). The paper establishes MVA, in addition to the deterministic design rules, giving qualitative insights in the uncertainties of the failure damage calculations.

Michos et. al. (2002) discussed reliability assessment of the control and protection system for a typical wind turbine. In the first part the authors have described the limits and boundaries of a protection system highlighting what task it should perform and under what circumstances. The paper takes into account the standards of safety laid down by the *International Electrotechnical Commission* (IEC) named as Standard 61400. The computational aspect for reliability and safety assessment is discussed in the second part of this paper, which is closely related to the current study. The computational method of reliability assessment using an event tree and fault tree analyses is also discussed. The authors have considered different components of the protection and control system, which are as follows:

- Speed sensors
- Speed controller

- Relays
- Brakes & Aerodynamic breaking system.

However, it is argued that at times it is hard to draw a line between controller and safety systems due to a close relationship between them. The event tree analysis is done only for the speed control to avoid excessive speed. The above listed components are part of the speed control and protection system, which is the biggest threat towards the wind turbine system integrity. The working of the whole system is explained in detail and an event tree analysis is done using three different end states: Fail, Success or Partial failure. Minimal cut sets are established for each component and failure rates are determined using Markov analysis. However, the computation and model development for the system and components are not discussed. Some case studies were also performed to check different operation scenarios.

Sayas and Allan (1996) discussed the reliability of the wind turbine with a larger perspective of a wind farm setup where a number of wind turbines are networked to work in unison. The wind model is discussed with reference to Markov death and birth chain and is treated as a stochastic process. Different wind states are defined on the basis of wind speed and the state probabilities are determined along with the transition rates between different states. A wind turbine model is explained by output characteristics of different types of wind turbines that are stall and pitch regulated. The wind turbine is modeled as a binary state component having two states: fully operational and out of service. Based on the turbine model a wind farm model is developed. The authors have considered the state-dependence on the different wind-states. The failure and damage in

turbines are shown to be consistent with operation in increased wind speed states. Summarizing the work, the authors tried to establish a relation between different wind states and the output capability of a wind farm depending upon the wind turbine model.

Vittal and Teboul (2004) attacked the problem of wind turbine performance and reliability in a different way. They presented a method of jointly simulating both performance and reliability of the wind turbine. The approach is based on system simulation using Novel Monte Carlo algorithms driven from system transport theory, a method originally developed for nuclear physics applications. In the simulations both machine availability and energy produced are simulated as a function of the basic weather variables like wind speed, turbulence, intensity, etc. In addition to the simulations, Weibull log linear coefficients for blade, generator and gearbox are presented. Using these coefficients a more accurate failure distribution is presented that also considers the above-mentioned weather parameters. The repair distribution and parameters related to that are also discussed, keeping in view the major components of the wind turbine. The simulation output and results are presented for 8749 hours in the form of a turbine energy time series. Outputs are also presented in the form of percent availability, power output curve and downtime. In the end, the components' failure and sensitivities for a twenty-year period are presented.

Veer (1990) shed some light on the fatigue analysis of wind turbine components and structural reliability. In this specific paper the approach adopted is applied to components failing due to structural failure. The strategy adopted for performing the

reliability analysis is discussed in detail from problem formulation to transformations involved in data manipulation, approximation and computation. The analysis for a vertical axis wind turbine blade joint is performed. The formulation of a relation is performed, which is a function of nine variables out of which seven are said to be random. Damage **D** is calculated as a function of variables, and *time to failure* is computed as Number of cycles of failures divided by frequency of cycles. The fatigue reliability is computed as failure state functions, which is based on the difference of time between *time to failure* and *target lifetime*. Variability in fatigue is modeled as the variability in random parameters. All random variables are assumed to be normally distributed except for fatigue coefficients. The variables following Wiebull distribution are transformed to normal random variables using transform equations. The author discussed the selection of the distribution for random variables based on the data patterns. A comparison is made between Normal and Wiebull distributions from random variables keeping structural reliability in perspective.

The work of other authors listed below was also consulted and reviewed before conducting the reliability analysis. The discussed work may not be related to the research as strongly as the work discussed previously but it provides a thorough insight into the system operation and problem formulation. Jonkman et. al. (2003) presented an investigation report on IEC safety standards for a small wind turbine in which safety conditions for several wind turbines including AOC-15/50 are discussed. Peterson et. al. (1992) discussed the structural dynamic behavior of stalled controlled HAWTs for mountain terrain. This work pertains to the loading of wind turbine in rough terrains and

compares the loads of two turbines. Winterstein and Lange et. al. (1995) discussed the estimation of the probability distribution of wind turbine loads from limited data. The Exponential and Raleigh distributions are used to model the parameters' probability. A new four moment Wiebull distribution model is developed and used to model the load. Uncertainty in damage estimates is also quantified along with the implied data needs. Veer et. al. (1990) developed the reliability methods to determine the wind turbine structural reliability depending upon the inherently uncertain environmental factors. In a similar paper, Veer and Winterstein (1998) summarized the cyclic loading phenomenon due to rain flow on a wind turbine blade. The progressive damage caused by the cyclic loading is also discussed. Finally Klein et. al. (1990) presented their work on FMEA for wind turbine generators. FMEA was conducted for different operation modes and components during their work.

During the process of review, some project reports were also examined that provided a better understanding of wind turbine systems in general. Jacobs and Johansen (2003) presented their final report for Riso National Laboratories. The report contains work with regards to the lifetime distribution of larger wind turbine components in a generic turbine that has real life dimensions. Another report presented under contract for Sandia National Laboratories (2002), which presented the results of a study of various parameters for the design of wind turbine blade as a function of blade length. The report provides a better understanding of blade structure, which will be helpful in reliability analysis in subsequent chapters. Viplay (2002) presented his report to NEG Micon Rotor Limited, which discussed the objectives of the project. The objective was to design,

procure, assemble and test the hardware and control software for a fully instrumented prototype hub and pitch system for a 2MW turbine. This report again provided the instrumentation requirement and a general idea of loads on a rotor.

2.3 Condition Monitoring (CM) Techniques in Modern Wind Turbines

There are different *condition monitoring* techniques that are being used in process and control industry. These techniques are developed after many years of research and study. A brief summary of work in relation to condition monitoring in Wind turbines is presented in the following text.

Institute of Solar Engineering Technology (ISET) Germany has worked on a number of projects involving condition monitoring and its developments for wind turbine industry. Caselitz and Giebhardt (1999) discussed the development of a system with German manufacturers SCHENCK VIBRO and ISET. The research highlighted the functionality of measurement routines for condition monitoring. Overall the Wind Turbine was monitored using remote access through computer networks. To perform the monitoring task a model of Wind Energy Converters (WEC) was implemented in the system known as VIBRO-IC using language developed named *VibroPlan*. This implementation is named as the '*object model standardization*' and is given in Figure 2.1 (Giebhardt and Caselitz 1999). Measurements of the parameters were done on a horizontal axis 600 kW wind turbine. The sensor configuration and filter specifications

were discussed for data acquisition system. Fault prediction algorithms were used to calculate the statistic values of parameters periodically. The authors discussed the gearbox and bearing fault detection methodologies using power spectral densities, which is closely related to the present research. Rotor faults and their detection were also discussed. This is to be kept in mind that this project was for a wind farm; however in the case of present study, one wind turbine system is in question. This model of the software was used for data acquisition routine and analysis of data obtained from sensors. A layered concept is used in signal processing, generation of characteristic values and diagnosis. The monitoring system is flexible to perform three main function summarized in the following:

- Continuous monitoring of power characteristics to compare an average power rating for all times.

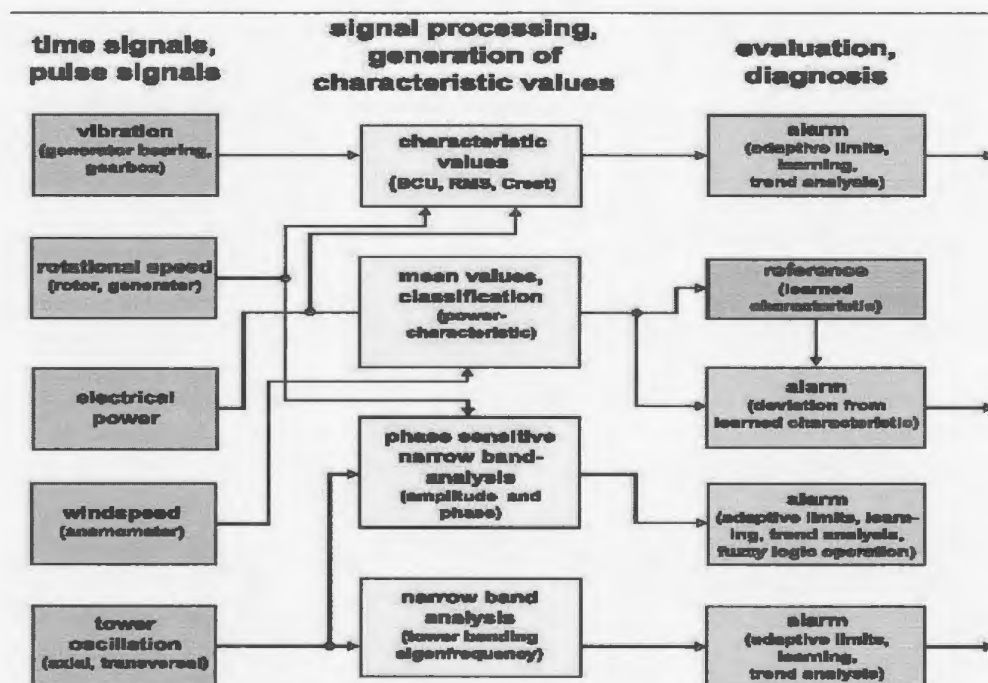


Figure 2.1. Standardized Object model for WEC monitoring (Caselitz and Giebardt 1999)

- Vibration monitoring
- Tower oscillations due to waves in Ocean.

Gearbox and bearing fault detection use the universal characteristic value like BCU and Crest, providing the overall information about the condition of bearing and gearbox. If a rising trend is detected, additional diagnosis of bearings can be derived from envelope curve analysis, which uses modulation of high frequency resonance to evaluate specific fault frequencies values. Besides gearbox and bearing the system will also keep in view the rotor faults by looking at the nacelle oscillations. As stated above several VIBRO-IC modules could be connected with serial line (RS – 422 or Ethernet networks). This allows data exchange and simultaneous access to all system.

In another instance Caselitz and Giebhardt (2003) highlighted the work on a similar project conducted by ISET. The work introduced a repair and maintenance project for offshore wind farms describing the requirements, scope and limitations of the project. Sensor mountings, specifications and overall operational characteristics of system are discussed. Monitored parameters like power, vibration amplitude and phase were explained with help of plots using real time data. Results of field test for a 300kW wind Energy Converter (WEC) are also discussed. A proposed solution for networked condition monitoring systems, using data from several WEC units is also mentioned. This solution describes the technology and hardware required for the system to work properly.

Popa and Boleda (2003) focused on the experimental investigation for incipient fault detection methods adapted for the use only in generators of a Wind turbine unit, which uses a doubly fed induction generators (DFIG). Fault detection discussed in this paper is concerning electrical faults listed as under:

- Inter-turn faults resulting in opening or shorting of stator phase windings.
- Abnormal connections of stator.
- Broken or cracked rotor bars.
- Static or dynamic air gap irregularities.
- Rub between rotor and stator can be catastrophic and can result in destruction of the entire machine.

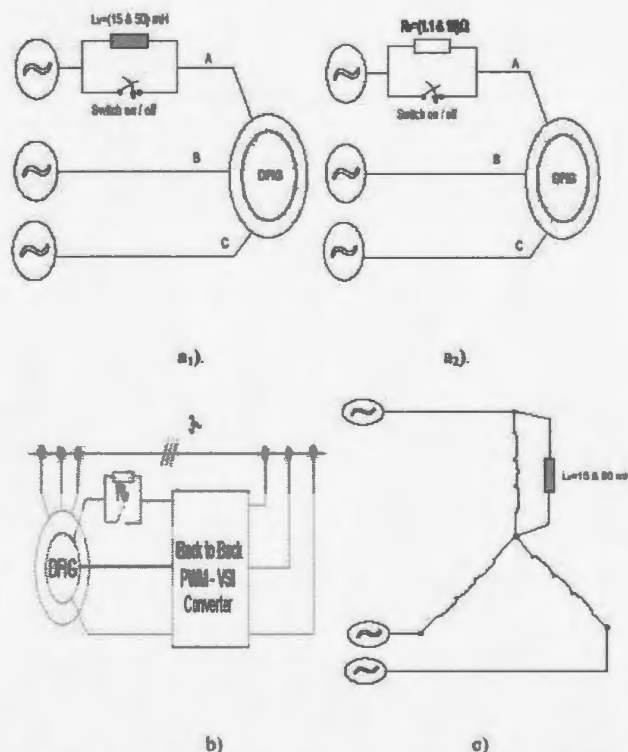


Figure 2.2. Scenarios of Resistive/Inductive imbalance.(a1) Stator Phase inductive imbalance, (a2) stator Phase resistive imbalance, (b) Rotor Phase resistive imbalance, (c) Turn to Turn Faults (Popa and Boleda 2003)

Faults like this were monitored using unbalanced air-gap voltages, increased torque pulsation and decreased torque. For experimental purposes the system used was rated at 11kW wound rotor induction generator with gearbox. The condition monitoring system consisted of many subsystems e.g. transducers, signal conditioning boxes and data acquisition devices.

Experiments of the stator and rotor faults were simulated. Three experimental investigations have been done to study the electrical behavior of induction machines:

1. Stator phase unbalance using a variable resistance and inductance in series on one phase.

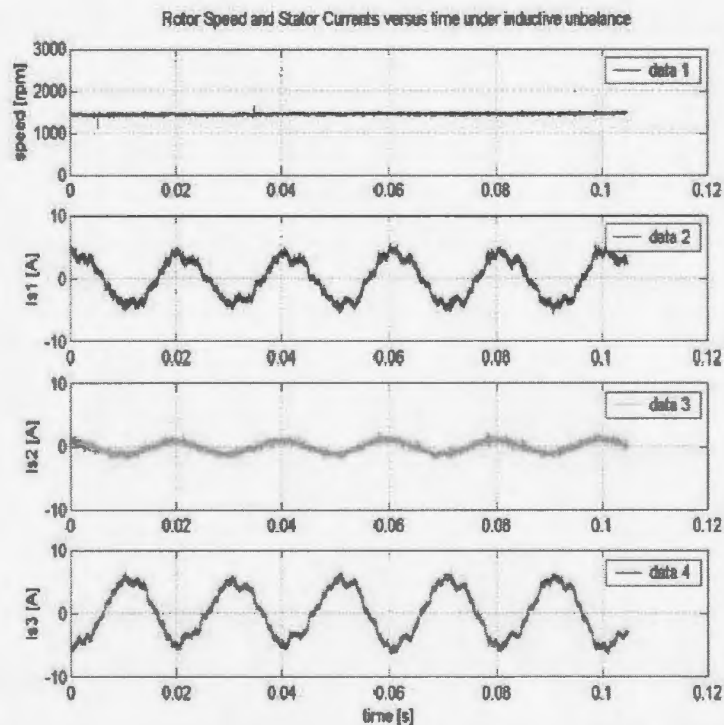


Figure 2.3. Inductive imbalance using Inductor in Series as shown in Figure 2.2 (Popa and Boleda et. al. 2003)

2. Rotor phase unbalance using a resistance of the same value as the rotor phase resistance inserted in series on one phase.
3. Turn-on turn winding fault, using inductance in parallel with one stator phase.

Different scenarios for resistive/inductive imbalance were simulated using the variable resistances as shown in Fig 2.2. The current characteristics were observed for all these cases. The data and graphs were recorded using Tektronics Oscilloscope TDS-50 and DAQ devices – ICS 645. DFIG was set to operate at a rotor speed of 1475rpm corresponding to stator active power of 2kW. Figure 2.3 illustrates the inductive imbalance. This phenomenon is known as Machine Current Signature analysis or MCSA. This method is a non-invasive method of finding rotor and stator faults. Afterwards the above-mentioned time domain signatures were converted to frequency domain by FFT for checking the generation of new frequencies due to faults.

Trutt et. al. (2002) presented similar kind of research as discussed in above (Popa and Boleda, 2003) but was limited to stator winding monitoring system only. Electrically excited vibrations were simulated in stator phases to look at the frequency spectra using resistors in series with the coil. The spectrum analysis shows that some additional vibrations are introduced in the bearing due to the simulation of electrical deterioration of stator winding. At first the motor was set to run at normal speed without the electrical excitation, afterward the excitations were used using resistors and the response was recorded using FFT signal spectra. This method is somehow similar to one discussed by

Popa and Boleda (2003), however MCSA is not used, rather direct vibration monitoring is used for any possible faults.

Work of some other authors was also considered with regards to condition monitoring and the operational aspects of wind turbine systems. Wilson (1990) discussed the optimization of mechanical braking systems for wind turbines. Horing (2003) conducted a probability study for the efficiency and the cost of operation of a wind turbine. Based on this study different condition monitoring strategies were developed. Billinton et. al. (2001) worked on supply reliability of small isolated power systems. The use of renewable energy sources is emphasized side by side with conventional electricity grids. Ugokwe (1992) discussed the working and reliability of a PLC unit in operation. Li et. al. (2002) presented the approach of fault diagnosis for motor roller bearing using neural networks. The simulation and real world results were obtained, which indicated that neural networks could be effective agents in diagnosis of various motor bearing faults. Similar type of work is presented by Wang and Kootsookos (1998) for modeling of low shaft speed bearing faults for condition monitoring in rotating machinery. The techniques of envelope autocorrelation were adopted for CM of speed shaft bearings. Rademarker et. al. (2004) presented the relation between condition monitoring and lowering of maintenance cost for offshore wind farms in their paper. New condition monitoring strategies such as optical fibers for strain monitoring on wind turbine blades were put to use. Bond and Clayton (1989) discussed their work on non-destructive testing of wind turbine blades in their publication. The work reviews the potential inspection capability available for use. Caselitz and Giebhardt (2003) discussed the work, which was discussed

in above paragraphs with the perspective of maintenance and repair of larger wind turbines systems in a separate publication.

A number of reports presented by different organizations and authors are also considered with regards to condition monitoring and other operation aspects of wind turbine system. Two such reports were presented by National renewable energy Laboratory and National wind technology Center (2003) for AOC-15/50. One report pertains to the safety and functionality of AOC-15/50 and the power performance is discussed in the second one. Both reports provided a thorough understanding of the system under study for the present research. Verbruggen (2003) presented the final report of a project, which was entitled as WT_Ω (wind turbine operation and maintenance based on condition monitoring). The report underlined some basic techniques for condition monitoring of a typical wind turbine and presented the case study for the instrumentation of Legerway 50/750 and Enron 1.5S wind turbine system.

2.4 Significance of Current Research

The previously mentioned work does cover many aspects of reliability related issues in wind turbines as well as condition monitoring techniques, but all of the mentioned work is conducted for larger systems. Due to the ever-increasing cost for providing electricity, the power companies are sometimes reluctant in installing a system that requires a large infrastructure. Such systems require continuous maintenance and immediate attention if there is some wear and tear. Systems like AOC-15/50 though smaller in capacity, have

the ability to withstand a longer lifetime. Due to the compact design of the drive train mechanism and passive yaw, the maintenance workload is reduced to half in the field. Even though, with greater *mean time between failures* (MTBF), the systems installed in remote rural locations require constant monitoring.

Reliability analysis is required for the groundwork of the Condition Monitoring system. But there are some other goals that will be met by conducting this analysis. Previous researchers have stressed on the analysis based on Event trees and fault tree analyses, which gives an insight into the mechanism of failure. These methods do pinpoint the scenarios, which will lead to a complete or partial failure of a setup, but have ignored the independent behavior of every component in working conditions. This type of analysis has become very important in asset management tasks. The budget constraints drive all power companies to conduct such analyses. These budget requirements put current research in perspective, which will be beneficial with regards to reliability modeling of individual components of a selected system and estimating their reliability, lifetimes and mean time to failures. The procedure and methods adopted will then be applicable to any wind turbine system. The aim is to provide a simple approach for the reliability analysis of individual components of a wind turbine system.

Condition monitoring techniques will be put into use after the reliability analysis is completed. The analysis will give insight into the causes of a component's failure. The health of each component will be translated in to a measurable parameter, which will be monitored independently by another on-board computer. The need to implement the

safety system independent to the control system makes sense. In event of a PLC failure, which is responsible for controlling the unit, the safety system can indicate the failure to remote control center and also be able to shut down the system in some cases. The development of this condition monitoring (CM) system for a smaller wind turbine can later be expanded in its scope. CM system can be set to monitor all the parameters of a unit, which are now being monitored by the controlling PLC. Another aspect of development of such a system is to reduce the condition monitoring cost for any smaller wind turbine unit. The conventional monitoring systems consist of data acquisition boards coupled with stand-alone Intel based Personal computer. Such a system adds up a few thousand dollars to initial installation and maintenance cost per unit. An effort will be made in future to implement an effective condition monitoring system with one quarter the cost of the Intel based PC. The future research will make use of the same single board computer used in this research that has the ability to communicate on Ethernet LAN for remote monitoring purposes and to acquire data from analog inputs at a sufficiently high speed.

Chapter 3

Reliability Analysis of AOC-15/50

3.1 Introduction

The description for the selected system, AOC-15/50 was discussed in chapter-2. This chapter illustrates the methodology adopted for the component based reliability analysis of the system. The introduction is followed by a flow chart explaining the main steps involved in this analysis. The first step is to perform the Failure Mode and Effect Analysis, which is followed by a general understanding of reliability models and their application in present study. The relationship among components is discussed which is later used in computing reliability of the system. The reliability of every component is computed for a period of one year. The Markov analysis is performed, to analyze the degraded performance of the system, which will give an understanding of the round the year availability of the system. To understand the failure mechanics and overall reliability, the fault tree analysis is also performed.

3.2 Methodology and Component Identification

The system selected for a component based reliability analysis can be divided into a number of different components. Methodology adopted for this study is outlined in the flowchart shown in Figure 3.1. Methodology is comprised of four main steps, which are conducted in sequence. Further details of these steps and the results are discussed in the subsequent sections of this chapter.

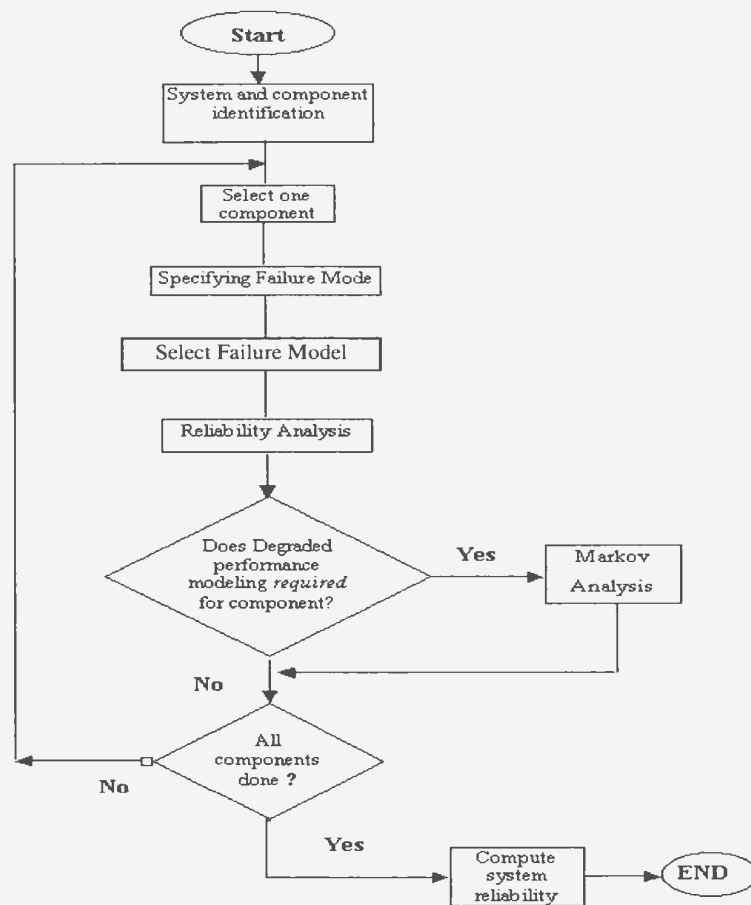


Figure 3.1. Flow chart of Tasks for Reliability Analysis

Wind turbine system in question can be divided into many components for analysis. It is important to define the system into a finite number of elements. The increased number of

elements will pose more problems in terms of collection of accurate data and making more assumptions. Assumptions in case of parameters such as *mean time to fail (MTTF)* can easily create undesirable and misleading results, which will lead to false reliability results. To keep the analysis precise, the system is divided into the following basic components. Further sub-division of these components is possible but is not adopted due to the unavailability of data. The relationship (series or parallel) between these components will affect the reliability of the entire system. Four basic operational areas are specified and components in the respective areas are listed in figure 3.2 and are as under:

- i) Blades.
- ii) Bolts.
- iii) Magnetic/Aerodynamic Brakes
- iv) Hub.
- v) Gearbox.
- vi) Generator.
- vii) Parking Brakes.
- viii) Yaw Bearing.
- ix) Tower.
- x) Anchor Bolts.
- xi) Controller and Constituent components.

A single AOC-15/50 wind turbine unit consists of above listed *major* components, which are considered for this study. Redundant components are provided to enhance system inherent reliability. However in case of wind turbines in general, due to the limitations of

cost and space it is not feasible. One of the components that is redundant in wind turbine is the blade, but here blade redundancy do not effect system reliability since three blades are considered as separate components. Figure 3.2 also clarifies the interrelationship of the components and how they contribute towards the proper functioning of the system.

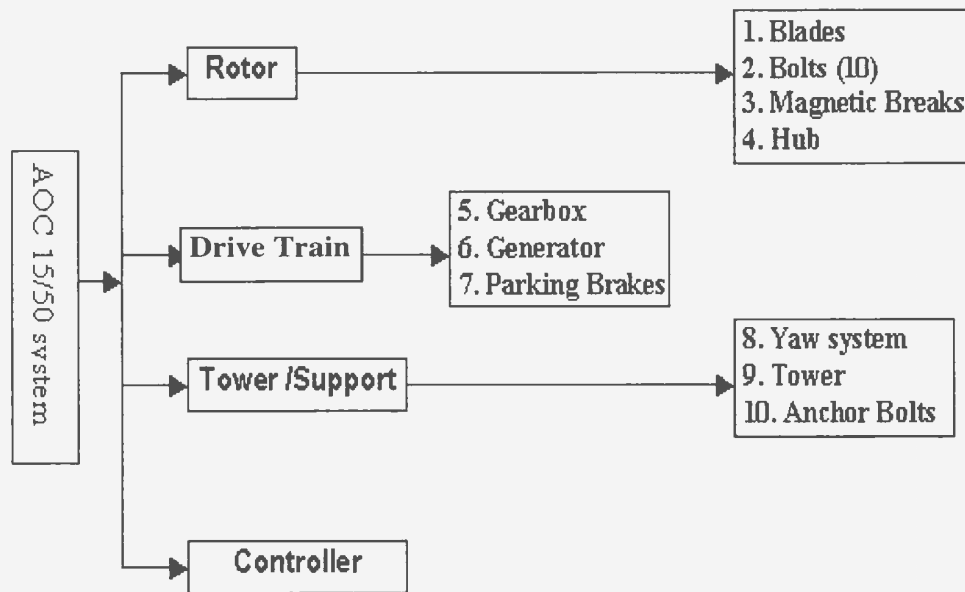


Figure 3.2. System Block diagram

After identifying the components and their relationship the next step is to conduct the Failure Mode and Effect Analysis. The discussion about the FMEA and rest of the analysis is done in the subsequent sections.

3.3 Failure Mode and Effect Analysis

The Failure Mode and Effect analysis (FMEA) is the study of different failure modes of system's components. This analysis enables the understanding of the causes and

consequences of failure of individual components. It also highlights the impact of failure of one component on the complete system. The results of FMEA for wind turbine system are presented in Table 3.1.

Table 3.1. Failure Mode and Effect Analysis table

No.	Component	Failure Modes	Causes	Consequences
1	Blades.	Fatigue failure.	Overloading due to wind load.	If any of blades fail, whole system will fail.
2	Gearbox.	Random failure /Over-speed.	Increased wind speed.	Complete failure or the system will result in failure of this component.
3	Generator.	Random failure/ Over speed.	Over speed due to disconnection from Grid. (No Load)	No generator, no electricity. So it will be a complete failure.
4	Brakes (parking).	Fatigue failure.	Continuous usage to stop.	If Brakes are unable to perform, a serious damage can happen in emergency situations when turbine is needed to be parked.
5	Brakes (Aerodynamic).	Fatigue failure.	Magnet failure, DC voltage failure or controller relay failure.	Failure can cause two problems, if open during normal operation: the system will deliver a degraded performance. If didn't work in over-speed conditions, can cause blades to brake or serious structural damage to blades due to high speed.

6	Tower.	Fatigue failure.	High-speed winds fatigue or over speed of rotor can cause excessive thrust on tower.	Total collapse of structure and hence the system fails.
7	Yaw Bearing.	Fatigue failure.	Roller bearing problems or lubrication maintenance.	Degraded performance as the angle of attack for wind will not be correct, Nacelle can fall down if alignment is lost.
8	Bolts (Hub – blade) 10 each.	Shear failure.	Increased wind speed during operation or parking can cause excessive shear on any of bolts.	Systemic degradation of support of blade that later can cause detachment during operation.
9	Hub.	Fatigue failure.	Constant stress on flanges can result in a crack.	Will result in detachment of blade if operation continues.
10	Controller.	Random failure.	Any of components may fail at any time.	PLC failure will result in no monitoring and can be catastrophic if not checked; Failure of circuit breakers can result in disruption of power supply to and from the system.

Knowing the causes and modes of failure for every component, a good judgment about the failure models that can be adopted for every component can be made. The discussion on generally used failure and reliability models is done in the up coming section.

3.4 Failure and Reliability Models

Reliability analysis of any component can be done once the failure data is known if a statistical analysis is required. However to select a failure model for such an analysis is in itself a task. Components are analyzed considering their individual working environment. Some components that remain under the same working loads and only fail randomly are governed by *Random failure* models. Three main components modeled on random failure basis are generator, gearbox and controller. However other components when start their life in service start to wear out. Such components have to be modeled on basis of time dependent failure models. There are two most commonly used time-dependent distributions that can be used, that are *Lognormal* and *Wiebull*. Both are characterized by the same principles of time dependence but have different distribution parameters. Wiebull model is more appropriate then the lognormal model because of its ability to address most of the failure and fatigue data distribution.

The two parameters in a Wiebull distribution are β and θ , the *shape parameter* and the *characteristic life* or *scale parameter* respectively. Shape parameter by its name defines the shape of the distribution and a value between 1 and 3 is desired in the present case for an increasing failure rate assumption. It is because $\beta < 1$ signifies significant improvement in reliability with time (infant mortality) and $\beta > 3$ specifies as normal distribution, which are not desirable to analyze a physical system (Ebeling 1997). For the intermediate values of β the distribution is positively skewed. Almost all components in any industry follow a positively skewed distribution function for the reason that they survive a viable lifetime

before they fail. If they follow a normal probability density function, half of them will fail and half will not, as normal distribution is symmetric about the mean value. The *scale parameter* on the other hand influences both the mean and the spread/dispersion of the distribution function. As θ increases the reliability increases at a given point in time or visa versa (Ebeling 1997). This method is used for parking Brakes; tip Brakes and yaw bearing in this study. For better understanding the behaviors of Shape parameter is explained in Table 3.2.

Table 3.2. Weibull Shape Parameter β (Ebeling 1997)

Values	Property
$0 < \beta < 1$	Decreasing Failure rate DFR
$\beta = 1$	Exponential Model or Random Failures
$1 < \beta < 2$	<i>Increasing Failure rate IFR</i>
$\beta = 2$	Linear Failure: Rayleigh Distribution Model
$\beta > 2$	<i>Increasing Failure rate IFR</i>
$3 \leq \beta \leq 4$	FR Values approach Normal distribution

The components, which cannot be analyzed by using either of the above statistical models and are subjected to excessive stress, are analyzed by using physical reliability model involving static reliability at an instant of time. These static values are then modeled for periodic loads for dynamic reliability of the component. This method is very effective and important for accessing structural components under constant load and can be applied in this case to blades, bolts connecting the blades, Hub, tower and anchor bolts. For modeling the *load* and stress on these components the load distribution is taken to be a lognormaly distributed.

3.4.1 Significance of the Bathtub Curve

The bathtub curve is a result of composition of several different distribution patterns as can be seen from the following diagram:

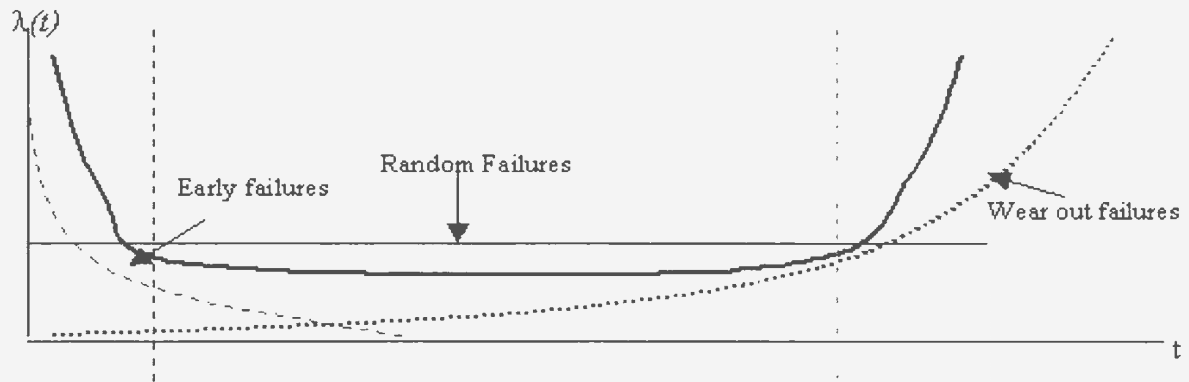


Figure 3.3. Bathtub curve and failure regions.

The pattern marked as early failures in figure 3.3 above depicts an infant mortality of components, the straight line indicate a constant failure rate when the component have crossed the early life stage and finally curve marked as “wear out failures” indicates the wear out period of life. Early or burn in failures are not of interest in present study. The components have to be tested for burn in failures in manufacturing facility, however the other two patterns will be useful as they depict the real situation faced by most of the wind turbine components/system. As mentioned above that not all components are working in the same environment and do not follow a same failure pattern, some fail in useful life stage randomly and some are in wear out stage. Wear out is a time dependent phenomenon and will be modeled using a Wiebull failure distribution model while random failures will be modeled as an exponential distribution model. Based on

discussion in Table 3.1, the failure model to be used for each component is given in Table 3.3.

Table 3.3. Reliability models used for components.

No	Component	Failure Mode	Reliability Analysis method.
1	Blade	Fatigue	Physical Reliability model
2	Gearbox	Random	Random failure model
3	Generator	Random	Random failure model
4	Brakes (Parking).	Fatigue	Wiebull reliability model
5	Brakes (Aerodynamic)	Fatigue	Wiebull reliability model
6	Tower	Fatigue	Physical Reliability model
7	Yaw bearing	Fatigue	Wiebull reliability model
8	Bolts 10/blade	Fatigue	Physical Reliability model
9	Hub	Fatigue	Physical Reliability model
10	Controller	Random	Random Failure model

After identification of components, their failure modes and selection of reliability/failure model to be used for all the components, the reliability analysis can be carried out.

3.4.2 Defining Reliability

Reliability is defined as probability that a component or a system will function over some period of time t when used under stated condition. If T is the continuous random variable

the time to failure of the system and $T \geq 0$. Then reliability can be expressed as follows (Ebeling 1997):

$$R(t) = \Pr\{T \geq t\} \quad (3.1)$$

For a given value of t , $R(t)$ is the probability that the time to failure is greater or equal to t also known as *Reliability function*. $F(t)$ is defined as cumulative probability that the failure will occur before time t it is represented as *cumulative distribution function*.

$$F(t) = 1 - R(t) = \Pr(T < t) \quad (3.2)$$

Another function that describes the shape of the failure distribution is known as *probability density function* is specified by the following relationship.

$$f(t) = \frac{dF(t)}{dt} \quad (3.3)$$

In addition to the reliability function defined above, there is another function that plays an important role in analysis and often available as a numeric value for different components know as *failure rate* or *hazard rate* $\lambda(t)$. From figure 3.3 we can see the transition effect on failure rate with time in the life of a system (component) and is defined as under using $f(t)$ and $R(t)$ described in equations (3.1) and (3.3):

$$\lambda(t) = \frac{f(t)}{R(t)} \quad (3.4)$$

Based on discussion mentioned in Table 3.1, 3.2 and 3.3, the specified reliability models will be used for the reliability computation from the available data (failure rate or available parameter values).

3.5 Reliability Modeling

The discussions carried out in the previous sections of this chapter were the groundwork for the reliability computation for every component, which is a matter of interest in the reliability analysis of this system. The details of computation and analysis discussed in the section are of pivotal importance to this research and thesis.

3.5.1. Reliability Model Block diagrams

As mentioned before that no component is redundant in the system. It is observed that components have series dependency which means that failure of a single component will lead to a complete failure of the whole system or will result in a degraded performance. For ease of analysis, the system is divided into four sub-systems.

- i) Blade Assembly/Rotor.
- ii) Drive train.
- iii) Tower and supports.
- iv) Controller.

Components in these sub-systems are represented in block diagram according to reliability modeling principles.

i) **Blade Assembly:**

Blade assembly for AOC-15/50 can be divided into four different parts, Blade, Aerodynamic Brakes, Bolts/Nuts and Hub. Failure of any of these components will

completely or partially fail the whole system. Partial failure pertains to a state in which one of the aerodynamic brakes or bolts are failed but system is still able to operate.

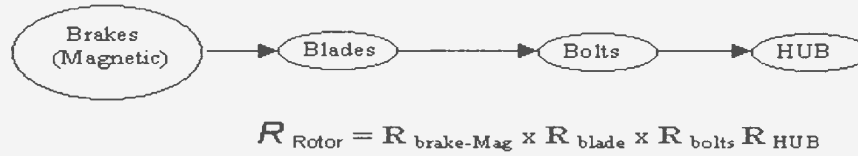


Figure 3.4. Rotor components in Series

There are 10 bolts in one blade and there are 3 blades. Each blade is considered as separate component in series as failure of one will result in the failure of whole system.

ii) **Derive Train.**

Derive train is custom build by AOC however the components are from different manufacturers. It consists of generator, gearbox and parking brakes. Generator is made by **Elliot MagneTek, California**. The gearbox is manufactured by **Fairfield manufacturing Co.** having two stage planetary gear mechanism. Brakes are from standard product line of **Stearns 81000 series** disk/parking brakes. This part contributes to the center of all generation and transmission activity and can play crucial role in the system's reliability. There is no redundancy in this sub-system so all of the component will be in series.

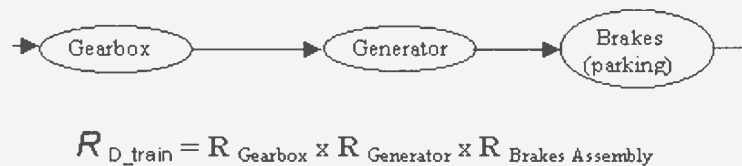


Figure 3.5 Drive Train in series

iii) Tower and Support.

Tower and support include two different components, Yaw bearing mechanism and tower components. One big roller bearing, which is fixed with tower top provide the yaw capability. This mechanism is passive in nature and is not driven or control by motors, so that the turbine will automatically orient itself in the direction of wind. Tower is made of Galvanized steel with three legs and truss-members. There are 4 sections of this tower, each section is 6 meters in length and weigh 900Kg. However given the structure of tower and scope of study, forces on each and every truss-member cannot be analyzed. It can be accomplished by a detail *finite element analysis* of the tower in a separate study. Tower is considered as one component, yaw mechanism as one and support that will include the anchor bolts. Anchor bolts will themselves be a system of three components in series as failure of one-leg can induce vibrations and that can lead to toppling of the whole structure in high winds only. Failure of the tower can also be represented as a *common mode failure* as failure of tower will be the system failure.



$$R_{\text{Support}} = R_{\text{Yaw_sys}} \times R_{\text{Tower}} \times R_{\text{Anchor-Bolts}}$$

Figure 3.6 Tower and Support components in series.

After looking into the reliability block model of these sub-systems we can now compute the whole reliability block diagram of the system as follows.

$$R_{\text{SYS}} = R_{\text{Rotor}} \times R_{\text{Drive Train}} \times R_{\text{Support}} \times R_{\text{Controller}} \quad (3.5)$$

3.6 Random Failure Models

As discussed previously that random failure model will be used for only those components where the failure is due to completely random or chance events. This model is also referred to as CFR (constant failure rate) or exponential model. In this study this model is applied to the analysis of three major components i.e Generator, Gearbox and Controller (PLC). Failure rate for generator and gearbox are adopted from (Non Electric Part Reliability Data, 1995). For PLC (Lees, 1996) is consulted.

3.6.1 Generator

Failure rate = $\lambda(t) = 0.796 \times 10^{-6} / \text{hr.}$

Estimating the reliability using CFR model for; $t = 1 \text{ yr} \Rightarrow 8760 \text{ hrs.}$

$$R(t) = e^{-\lambda t} \quad (3.6)$$

$$R(t) = 0.99305$$

3.6.2 Gearbox.

Failure rate = $\lambda(t) = 0.63 \times 10^{-6} / \text{hr.}$

Similarly;

$t=1 \text{ year} ; \Rightarrow 8760 \text{hrs.}$ Using equation (3.6)

$$R(t) = 0.9944$$

3.6.3 Programmable Logic Controller.

Failure rate = $\lambda(t) = 0.25/\text{year}$ provided in (Lees, 1996);

$$\lambda(t) = 2.85 \times 10^{-5}/\text{hr. } t=8760 \text{ hrs}$$

$$R(t) = 0.7788$$

3.7 Time Dependent Reliability Model

Time Dependent reliability model adopted is Weibull distribution model. The calculation of reliability from this model depends on the availability of two modeling parameters as stated in the section 3.4 of this chapter. This model is applied to three components, namely yaw bearing, parking brakes and aerodynamic magnetic brakes. In case of yaw bearing the parameters values are available on an Internet based reliability database (www.barringer1.com, recorded May 24, 2004). These values are used in conformity with the working condition of yaw bearing.

3.7.1 Yaw Bearing.

Data available for ball bearing .

$$\beta = 1.3.$$

$$\theta = 50,000 \text{ hrs.}$$

$$R(t) = \exp -\left(\frac{t}{\theta}\right)^\beta \quad (3.7)$$

Time dependent reliability models show a change in reliability with time t in equation (3.7). Where t is hours of operation for any component. Reliability of yaw bearing for adopted parameters and different time values is presented in the table 3.4.

Table 3.4 Reliability of Yaw bearing R (t)

T (years)	R (t)
30	0.00017
10	0.12588
5	0.43811
3	0.64384
2	0.77428
1.5	0.83861

For 1 year; t = 8760 hrs

$$R(t) = 0.9013$$

3.7.2 Aerodynamic Tip Brakes

The parameters for the yaw bearing were used directly as they were provided in 3.7.1, however in the case of brakes (parking and aerodynamic) this is not the case. The data available for analysis is the failure rate. One of the parameters in equation (3.7) has to be assumed on the basis of discussion made in section of 3.4. In the following it is shown how the available data (failure rate) is used in developing the required parameters for parking and aerodynamic brakes.

The failure rate is provided for magnetic brakes in (Non Electric Reliability Part Data, 1995)

$$\lambda(t) = 100.00 \times 10^{-6} / \text{hr.}$$

$$MTTF = \frac{1}{\lambda} \tag{3.8}$$

$$MTTF = 10,000 \text{ hrs}$$

For Wiebull reliability model the *mean time to failure* (MTTF) for a given component can be computed as under provide in Ebeling (1997):

$$\text{MTTF} = \theta \Gamma\left(1 + \frac{1}{\beta}\right) \quad (3.9)$$

With reference to the discussion in section 3.4 and from the Table 3.2, a suitable value of β is selected for both remaining components. A suitable value ranges from 1.1 to 2.9; value of β chosen for aerodynamic brake is 1.85 indicative of an increasing failure rate as per Table 3.2.

From equation (3.9) computing the value of θ ; when $\Gamma(x)$ provided in the any standard reliability book.

$$\theta = 11258.99 \text{ hrs} \cong 11260 \text{ hrs (approx).}$$

Wiebull reliability model from equation (3.7) gives the reliability at: $t = 8760$ (1 year).

$$R(8760) = 0.5334$$

3.7.3 Parking Break

The analysis for parking break will proceed in a similar fashion as above. Failure Rate is used from the same resource.

$$\lambda(t) = 2.10 \times 10^{-6} \text{ /hr.}$$

$$\text{MTTF} = \frac{1}{\lambda} : \quad \text{From equation (3.8)}$$

$$\text{MTTF} = 429.962 \times 10^3 \text{ hrs}$$

Assuming $\beta = 2.2$ considering an Increasing Failure Rate and using equation (3.9) will give $\theta = 537,688$ hrs. A one year reliability at $t = 8760$ is then computed using equation (3.7) as under;

$$R(t) = 0.999$$

3.8 Physical Reliability Models

In many situations it is not appropriate to assume that the reliability is merely a function of time as in the case of all remaining components under discussion. These components experience unusual stress during normal operation and their proper functioning and life depends on the periodic loads. Development of a *static model* from the available distributions will be the first task as stated in Ebeling (1997). These static models estimate the point reliability at any instant of time under stress; afterwards this model is subjected to periodic loading, which is a time dependent analysis and is termed as *dynamic modeling* in literature (Ebeling 1997). Based on the physics of the problem a *constant strength – random stress* model is used.

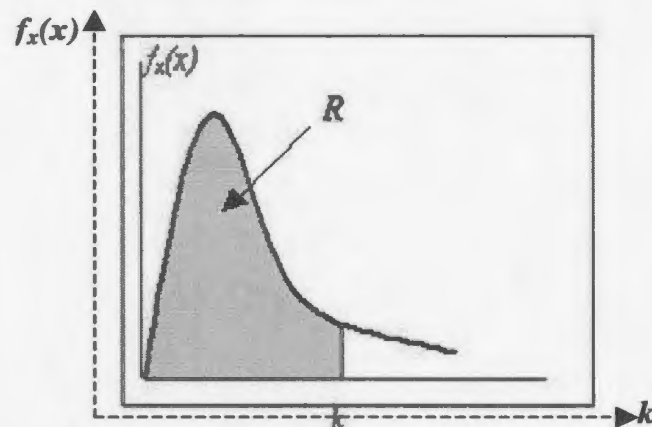


Figure 3.7. Reliability of a component - Fixed strength and random load model

If the system/component strength is a known constant k , and stress is a random variable with Probability Density Function (PDF) as defined under, then the system's static reliability can be defined as *the probability that stress does not exceed strength value k* . That is adopted from Ebeling (1997).

$$R = \int_0^k f_x(x) dx = F_x(k) \quad (3.10)$$

Specific stress distribution is required for static reliability modeling. In present study all stresses are assumed to be log normally distributed. The point reliability for a lognormal stress distribution is given in the following expression.

$$R = \phi \left(\frac{1}{s} \ln \frac{k}{x_{med}} \right) \quad (3.11)$$

Where :

s = Shape parameter of lognormal distribution.

x_{med} = Median value of load.

Where s is shape parameter taken to be $s = 0.1$ in all cases. Additional relationship that will help in the analysis is given as:

$$x_{mode} = \frac{x_{med}}{\exp(s^2)} \quad (3.12)$$

Where x_{mode} is the mode value of load acting most of the time for a specific situation (normal operation or in a storm conditions). In the following the analysis is performed for blade, bolts, hub, tower and anchor bolts.

3.8.1 Blades

Moments on one blade are estimated based on the total thrust produced by the rotor disk of a wind turbine (Manwell et. al. 2002). The thrust on the disk is given as;

$$T = C_T \frac{1}{2} \rho \pi R_r^2 U^2 \quad (3.13)$$

Where;

C_T = Thrust coefficient (8/9 for a rigid rotor assumption)

ρ = Density of Air.

R_r = Radius of Rotor.

U = Free Stream Wind Speed.

There are two kinds of moments that will primarily act on the blade and are of interest. These are Flap wise and Edgewise moments. Edgewise moment is responsible for the lift of the blade and does not contribute in any failure mechanism. Hence it is not considered here for strength analysis. The Flapwise moment will be responsible for failure due to fatigue during normal operation or increased stress during high winds when turbine is parked. The Axial forces and moments on the blade can be found by models provided in (Manwell et. al. 2002) which is;

$$M_\beta = \frac{1}{B} \int_0^{R_b} r [1/2 \rho \pi 8/9 U^2 2r] dr \quad (3.14)$$

Where:

M_β = Flap wise bending moment on one blade root.

r = instantaneous radius.

B = No. of blades. (Three)

R_b = Radius of the blade.

Computing the integral for (3.13): we have

$$M_\beta = \left[\frac{\rho \pi 8 U^2}{2B9} \right] \int_0^{R_b} 2r^2 dr$$

Substituting from equation (3.14) when $C_T = 8/9$; $2T = 8/9 \rho \pi R^2 U^2$ we have;

$$M_\beta = \frac{2T}{3B} R_b \quad (3.15)$$

This moment value can be translated into maximum instantaneous Stress as follows;

$$\sigma_{max} = M_\beta \cdot \frac{C}{I_b} \quad (3.16)$$

Where;

σ_{max} = Maximum Stress.

C = Distance to neutral axis of force.

I or I_b = Blade root moment of inertia.

The moment calculated and discussed is on the blade root and the reason for doing so is that the root is directly attached to hub via 10 bolts per blade. The blade root will be experiencing the affect of the bending moment on the blade eventually. Model Equation (3.13) and (3.15) are used to for peak values of input variables like cutout *wind speed* = 23 m/sec, *Radius* = 7.2 m; $\rho = 1.29 \text{ Kg/m}^3$ to calculate moment on one blade root.

$$T = 49.3945 \times 10^3 \text{ N}$$

$$M_\beta = 79.031 \times 10^3 \text{ N.m}$$

In Equations (3.16) the value of I_b is unknown, the blade root section is assumed to be rectangular in this case and on the basis of data provided from manufacturer the dimensions of the cross-section of blade root are l or Chord Length = 451 mm and t thickness = 281mm. Moment of inertia is given by:

$$I_b = \frac{l}{12} t^3 \quad (3.17)$$

$$I_b = 8.977 \times 10^{-4} \text{ m}^4$$

Equation (3.16) will provide with maximum stress on the root with $c = \frac{t}{2}$ being flap wise neutral axis.

$$\sigma_{max} = 12.677 \text{ Mpa}$$

3.8.1.1 Static Reliability Computation

From the above analysis we have established the maximum value of bending stress on the blade root. Using the static reliability models discussed in (3.11) and (3.12), and taking $\sigma_{max} = x_{med}$, material strength of wood epoxy k is a *range of values* ranging from 49 to 125 Mega Pascal (M Pa) for different resins. Assuming the lowest value of strength being conservative in analysis, static reliability can be computed as under:

$$x_{med} = 12.794 \text{ M Pa.}$$

The parameters discussed for equations (3.11) in start of section 3.8 and using above values of x_{med} .

$$R = \phi \left(\frac{1}{s} \ln \frac{k}{x_{med}} \right); \quad \text{Equation (3.11)}$$

$$R = \phi (14.069)$$

From tables in Ebeling (1997); $\phi(x)$; where $x > 4$ implies $R = 0.9997$ however when ever $x \gg 4$ we take $R = 0.99999997$ as in this case.

3.8.1.2 Dynamic reliability Model (periodic loading)

Dynamic reliability model as stated Ebeling (1997) is given as;

$$R = \exp^{-(1-R)\alpha t} \quad (3.18 a)$$

Where α is defined as load cycles. For a wind turbine blade and related components the cyclic loading phenomenon is described in detail in (Manwell et. al. 2002) as under;

$$\eta_L = 60 K n_{rotor} H_{op} Y \quad (3.19)$$

Where:

η_L = cyclic loads are *same* as α in equation (3.18a).

$K = 1$: the number of *cyclic events of bending*; in this case it is the minimum.

$n_{rotor} = 62$: rotational speed of rotor in revolutions per minutes (rpm) which is the maximum speed for AOC15/50.

$H_{op} = 8760$: hours of operation for one-year period.

Y = number of years same as t

For a 1-year reliability estimate ($Y = 1$) assuming round the clock operation without any maintenance; we have:

$$R_{\text{blade}} = \exp^{-(1-R)\eta L} \quad (3.18 \text{ b})$$

$$R_{\text{blade}} = 0.9068$$

As there are three blades in a series configuration according to reliability block model, the reliability will reduce. For the sake of analysis if the period of operation is increased the reliability will further decrease as shown under:

$$H_{op} = 4000 \text{ hrs and } Y = 20 \text{ yrs.}$$

$$R_{\text{blade}} = 0.4095$$

$$R_{\text{blades}} = [R_{\text{blade}}]^3$$

These values corresponds to a 20 year continuous operation for almost 6 months a year; $4000 \times 20 = 80,000$ hours of operation at peak operating speed of 23 m/s (worst case scenario). Due to the variation in speed these operating hours can increase because the resulting load and stress on blade will be less in those conditions and will provide a longer lifetime.

3.8.2 Bolts

The failure of bolts, which connect blade to the hub, is associated with shear forces that can cause the bolt to break away. Once in a rotation every blade will be faced downward. During this position, the component of thrust will be acting down along with the weight of blade; contributing to a worst load case for bolts, as they will be experiencing a maximum shear at that time. In addition of the weight of blade acting downward, there will be additional centrifugal force that will add to the total force acting on the bolts

supporting one blade. So the total stress on one bolt will be stress due to weight (σ_{gb}) and stress due to centrifugal force (σ_{cb}). Give by the following equation:

$$\sigma_b = \sigma_{gb} + \sigma_{cb}$$

$$\text{Weight of Blade} = W = 150 \times 9.8 = 1.470 \text{ k N.}$$

Models for moments due to weight and centrifugal force on a blade are adopted from Manwell et. al. (2002) given $M_w = W \cdot r_{cg}$; where r_{cg} is the center of gravity distance of blade (radius of blade/2)

$$M_w = 5.292 \text{ k Nm.}$$

Considering the dimensions of blade root and that root is directly connected to the bolts supporting the blade; we have stress due to weight on blade root provided in Manwell et.

$$\text{al. (2002) as: } \sigma_g = \frac{M_w}{I_b} \left[\frac{c}{2} \right]; \text{ where } c \text{ and } I_b \text{ provided in section 3.8.1.}$$

$$\sigma_g = 8.47 \text{ M Pa}$$

$$\text{Stress on One bolt due to weight} = \sigma_{gb} = \sigma_g / 10 = 8.47 \times 10^5 \text{ Pa}$$

$$\text{Centrifugal force for one blade} = F_c = \frac{\text{Mass of Blade}}{g} r_{cg} \Omega_s^2 \text{ as stated in (Manwell et. al. 2002)}$$

$$F_c = 211.18 \text{ k N}$$

$$\text{Centrifugal force on one bolt } F_{cb} = F_c / 10 = 21.18 \text{ k N}$$

$$\text{Stress on One bolts is given} = \sigma_{cb} = F_{cb} / A = F_{cb} / \pi r_b^2$$

Bolts specification listed in AOC 15/50 Manual (2002); A193 heavy- hex bolts, standard for those are governed by American Society on Mechanical Engineering;

$$r_b = 8.1534 \times 10^{-3}.$$

$$\sigma_{cb} = 101.41 \text{ M Pa}$$

$$\text{Total stress on bolts} = \sigma_b = \sigma_{cb} + \sigma_{gb} = 102.26 \text{ M Pa.}$$

3.8.2.1 Static and Dynamic Reliability Model.

Ultimate strength of Grade –8 Steel bolt used here is =640 M.Pa. Using (3.11) and (3.12) for the analysis;

$$x_{mode} = 102.28 \text{ M Pa.}; k = 640 \text{ M Pa.}$$

$$R = \phi (6.25)$$

The value implies the same results as observed in Blade with $R = 0.99997$. For the periodic loading 8760 hours of operation using (3.18) and (3.19);

$$R' = 0.9068$$

$$R_{bolts} = [0.9068]^{10}$$

This will compute the reliability if 10 bolts per blade. However a degrading analysis will be performed in Markov analysis.

3.8.3 Hub

Failure of hub can be a result of two distinct events; crack in the hub branch to which blade is connected, or crack of flange to which blade is bolted on the hub-branch. Worst case of loading will be 90° angle with vertical axis of blade when it will behave momentarily as a cantilever beam. The following analysis is performed for finding the bending moments on the Hub branch.

$$M = \text{Moment due to weight} + \text{Torque} \quad (3.20)$$

$$M = M_w + T'$$

M_w was calculated in previous section to be 5.292 k Nm

Force due to torque can be calculated using the model given by (Morrow, 1999)

$$\text{Power} = \frac{T' \Omega_s}{9550} \quad (3.21)$$

Where: T = torque, Ω_s = Speed of rotor Rev Per Minutes, P = Power (K Watts)

$$T' = \frac{9550}{62} \times 50$$

$$T' = 7701 \text{ N. m}$$

Total moment on one Hub Branch is given by equation (3.20) is;

$$M = (5.292 + 7.701) 10^3 \text{ Nm} = 12.993 \text{ k Nm}$$

With dimension of the Hub Branch known; width = 0.231775 m; Height = 0.1501 m and using equations (3.16) and (3.17) we can have the $\sigma_{\max} = 8.058 \text{ M Pa}$.

3.8.3.1 Static and dynamic Reliability Model.

Following the same procedure carried out in case of blade and bolts with $x_{mode} = 8.14 \text{ M. Pa}$. with $k = 170 \text{ M Pa}$, $R = 0.99997$. The reliability for 1 year period with 8760 hours of operation per year using (3.18) and (3.19) is given as under:

$$R'' = 0.9068$$

$$R_{\text{hub}} = [R'']^3$$

$$R_{\text{hub}} = [0.9068]^3 = 0.7456$$

3.8.4 Anchor Bolts and Tower

The guidelines for analysis of tower are followed directly from Guideline for Electrical Transmission line Structural Loading (American Society of Civil Engineering 1991). It provided a useful and easy approach to a number of transmission structures. However same approach is used for Wind Turbine tower keeping in consideration the environment and terrain conditions. The wind force acting on a tower or transmission component as stated in Guidelines for Transmission line Structural Loading (ASCE 1991) is given as under:

$$F = Q (Z_v V)^2 G C_f A' \quad (3.22)$$

Where:

Q = Air density factor [$0^\circ\text{F} = -17.7\text{C} \cong 0.00289$] specified by elevation above sea level.

Z_v = Terrain factor [open land = 1.14, open shore = 1.29 @ 80ft.]

V = wind speed = 51mph = 22.5 m/sec (peak speed of operation).

$G = G_t$ = Gust response factor for tower only.

G_t can be calculated by direction and tables in same Guideline from ASCE (1991)

C_f = force coefficient value.

A' = Projected area of tower in ft^2 .

Using the appropriate parameters for the equation (3.22), which are all selected from Guidelines from (ASCE, 1991), the analysis is conducted in the upcoming sub-section.

3.8.4.1 Area of projected tower face

Face of the tower experiencing the winds will be the most crucial case of loading, face of the tower has a trapezoidal face with dimensions; $h = 80$ feet, $b_1 = 10.75$ feet, $b_2 = 2.75$ feet. With area $A = \frac{1}{2} (b_1 + b_2) h$ which gives area of one face of tower to be 540 ft^2 . Assuming a solidity factor of 30% effective area is 162 ft^2 . Force coefficient given for 30% solidity in Guidelines for Transmission line structural loading (ASCE 1991) is 3.75. Substituting all of above values in equations (3.22) we get:

$$F = 7.0856 \times 10^3 \text{ Kip}$$

$$1 \text{ Kip} = 4.448 \text{ KN}.$$

$F = 31.517 \times 10^6 \text{ N} = 31.517 \text{ MN}$. Forward thrust produced by the rotor disk in the direction of wind will also be added to this force value;

$$F = 31.517 \text{ MN} + 49.39454 \times 10^3 \text{ N} = 31.566 \text{ MN}.$$

If it is assumed that tower behaves as a cantilever beam, with forces on tower known it is possible to compute maximum stress, however moment of inertia has to be known for that computation. That is not possible in a simplistic way as tower is lattice bolted and a truss structure. A similar analysis is presented for a telecommunication tower for a service life of 30 years by Fashny, Chouinard and McClure (Canadian Journal of civil engineering 1998). The work presents the upper and lower bound values of probability of failure taking in consideration different wind speed and ice loading scenario for the telecommunication tower. Keeping in view a large number of values presented in the paper and our computational limit of nine significant figure we adopt a failure probability

as $F(t) = 0.33 \times 10^{-9}$ corresponding to the lower bound group with ice thickness $\leq 35\text{mm}$ and wind speeds of $\leq 150\text{km/h}$. Using equation (3.2) we have

$$R(t) = 0.99997$$

With this value of reliability of tower under winds up to 150km/h , there is no possible cause of failure for anchor bolts. The specification of bolts also rule out such a failure possibility due to their extraordinary tensile strength, stainless steel material and the fact that they are bolted to foundation and supporting a heavy structure not allowing it to vibrate/topple as mentioned in AOC-15/50 Manual (Version 5.0 2002).

3.9 Markov Analysis

The Markov analysis looks at the system as being in one of several states. States are defined as *total operation* or *degraded operation* states. Every degraded state differs from the other depending upon which component has failed and what effect will it have on the overall performance and production level. For this study the components that may lead the system to a degraded performance or a sequential failure scenario are the bolts, tip brakes and yaw bearing. This implies that the total number of states will be five. According to Ebeling (1997) “the fundamental assumption in a Markov process is that the probability that system will undergo a transition from one state to another depends only on the current state of the system and not on any previous state system may have experienced. In other words this property is equivalent to the memorylessness of

exponential distribution and it is not surprising that exponential time to failure satisfy markovian property”. From the discussion regarding reliability analysis, the failure rates of most of components are known. For those components they are not known, and will be calculated in the next section.

3.9.1 Conditions

As there are total of 30 bolts (connecting 3 blades to the hub), failure of any of two bolts on any blade will be considered as system failure as continuous operation at that point can cause sever damage. Mean time to failure can be found out from the following expression;

$$MTTF = \int_0^{\infty} R(t) dt \quad (3.23)$$

Where $R(t)$ is taken from equations (3.17-a) and (3.17-b) for the components analyzed by physical reliability model. In those equations if the value of variable time is ignored we will be left with the following:

$$R(t) = \exp^{-(1-0.999997)(60)(1)(62)t} \quad (3.18 - c)$$

Using the above two relations, the MTTF can be computed for components (blades, bolts and Hub) who have a static reliability of $R=0.9997$ and will be the same for all these components. The failure rate is in *per hour* units and can be computed as follows; here λ_1 is for bolts only.

$$MTTF = 89605 \text{ hrs} \cong 89600 \text{ hrs}$$

$$\lambda_1 = \frac{1}{MTTF} = 1.116 \times 10^{-5} / \text{hr}$$

In case of yaw bearing the failure rate λ_3 has to be deduced from Wiebull failure model given as under:

$$\lambda(t) = \frac{\beta}{\theta} \left\{ \frac{t}{\theta} \right\}^{\beta-1} \quad (3.24)$$

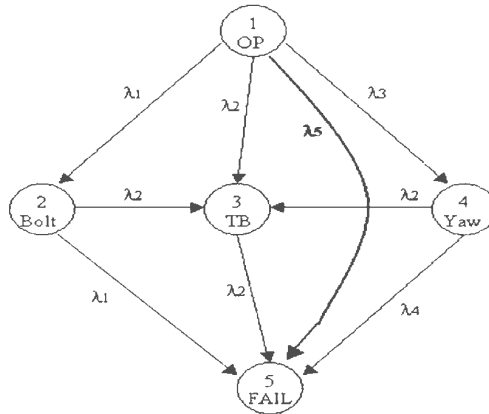


Figure 3.8 5-Stage Markov Model – Rate Diagram

3.9.2 Yaw failure Scenario

In case of yaw bearing the failure will cause system to go in a degraded state-4, from that state the system will go to a complete failure state (5). The failure rate from stage-4 to stage-5 will be the combined FR of all the remaining components in the model and λ_5 .

Wiebull FR for yaw bearing for an operating period of 1 yrs (8760 hrs) using (3.24) is;

$$\lambda_3 = 1.15 \times 10^{-5}$$

λ_4 according to above discussion can be calculated as follows:

$$\lambda_4 = \lambda_1 + \lambda_2 + \lambda_5 \quad (3.25)$$

3.9.3 Transition Rates for States and State Probabilities

Failure Rate for tip brake provided in section 3.7.2 of this chapter will be the transition rate from stage-1 to stage-3 and stage-3 to stage-5.

$$\lambda_2 = 100.00 \times 10^{-6}$$

There can be a scenario in which the system will directly go to a complete failure state (state-5) without going in a degraded operation mode as shown in figure 3.8. For such a case the failure rates will be the combined failure rates (λ_5) of all components failing randomly. Model equations for different states provided Ebeling (1997) will be used to model the probability of being in total operational state (1) over a period of time t . State 2, 3 and 4 are partially failed state.

$$\lambda_5 = \sum \lambda_i$$

Where $i = 3$ in this case for generator, gearbox and controller.

$P_i(t)$ is the probability for system staying in stage- i at time t , where $i = 1, 2, 3, 4, 5$; where $P_1(t)$ that is probability of being in a complete operational stage and it can be modeled as follows. The general model is provided in Ebeling (1997):

$$P_1(t) = e^{-(\lambda_1 + \lambda_2 + \lambda_3 + \lambda_5)t} \quad (3.26 a)$$

Transition of system from state-1 to any of the degraded state or failure state is hence the result of combined failure rate of bolt, tip break, yaw bearing and components failing randomly. The first step in the analysis will be performed for $t = 8760$ hrs. For the ease of analysis we can consult the following table for transition failure rates.

Table 3.5 Transition Failure Rates for Markov analysis

S No	Transition	Failure rate	Effective FR
1	State 1-2 & State 2-5	λ_1	$\lambda_1 = 1.116 \times 10^{-5}$
2	State 1-3 & State 3-5	λ_2	$\lambda_2 = 100.0 \times 10^{-6}$
3	State 1-4	λ_3	$\lambda_3 = 1.15 \times 10^{-5}$
4	State 4-5	λ_4	$\lambda_1 + \lambda_2 + \lambda_3 = 1.041 \times 10^{-6}$
5	State 1-5	λ_5	$(0.796 + 0.63 + 28.5) \times 10^{-6} = 2.99 \times 10^{-6}$

The failure probabilities for being in each state is provide in Ebling (1997) as follows and will be used to conduct the further analysis.

$$P_4(t) = e^{-(\lambda_4 + \lambda_2)t} - e^{-(\lambda_3 + \lambda_4 + \lambda_2)t} \quad (3.27)$$

The probabilities for state-2 and 3 are provided in a different manner then given in Ebling (1997). The transition *from* state-2 and 3 to state-5 is the result of the failure of same type of components that brought the system *to* state 2 and 3.

$$P_2(t) = e^{-(\lambda_1 + \lambda_2)t} - e^{-(2\lambda_1 + \lambda_2)t} \quad (3.28 \text{ a})$$

$$P_3(t) = e^{-\lambda_2 t} - e^{-(4\lambda_2)t} \quad (3.28 \text{ b})$$

Since total reliability is equal to 1, we have the following relationship for state-5.

$$P_5(t) = 1 - P_2(t) - P_3(t) - P_4(t) - P_1(t) \quad (3.29)$$

The above relation will provide the Markov analysis results presented in following table for 1 and 2 years operation. However the probability that the system will make a

transition from state-1 to any of the degraded states can be determined by $(1 - P_{I-a}(t))$ given by amendment in equation (3.25 a) as follows:

$$P_{I-a}(t) = e^{-(\lambda_1 + \lambda_2 + \lambda_3)t} \quad (3.26 \text{ b})$$

Table 3.6 Markov Analysis Results for States 1-5

S.No	State of System	One Year Probability $t = 8760$	Two Year Probability $t = 8076 \times 2$
1	$P_1(t)$	0.3326	0.1106
2	$P_2(t)$	0.0350	0.0024
3	$P_3(t)$	0.3868	0.1725
4	$P_4(t)$	0.0395	0.0309
5	$P_5(t)$	0.2066	0.6824

The values of $P_I(t)$ and $P_5(t)$ can give us a good idea about system availability, partially failed and completely failed states.

3.10 Fault Tree Analysis

Fault tree is a standard reliability analysis procedure for a multiple component system. It gives a better understanding of the failure scenarios and contribution of different components toward total failure of system. In the figure 3.9 the fault tree for the system is presented. The analysis of the tree can be followed by deducing the Cumulative Failure probability $F(t)$ from the preceding sections of this chapter. The basic analysis will follow as under where $P(T)$ is the probability of top event (System Failure);

$$P(T) = F_{\text{rotor}} \cup F_{\text{controller}} \cup F_{\text{drive train}} \cup F_{\text{tower support}} \quad (3.30)$$

$$P(T) = [F_{\text{blades}} \cup F_{\text{bolts}} \cup F_{\text{Hub}} \cup F_{\text{tipbrk}}] \cup [F_{\text{Controller}}] \cup [F_{\text{generator}} \cup F_{\text{gearbox}} \cup F_{\text{parkingbrk}}] \cup [F_{\text{yaw}} \cap F_{\text{tower}}]$$

Following the rules of binary algebra and set theory described in Ebeling (1997) or any other generic Math book and we have:

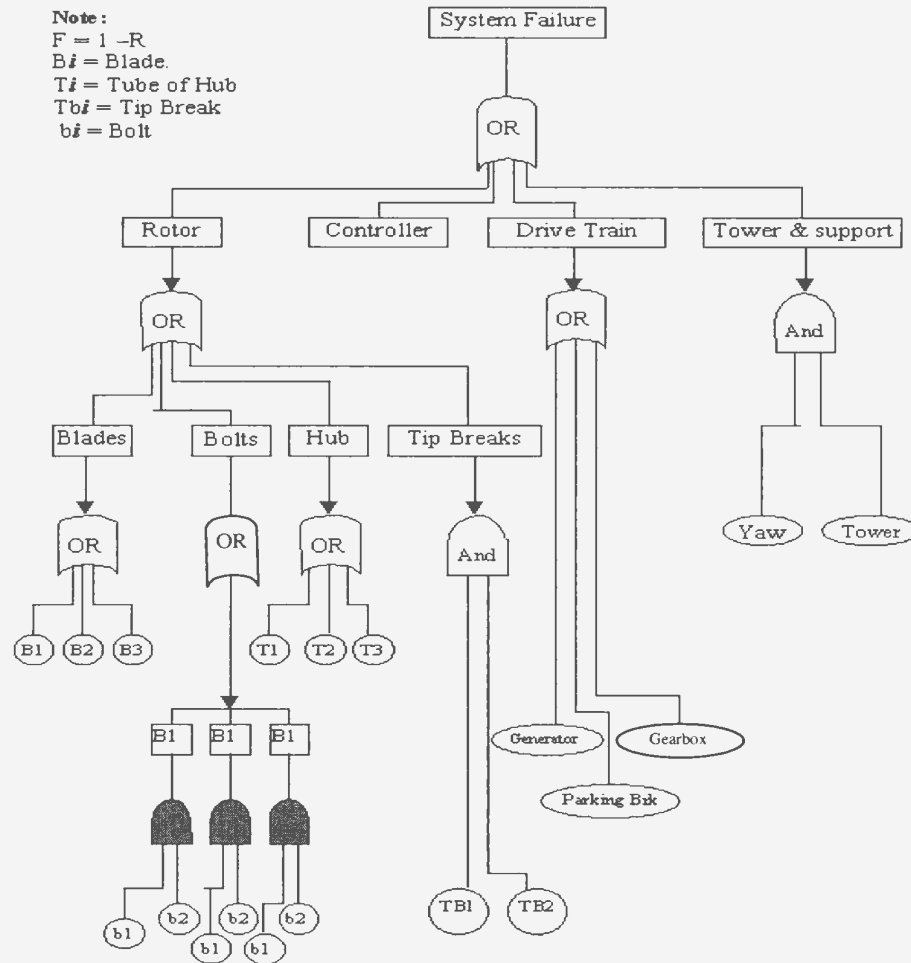


Figure 3.9 Fault tree Representation

$$P(T) = 0.0923 + 0.020 + 0.0932 + 0.217 + 0.2211 + (6.95 + 5.6 + 0.1) 10^{-3} + 2.96 \times 10^{-3}$$

$$P(T) = 0.6427$$

The results of analysis in fault tree are close to the analysis performed in markov analysis.

3.11 Summary

A detailed reliability analysis is performed for AOC-15/50 in this chapter based on the available data. After a detailed component analysis two famous methodologies are adopted to assess the system's reliability. Each method shows a different perspective in failure mechanics. According to fault tree analysis the probability of failure $F(t)$ is nearly 65% in one year, which gives a reliability value of 0.3573. In markov analysis $P_1(t) = 0.3326$ indicative of state-1 which is the total operational state. This value is very close to the value computed in fault tree analysis. It is to be noted that the failure of one blade is considered as one event; same as in the case of the failure of one section of the hub. This assumption plays a very important role in determining the final value of the probability of the top event $P(T)$ or failure probability of the system. If those events are considered independent of each other the probability of failure may increase considerably.

Chapter 4

Proposed Condition Monitoring System

4.1 Introduction

The need for an independent Condition Monitoring (CM) system has proven to be necessary for many electromechanical systems. Wind turbines installed in remote locations need continuous monitoring. Some variables like wind speed and direction, which are primarily important for basic operation, are always taken into account. However due to changes in environment, other parameters, which under normal circumstances may not pose any harm, may require attention. A condition monitoring system for wind turbines was proposed by Caselitz and Giebhardt (1999 & 2003) and many other authors; details for their work are discussed in Chapter 2 of the thesis. Most of the large commercial wind turbines have a condition monitoring system, but small wind turbines lack this feature due to the additional cost involved, as discussed in detail in section 2.4. This chapter lays the groundwork for condition monitoring design and instrumentation for AOC-15/50.

4.2 Component Reliability and Parameter Selection

A detailed reliability analysis was carried out for a 50kW small wind turbine AOC-15/50. The analysis provided reliability and sensitivity of some of the AOC-15/50 components while operating under normal conditions. It provides some valuable information about the components' lifetime and condition after one year of continuous operation. Table 4.1 describes the reliability analysis results for the wind turbine component discussed in Chapter 3. The tip brake and yaw bearing have been identified as the most vulnerable components in the system. The results are consistent with the problems faced by similar systems in operation.

Table 4.1 Component Reliability and Failure rate/hr.

Component	Reliability	Failure rates
Tip brake	R = 0.53340	1.00×10^{-4}
Yaw bearing	R = 0.90130	0.115×10^{-4}
Generator	R = 0.99305	0.769×10^{-6}
Gearbox	R = 0.99440	0.63×10^{-6}
Parking Brakes	R = 0.9990	2.16×10^{-6}
Blades	R = 0.90680	1.116×10^{-5}
Bolts	R = 0.90680	1.116×10^{-5}
Hub	R = 0.90680	1.116×10^{-5}
Tower and anchor Bolts	R = 0.99970	1.000×10^{-7}

The steps involved in the development of the condition monitoring system are outlined in the following subsection. The work carried out is covered in this chapter and chapter 5.

4.2.1 Methodology Adopted for CM System Development

The flowchart shown in figure 4.1 elaborates the process involved toward the design and implementation of a condition monitoring system.

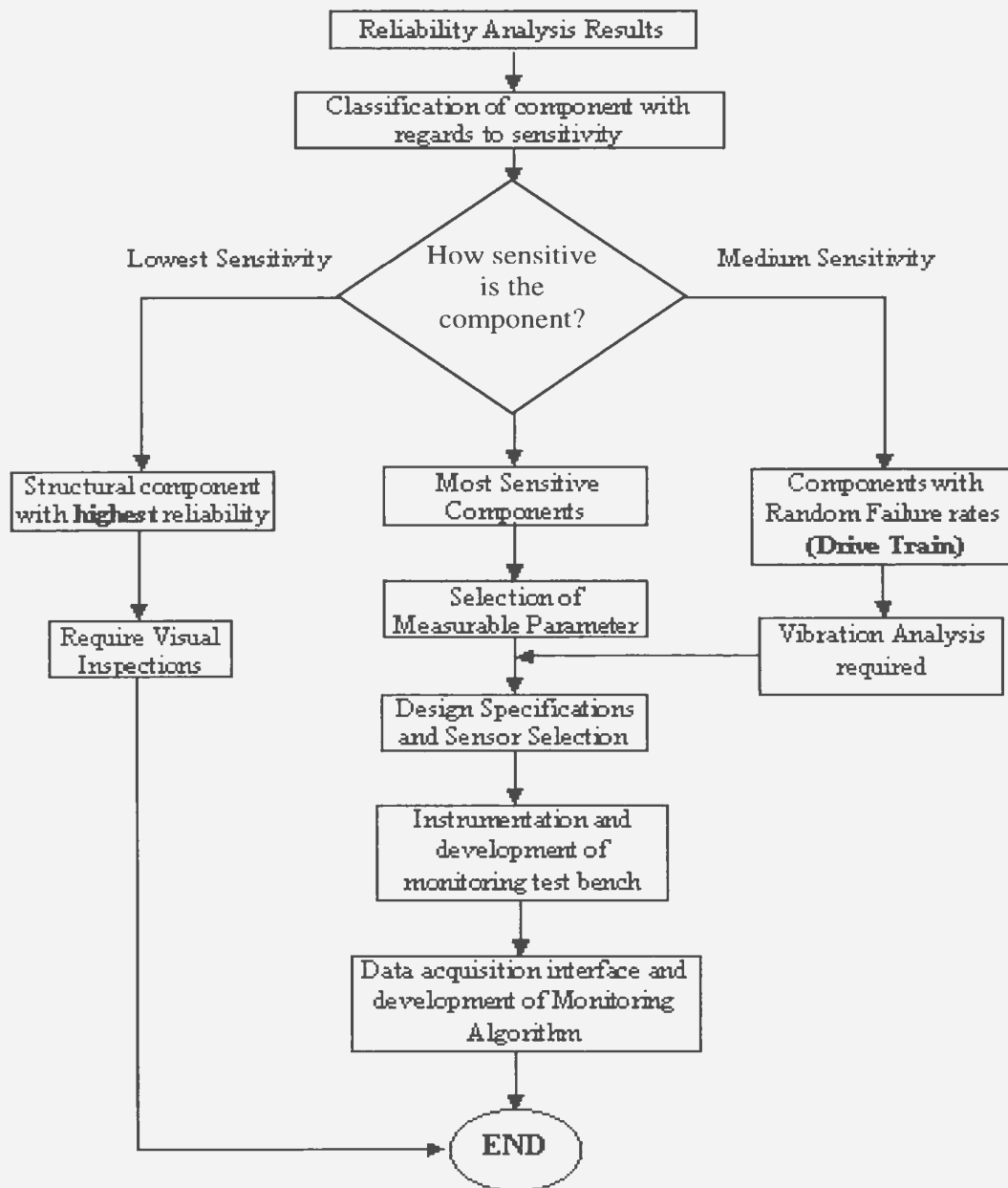


Figure 4.1 Flow chart of methodology adopted in CM system development

4.2.2 Parameter Selection

Based on the reliability analysis, the components can be classified into three groups as per their vulnerability to fail, as shown in Figure 4.1 and listed in Table 4.2. The groups are: most sensitive components, components with medium sensitivity and least sensitive components. The most sensitive components are those that are highly sensitive to their loads and working environment and require continuous monitoring. The components in the medium sensitive group show a random or wear-out failure pattern and could be monitored. They may require periodic maintenance on an annual basis. The last group of components, which are structural in nature, may not require a technical monitoring method and periodic visual inspection is sufficient after a constant period of time. Parking brakes are classified as medium reliability group component. However, they show a high reliability value of 0.999 as compared to bolts and the hub. The reason for this is the difference between statistical and physical reliability analysis. The structural component may show a lower reliability value for one year but they can sustain a longer life when periodically loaded for a 30-year life time, which does not happen in the case of parking breaks since the Weibull reliability model is used for analysis.

In order to monitor the health of any component, it is necessary to identify and select a measurable parameter. The parameter will specify the type of sensor to be used. The instrumentation is required for data acquisition purposes, which is discussed in detail in chapter 5. Every component exhibits a unique attribute related to it, which is affected during its use. That attribute can be translated into a measurable parameter like voltage or current, which may vary depending upon different operating conditions. This change will

provide information about the operating conditions of different parts of the system. A list of all components and the related parameters are given in table 4.2.

Table 4.2 Component and Selected Parameters

Component	Sensitivity	Parameter for monitoring.
1. Tip Brake.	Both components are highly sensitive due to wear out effects.	1. Current sensors for electromagnetic brakes.
2. Yaw bearing.		2. Strain Gauge measurement for strain on bearing.
3. Generator.	Random failure. Low sensitivity toward working loads	3. Vibration Monitoring for bearing faults. Torque.
4. Gearbox.		4. Vibration Monitoring for Gear Mesh fault and spike frequency methodology specific gear problems.
5. Parking brakes.	Wear out failure but comparatively longer life and lower failure rates.	5. Mostly dependent on component life but temperature can be monitored during every braking cycle. Visual Inspection.
6. Blades.	Structural components show a high reliability for design life of 30 years	6. Visual monitoring for blades + stain sensor may be mounted on blades to record bending.
7. Blots.	-Same as Above-	7. Visual monitoring for rusting and tightening conditions.
8. Hub.	-Same as Above-	8. Visual monitoring for rusting and cracks.

9. Tower.	Structural components show a high reliability for design life of 30 years	9. Oscillations for tower integrity in case of high winds and visual inspections for tower conditions.
-----------	---	--

The following discussion will establish the rational for selecting the specified parameter for each component along with the sensor specifications.

4.3 Monitoring of Tip Brakes

The spoilers or the tip brakes are mounted on the tip of each blade that provides aerodynamic traction while stopping. They are a part of the regular stopping mechanism and have to be deployed when a stop cycle commences. However, it was discovered that tip brakes, being mechanical in nature, have some problems. They are prone to failure during regular operation, especially when they are in a closed position. The centrifugal forces acting on them can also lead to failure. Even in the case of magnets activated for keeping them closed, brakes seem to open partially or deploy without an instruction from the system's PLC. This situation can cause problems in a smooth operation of the turbine and energy production. On close observation it was discovered that before the occurrence of a complete failure, the spoilers would experience a mechanical play. This play introduces a change in the supply current. The change in current is more significant as the brake (which essentially is a metal plate connected to the spring mechanism and magnet) vibrates while rotating. Due to the centrifugal force, plates may disconnect from the magnets sending current surges in the supply, as shown in Figure 4.2. These variations in current can be recorded to keep track of the health of every tip brake. Any sudden

variation or pattern observed by the system can be recorded and appropriate action to shut down the system if more than two brakes are damaged can be taken. However these variations might appear in the main power supply to the brakes. The main power supply to the brakes is rated at 120V/5A. A current of 0-5Amp is expected; it is shown that the brakes work on a constant AC current value, which implies that any sudden changes in current can be detected (AOC 15/50 Manual, revised April 2002). The operating voltage and current require a sensor that is good for the same current and voltage ratings.

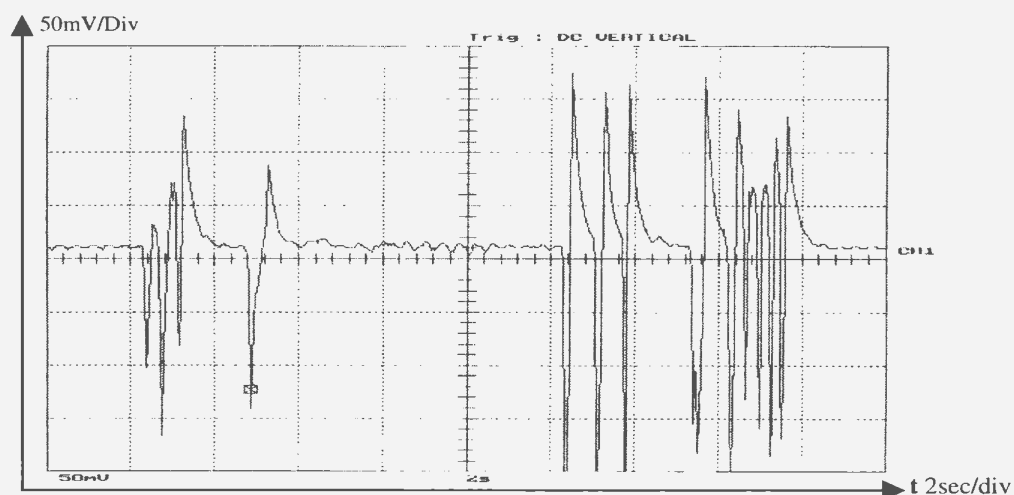


Figure 4.2 Expected variations in Current supply to Tip Brakes

4.4 Monitoring of Yaw Bearing

Strain measurements are mostly meant for structural loading; here it will be serving a slightly different purpose. From the analysis in chapter 3, the second most sensitive part of the AOC-15/50 appears to be the yaw bearing. It has been observed in similar and other systems of larger capacity, that yaw bearing is a prime source of service disruption.

This happens in the case of bigger yaw bearings, but AOC-15/50 has a yaw bearing not exceeding a diameter of 2 feet. This custom-designed bearing under normal operating conditions experiences some unusual moments. The reliability data also suggest the same finding. Due to the passive nature of the yaw mechanism in AOC-15/50, the operating conditions of yaw bearing become vulnerable, as there is nothing to reduce the increased forces from the severe weather and wind conditions. Such circumstances can trigger unusual loading scenarios and irreversible damage can be caused to the *bearing's shape*, and later on it may result in a major system failure. However if such a change is detected beforehand, a lot of potential loss can be saved. Before proceeding toward instrumentation and implementation of the condition monitoring system, the following analysis is deemed necessary. With reference to structural details discussed in the AOC-15/50 Manual (revised 2002) and Byers and Snyder (1969), the following will be helpful in designing and calibrating any appropriate sensing arrangement. Figure 4.3 is a reduced-scale drawing provided by the manufacturers. The analysis follows as under:

$$m_1 = \text{Mass of Generator} \qquad \cong 120 \text{ Kg}$$

$$m_2 = \text{Combined mass of Three blades at hub} \cong 450 \text{ Kg}$$

The downward force exerted by both masses *as ignoring the mass of gearbox* is given by;

$$F_1 = 1.176 \text{ K N and } F_2 = 4.410 \text{ K N}$$

The moment arm are indicated in Figure 4.3 as L_1 and L_2 for both forces respectively, therefore the moment of force on the rotating ring of bearing would be:

$$M_1 = 514.73 \text{ Nm} \quad \text{and} \quad M_2 = 4890.48 \text{ Nm}$$

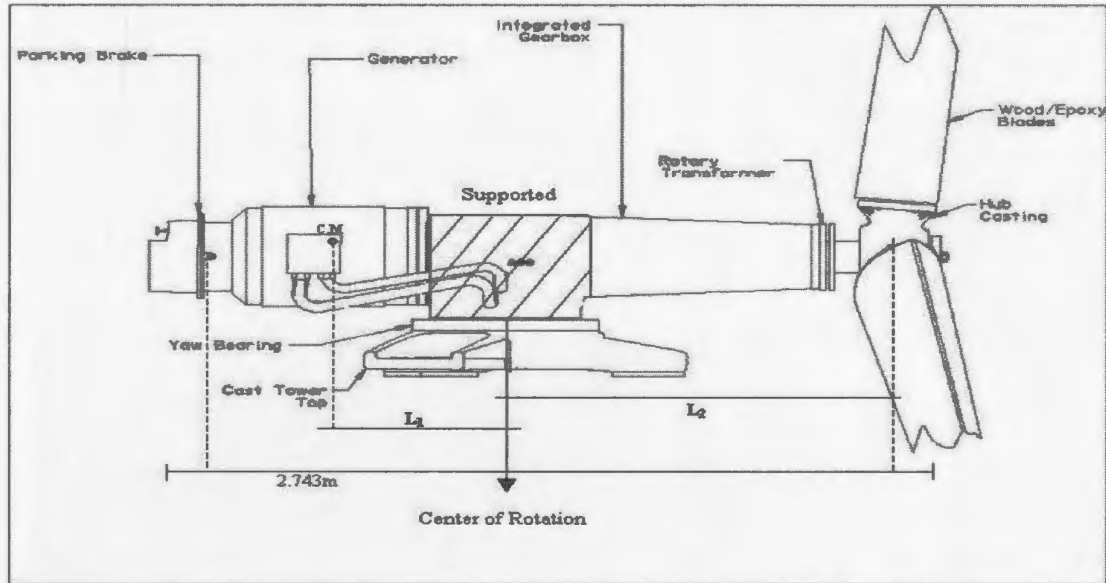


Figure 4.3 Drive Train and Yaw support with Tower top

The inherent imbalance of the moment is of about **4375.752 Nm** can be observed by values of M_1 and M_2 . It is also important to note from figure 4.3 that the center of gravity is also slightly towards the hub rather than being on the *center of rotation*. This also adds to the imbalance effect on the bearing. The rotor disk thrust phenomenon is discussed in detail in chapter 3 (section 3.8.1). This thrust can also affect the imbalance conditions. If it is assumed that while rotating, a blade experiences the maximum thrust when they are in a vertically upward position. At the same time, the other two blades are at an angle of 120 degrees from it and in a position where they might not be receiving an equal thrust, thus creating a net downward moment on the hub end of the assembly. To keep the analysis conservative, a worst-case scenario of the downward moment due to difference of thrust is taken to be *the total thrust*. It is assumed that no thrust force is acting on other

blades in this scenario providing a net downward moment. From equation (3.12) and subsequent analysis in section 3.8.1, we have the *thrust* on rotor disk, given as:

$$\Delta T = T' = 49.394 \text{ k.N}$$

$$\mathbf{M}_T = 54.775 \times 10^3 \text{ Nm}$$

Hence the total bending moment on bearing comes out to be;

$$\mathbf{M}_\beta = 59.1513 \text{ K Nm}$$

Which translates into stress φ of 0.18640 M Pa. Using Hook's law (Byers and Snyder, 1969) to observe *change in length per unit length* when the above-mentioned stress is applied;

$$\mathbf{E} = \frac{\varphi}{\varepsilon} \quad (4.1)$$

Where:

ε = Strain

\mathbf{E} = Young modulus of the material (steel 316)

We have a strain value;

$$\varepsilon = 9.65 \times 10^{-7} \text{ m/m}$$

After studying the dynamics of the Yaw bearing which is an 8-point slip bearing designed for heavier loads, the mechanics of transfer of force to the outer bearing ring (mounted to tower) may not be linear. However, it is assumed that strain will be transmitted to the outer ring (on which the measuring instrumentation will be done) with the same

magnitude. For sensitivity and calibration purposes and by convention, the above value of strain is converted into **in/in** units and comes out to be:

$$\epsilon = 0.00003799 \text{ in/in}$$

For an available strain gauge with a ***gauge factor*** of 2.0 and $R = 120\Omega$ the relation is given in Byers and Snyder's (et al 1980) as:

$$\Delta R = \epsilon \cdot (GF) \cdot R \quad (4.2)$$

$$\Delta R = 0.009118 \Omega$$

$$\Delta V \propto \Delta R$$

Ohm's law implies that there will be a proportional change in the value of voltage with changes in resistance. This provides a basis for the detection of strain on the ball bearing for a given load. The change in voltage will be of the order of millivolts that can be detected using some instrumentation.

4.5 Vibration Monitoring for Drive Train

Vibration measurement has now become a norm in modern condition monitoring systems. The use of such a system is not directed by reliability analysis, however to determine the health of rotating machinery a real-time vibration measurement technique is required. There are many existing monitoring systems available in markets by different vendors. These systems use Fast Fourier Transform (FFT) routines to compute the FFT and display the magnitude spectrum on the monitor or system display. Most of these

systems are custom-made and have to be calibrated, moreover they are installed as a software program/application on a Windows/DOS based operating system along with a separate data acquisition card that will take the real-time data samples and compute the FFT spectrum. These types of systems are suitable for bigger wind turbine systems, having a staggering installation and repair cost. However, for smaller systems like AOC-15/50 the addition of this type of a separate data acquisition and monitoring system will come out as a huge price issue if one system is to be provided with each wind turbine unit. Keeping in view the financial restrictions, there is a need to develop a cost effective and equally efficient solution. An effort is being made during this research to develop such a system that is able to keep track of vibration activity for the whole unit and thus be able to detect sudden changes in frequency spectrum. These changes will be indicative of any upcoming faults as well as of any imbalance within the frame of turbine. FFT is an improved way of computing Discrete Fourier Transform (DFT), which is the crux of the solution. DFT can be computed on any band-limited time varying signal. From its name it is clear that discrete time sample values are required. Mathematical representations of Fourier transform of a continuous time and discrete time signal are given by following equations:

A continuous time signal $x_c(t)$ can be represented in a discrete time representation as follows;

$$x_c(t) = x_k(n\Delta T_s) \quad (4.3)$$

$$X_N(\omega) = \sum_{k=0}^{N-1} x_k e^{-jk\omega} \quad (4.4)$$

Where T_s be the sampling time and X_N is the DFT of the discrete signal x_k .

$$\text{Now } \omega = n\omega_s; \quad \omega_s = 2\frac{\pi}{N} \quad (4.5)$$

Which gives us the final relation as under;

$$X_N(n\omega) = \sum_{k=0}^{N-1} x_k e^{-jkn\omega_s} \quad (4.6)$$

This theoretical interpretation of DFT can be implemented in many ways in code. Fourier transform represented in above equations are known as exponential Fourier transforms, the trigonometric series can also be used to compute the same spectrum. In this particular case *Compact Trigonometric Fourier Series* is used to represent the Fourier spectrum and is given as under:

$$a_n \cos n\omega_s t + b_n \sin n\omega_s t = C_n \cos (n\omega_s t + \theta_n) \quad (4.7)$$

Where a_n and b_n in above equation represent the real and imaginary parts of a frequency components. The magnitude and Phase spectrum for the above representation given below is used in the code:

$$C_n = \sqrt{a_n^2 + b_n^2} \quad (4.8)$$

$$\theta = \tan^{-1} \left(\frac{-b_n}{a_n} \right) \quad (4.9)$$

Phase spectrum is always given a secondary importance as magnitude spectrum provide enough information in terms of harmonics and amplitude, which changes with machine health.

4.6 Proposed System – Block Diagram

In the following, the block diagram of the purposed setup is presented to establish a better understanding of the design of the test bench and required instrumentation. The specific details will be discussed in the upcoming chapter. The work described in this chapter was required to proceed with the implementation of the instrumentation test bench, design of instrumentation and conditioning board, inputs and outputs for the system and intermediate blocks. Figure 4.4 shows the test bench setup in the right-most block.

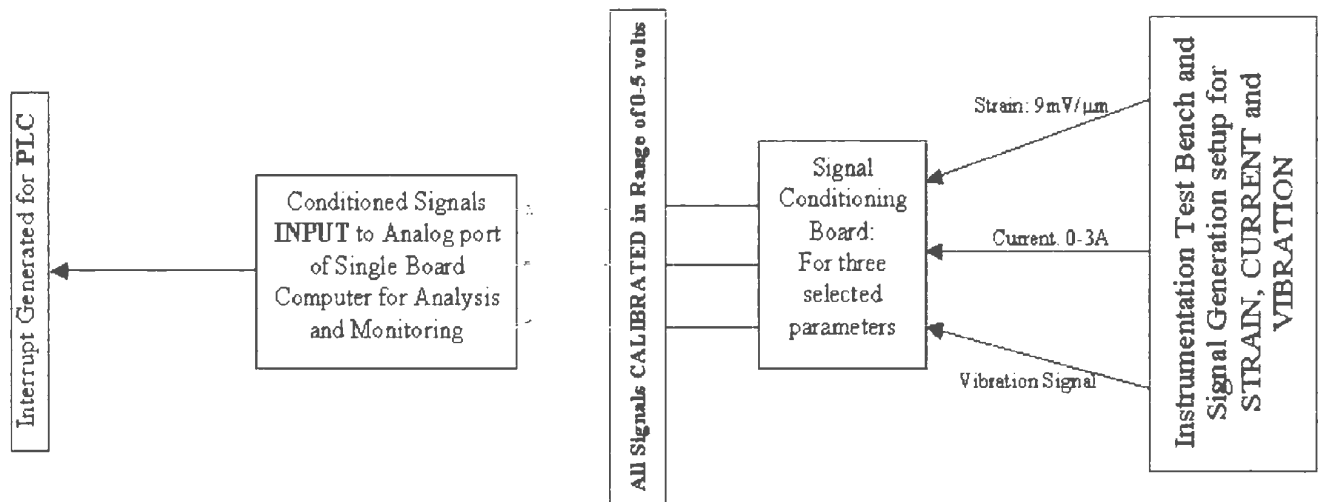


Figure 4.4 Block Diagram of Setup proposed for CM system

Three real time signals originate from that setup and are fed to the Instrumentation board where they are amplified and calibrated as per single board computer's requirements. Then those signals are fed to single board computer for monitoring. Finally an interrupt is generated, depending upon the condition of parameters, which are monitored by single board computer.

Chapter 5

Condition Monitoring System Implementation

5.1 Introduction

On the basis of the design of the condition monitoring system discussed in chapter 4, a condition monitoring (CM) system has been implemented for AOC-15/50. This chapter deals with all the intricate details involved in the implementation of the CM system with issues ranging from sensor selection, to the board layout and interface with the single board computer. This chapter also sheds light on the test bench setup developed for testing data acquisition and analysis routines from real-time signals. The later sections of this chapter discuss the monitoring routine, which is custom to this specific design along with calibration requirements for instrumentation board.

5.2 Sensors and Instrumentation Board Layout

It is clear from the discussion in chapter 4 that the monitoring of three parameters, namely strain, current and vibration is required. For monitoring a physical and

measurable parameter a proper sensor is required. A sensor is always selected keeping in mind its range of operation and the working environment. Sensors selected in this case were given similar considerations. The test bench will be tested in a lab environment, though for mounting the sensors on the wind turbine, the weather conditions are to be kept in mind. The important thing in this regard is the temperature range. All sensors have been selected with dynamic operation range. Each sensor is discussed with its make and specific characteristics.

5.2.1 Current Sensor

The ratings of the tip brakes, which are electro-magnetically controlled for deploying, are given by manufactures as 120V/5A. The power to each blade is supplied by a rotary transformer, which is mounted in between the gearbox and the hub. From the hub the power supply is integrated into each blade with a rectifier within each blade for the operation of the brake. The sensor required should be able to detect any surges or spikes in the power supply to the brakes. After careful research from different sources, the sensor manufactured by CUI INC, Oregon USA is selected. Catalog specification is named as SCD05PUN. The sensor is specified to operate for a 0-5A range. It requires 12-volt DC input and outputs an AC voltage corresponding to the supply current having a DC shift with a maximum voltage of 5-volts peak to peak on the rated current. The sensor will be mounted on the instrumentation board with independent power supply to provide constant 12-volts DC for its proper operation. Figure 5.1 shows the picture and pin configuration for the current sensor, which is directly adopted from the data sheet of the sensor. The sensor has a hysteresis specification of about $\pm 1.5\text{mV/C}$, which is to be

considered for extreme weather conditions. It is designed to withstand a 2000V surge in the measured AC voltage, with 50/60 Hz supply. Output voltage is $\pm 0.5\%$ linear at rated current. Proper signal conditioning instrumentation will be required before setting up the sensor for monitoring and analysis.

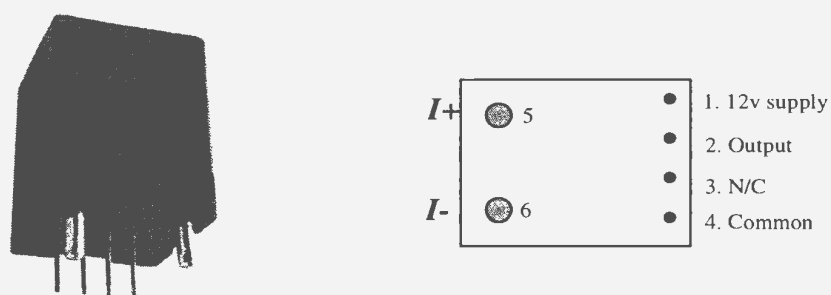


Figure 5.1 *Current Sensor SCD05PSN and Pin Configuration

5.2.2 Strain Sensor

Different types of strain sensors/gauges are available. A metal strain gauge is used in this case due to temperature conditions. Strain gauges are often used in a bridge configuration to provide higher gain using a dummy gauge, which is also used for providing temperature compensation. As discussed previously, this gauge changes its resistance with a change in the length of the material it is mounted on. The material has to be steel for this type of gauge. The Gauge Factor (GF) is 2.0 with resistance of 120 ohm. Figure 5.2 further illustrates the structure of the gauge. The gauge factor is discussed in the previous passage. GF is indicative of the physical properties of the metal with which it is made of and can be represented by the equation (5.2), which is used in previous chapter (section 4.4) in a different representation to calculate change in resistance per unit length.

* Sensor picture adopted from www.digikey.com

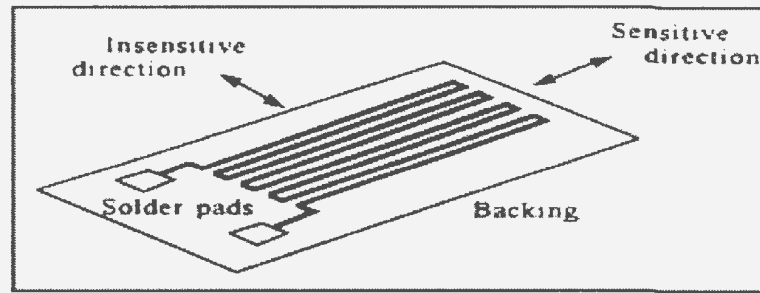


Figure 5.2 * A typical metal strain gauge

GF is given as the ratio of change in length per unit length to strain applied to the surface it is mounted on (Byers and Snyder 1969).

$$\mathbf{GF} = \frac{\Delta R}{R} \left(\frac{1}{\text{Strain}} \right) \quad (5.1)$$

5.2.3 Vibration Sensor

Vibration is usually monitored using a piezoelectric transducer. The piezoelectric effect of some crystals like quartz enables them to generate a faint electrical signal when the load is changed on them. This property is used to track the changing parameters like acceleration in rotating machinery. Besides this, they can also be used to keep track of velocity, linear displacement and vibration frequency. Certain features have to be taken in consideration before selecting the sensor. These are the measuring range, frequency range, accuracy, and ambient conditions. The measuring range differs for every measuring quantity, for example G's for acceleration, Hz for frequency, in/sec for linear velocity and length of linear displacement and proximity. The electrical output options

* Strain Gauge picture adopted from <http://zone.ni.com>

depend on the system being used with the vibration sensors. Usual analog outputs are current, voltage or frequency. Accuracy can vary in this process depending upon the system's sensitivity.

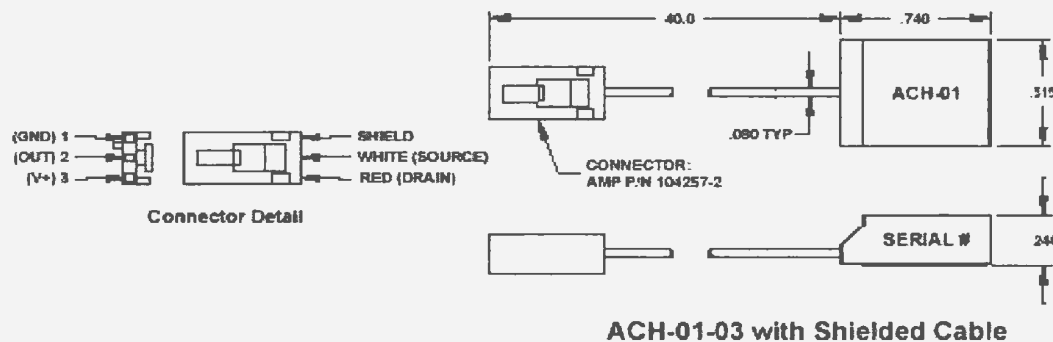


Figure 5.3 * ACH-01 diagrams adopted from product datasheet

A similar type of accelerometer is used here, which is manufactured by MEASUREMENT SPECIALIST and listed in the **Digikey** database. ACH-01 is a general-purpose acceleration transducer with impressive output characteristics. The datasheet of ACH-01 suggests that it is specifically designed for high volume applications which require the permanent installation of accelerometers, such as machine health monitoring, modal analysis, automotive sensors, appliances and feedback control systems. The typical features like lower frequency of 2 Hz to high frequency cutoff at 20 kHz with 0.1% linearity; 3 to 40 volts of DC voltage supply range; dynamic temperature range of -40 to 85°C and weighing only 8 grams, listed in datasheet makes ACH-01 an excellent candidate for this application. These parameters are only important for acquiring a

* Data sheet available on Digikey website www.digikey.com

vibration signal. The typical interface circuit for ACH-01 is provided in the datasheet, which is adopted in the implementation with some modifications. Figure 5.3 is adopted from the datasheet, which gives a better idea of dimensions, size and pin configuration of the device.

5.2.4 Instrumentation Board Layout

Once the sensors are selected, the interface circuits can be designed, implemented and then calibrated depending upon the requirements that will be specific to the analog channels of the single board computer. Details of all three circuits and individual components are discussed in the subsequent section. The preliminary layout of the custom design board is shown in Figure 5.4, which was developed as a part of this research.

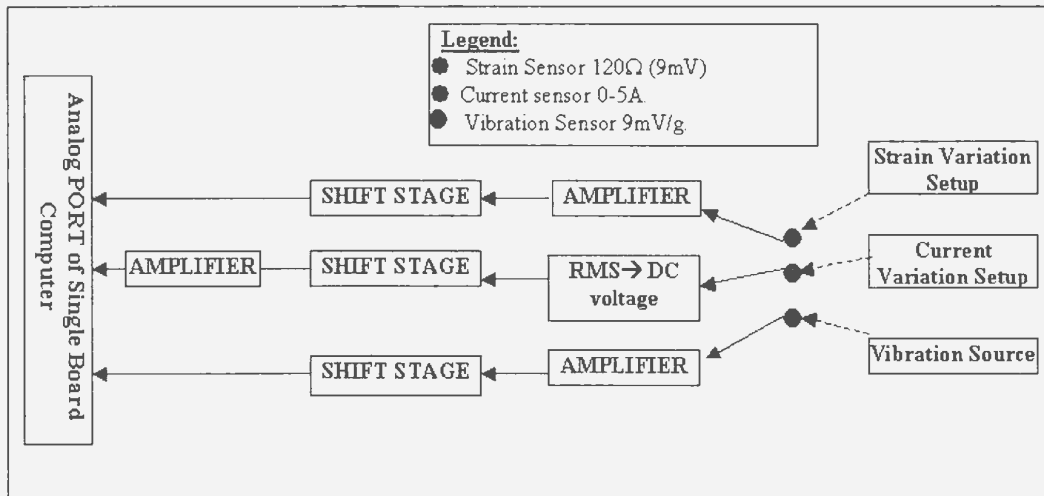


Figure 5.4 Instrumentation Board Layout

5.3 Single Board Computer

Single board computer (SBC) selected for this application is manufactured by JK-micro systems. The selection is made keeping in view the requirement of the system and its scope. This SBC has the Intel-186 architecture and is named as **Pico Flash**. It has a built-in 256K program-memory with extra slot for a 512 kByte RAM chip if required. The 40 MHz processor frequency and specified memory will enable the system to perform the monitoring task efficiently, keeping in mind the speed requirement for Fast Fourier Transform (FFT) computation. Two console ports are provided, one of which is used for programming. This board has a dynamic programming environment, which is very easy to use. It is designed to have a built-in DOS, with two drives A and B on it. Borland C++ compiler is provided to program and create **.exe** files for embedded applications, which do require a specific project setup in accordance with the board speed and memory specifications. The **.exe** file is then downloaded in SBC using the console port, interfaced with standalone PC or Laptop using the HyperTerminal software provided by Microsoft Windows. Pico Flash is a digital board with digital input and output capability. However expansion slots are available for a separate board by the same manufacturers for analog input. The expansion board is called **Pico I/O** and it is capable of 11 channels of 12-bit analog input, which makes it favorable to use for measuring physical parameters, as required in this research. The analog channels can only measure a range of voltage levels from **0** to **+5** volts, which is important to note as the calibration will be required for all interface circuits to give an output in the similar range. Voltage levels more than +5V can damage the inner circuitry of the board and will render it unfit for use. Therefore proper

handling is required to protect the board from getting damaged. The interrupt is generated using bit-01 of the digital port indicated by Light Emitting Diode (LED). Figure 5.5 shows the both the Pico Flash and the Pico I/O board mounted together.

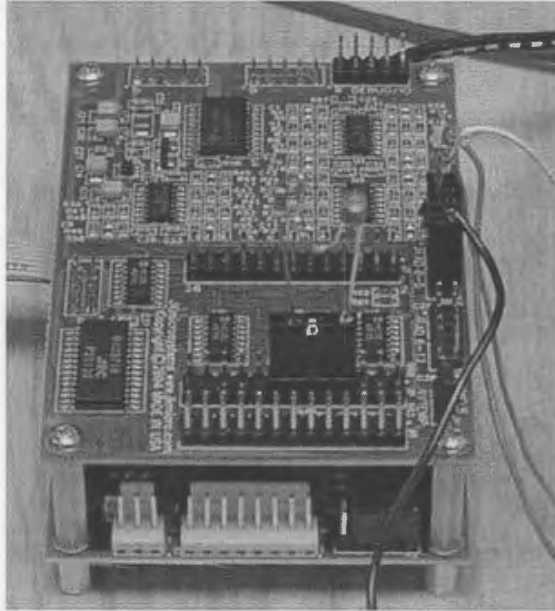


Figure 5.5 Pico Flash with Pico I/O and the interrupt LED

5.4 Test Bench Setup

Before moving forward with the instrumentation board implementation, it is required to build signal sources for three parameters. The setup is created in the lab with available resources. The strain setup was mentioned previously. Two strain gauges are mounted on a cantilever beam setup to provide the variation in the strain. A bolt is provided at the unsupported end of the beam to slowly apply the strain and record the observations, which will be used in calibration later on. Figure 5.6 shows the beam with bolt and strain gauges mounted on it.

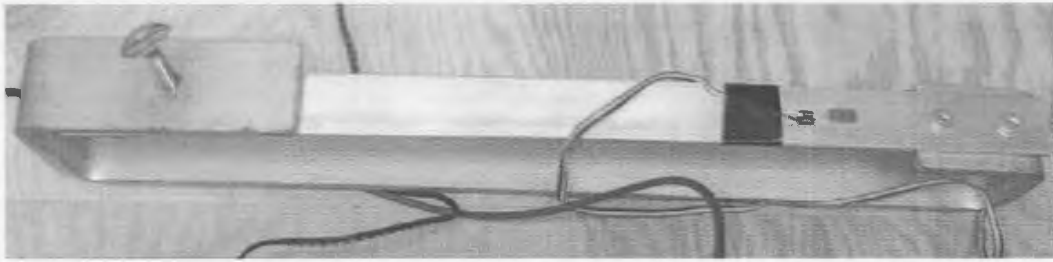


Figure 5.6 The strain variation setup

Current variation was provided by using a variable transformer with 0-120 volts in series with four 300-watt resistors in series. With the equation $P = I^2R$, the current through the resistors in series cannot exceed 6Amps, though for safety purposes 2.5 Amps current is used as a maximum input current. The variation setup is shown in Figure 5.7.

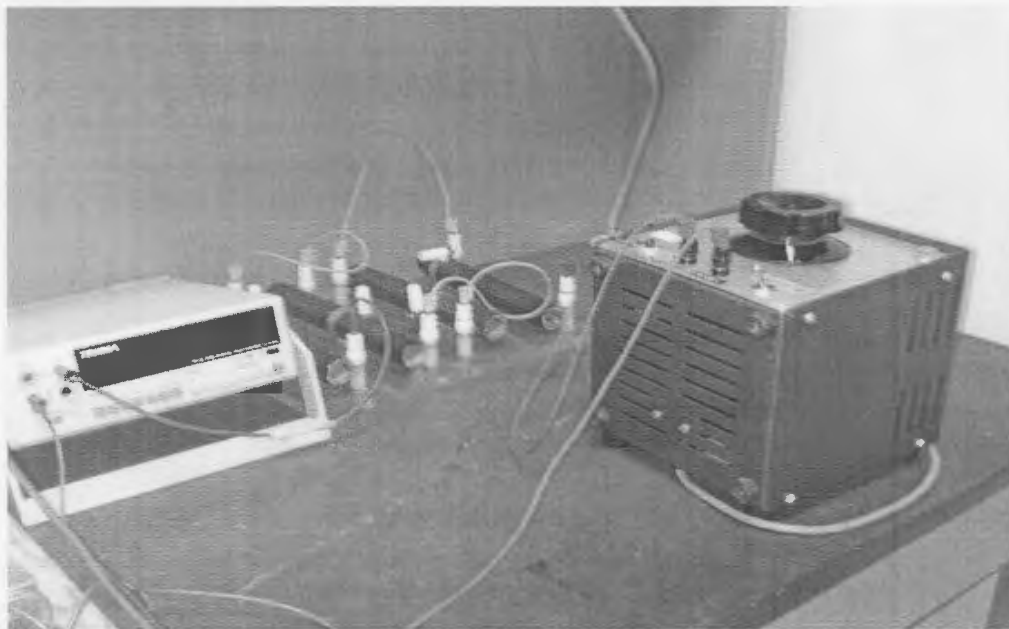


Figure 5.7 Current variation with ammeter used for safety purposes

For vibration signal generation a rather simple procedure is adopted to produce a signal, which can provide sufficient vibration for analysis. A three-volt DC motor with an

unbalanced shaft is used for that purpose. The motor setup and one of the vibration signal is presented in the following figures. The accelerometer is mounted on the motor with adhesive tape to provide sufficient contact with motor surface.

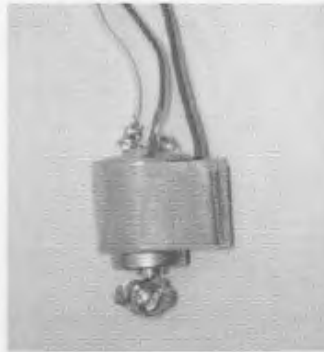


Figure 5.8 Motor with Accelerometer mounted on motor body

The result of motor vibrations for an input voltage of 1.77 volts is shown in Figure 5.9.

Results for different vibration levels are provided in Appendix 2.

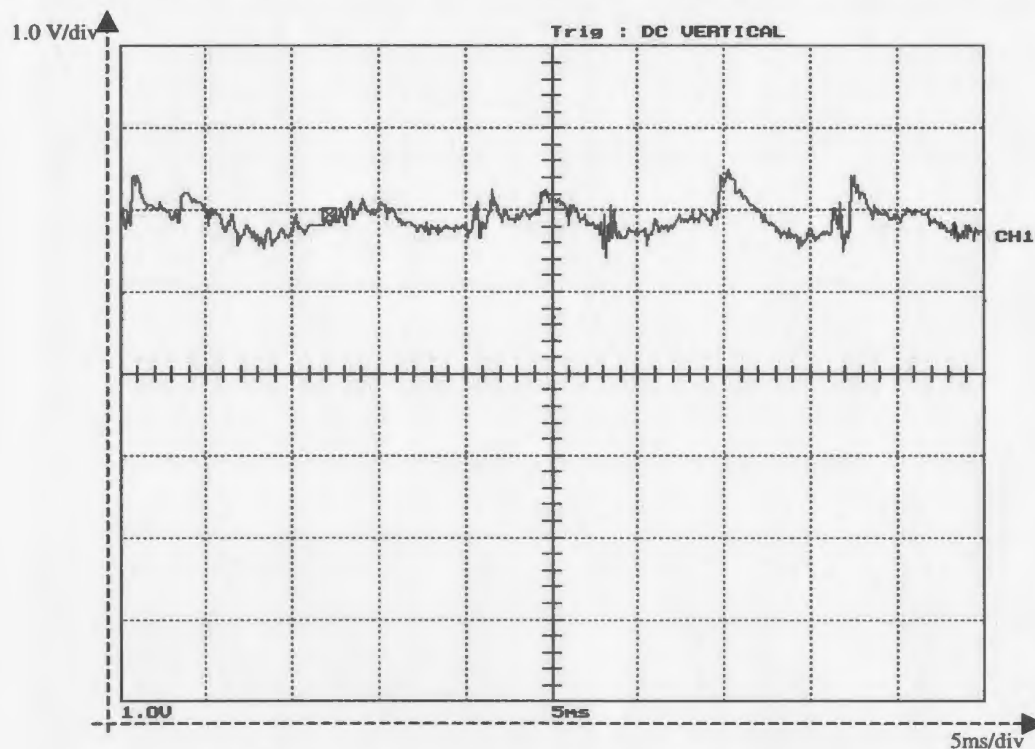


Figure 5.9 Vibration signature at 1.77 volts

5.5 Signal Conditioning

The ranges for analog inputs for SBC are discussed in the preceding sections. All the instrumentation circuitry should be able to bring the detectable signal within the range of 0 to +5 volts. For protection purposes this range will not be utilized to its fullest and all the signals will be restricted to a + 4.7 volts level by using Zener diodes. The conditioning circuits are implemented in conjunction with the principles and rules of analog electronics mentioned in electronics literature, Sedra & Smith (1998) and Byers & Snyder (1969) can be consulted for any relevant details. The detail description of the circuit is mentioned in the following subsections.

5.4.1 Strain Instrumentation Circuit

The strain gauges are to be mounted on a cantilever beam, which have an ability to bend. A specific adhesive is provided with the strain gauges to provide a compact surface contact. Gauges are soldered with soft copper wire, which are then carried to the board to be connected to the bridge. Since it is a half bridge two strain gauges are used. In a bridge for providing null offset, generally a variable resistor of the similar value is used in place of the third resistor. A variable resistor of 100 ohm is used in this case to provide DC-offset calibration necessary for the output conditions put forth by the single board computer (0-5 volts). The calibration will be discussed in the next section. Figure 5.6 illustrates the circuit diagram of the implemented circuit. General-purpose instrumentation amplifier INA-128 is used, which is a preferred device for the bridge circuit amplification. The dual power supply of ± 15 volts is supplied to the setup.

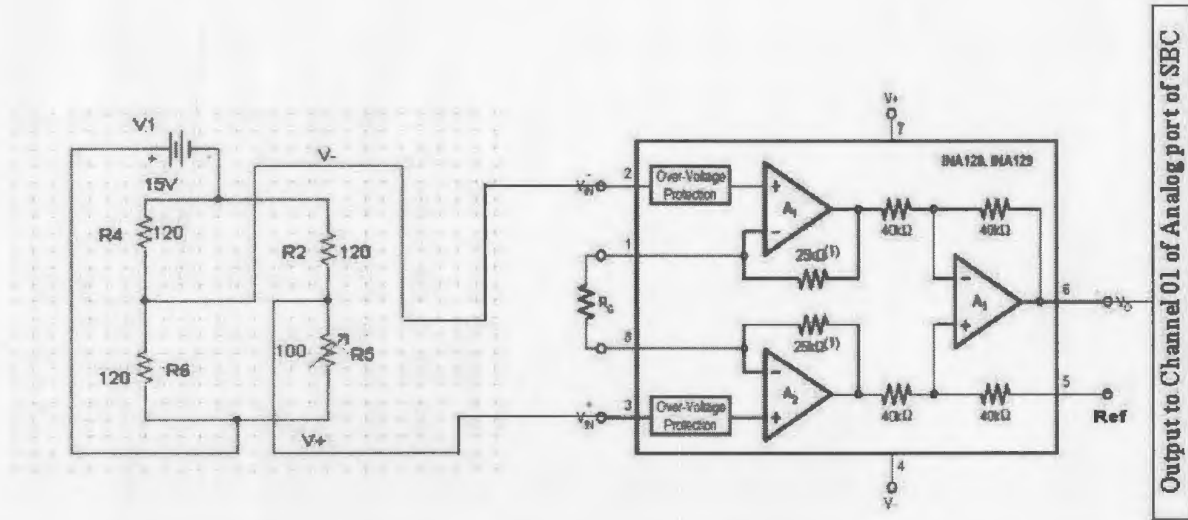


Figure 5.10 Strain Instrumentation circuit- in the center INA-128 is visible

The gain of INA-128 is controlled by R_G visible outside the amplifier box in the middle of figure 5.10. R_G is selected depending upon the gain requirements for the circuit. The equation (5.2) is adopted from the datasheet however the details on instrumentation amplifier application and uses are provided in Sedra & Smith (1998).

$$\text{Gain} = 1 + \frac{50k\Omega}{R_G} \quad (5.2)$$

To keep the gain under the prescribed range (0-5 volts DC) R_G is selected as 48K Ω by giving a gain of $\cong 2$. The output of circuit in figure 5.6 is send to SBC analog channel 01.

5.4.2 Current Instrumentation Circuit

As compared to strain, current instrumentation and interface is more complicated. More number of intermediate signal-stages make the implementation hard to handle. Current

sensor operates on a 12volts DC input (max). All other circuitry is capable of operating at ± 15 volts as mentioned earlier. A separate arrangement is required to step down the power supply to 12 volts by using a *National Semiconductor's* voltage regulator LM7812. The current ranging from 0-2.5 A is supplied from the current variation setup discussed in test bench setup. For 0 Amp current the output of the sensor is a 2.5VDC. As the current is increased the output exhibits an AC voltage having a 2.5 volts offset corresponding to supplied AC current as specified in the product data sheet. The output voltage will increase to 5 volts peak to peak for maximum of 5A current. This output is not measurable by the SBC being an AC voltage; an RMS to DC converter (AD636) is used to convert the AC voltage from the current sensor to a DC voltage. After configuring AD-636 as specified in the datasheet, the output of AD-636 is 11.5 volts DC for 0 Amp current, the output increases to 12.2 volts DC for a 2.5A current. The next step comprises of two tasks: first to bring the voltage down to specified range of 0 to +5 volts in order for it to be read by SBC analog port, secondly that the 0.7 volts resolution for the supply current range is needed to be amplified for monitoring in an effective way.

A shift stage is used to bring the 11.5 volts at 0 amp current to zero volts. The circuit is provided with all details in Figure 5.11. An inverting amplifier with unity gain and offset voltage at non-inverting terminal provides the output voltage range from 0.0 to -0.76 volts DC. This voltage is then fed to another inverting amplifier with a gain of 4.7 for achieving the required voltage range to be read by SBC analog channel 0.

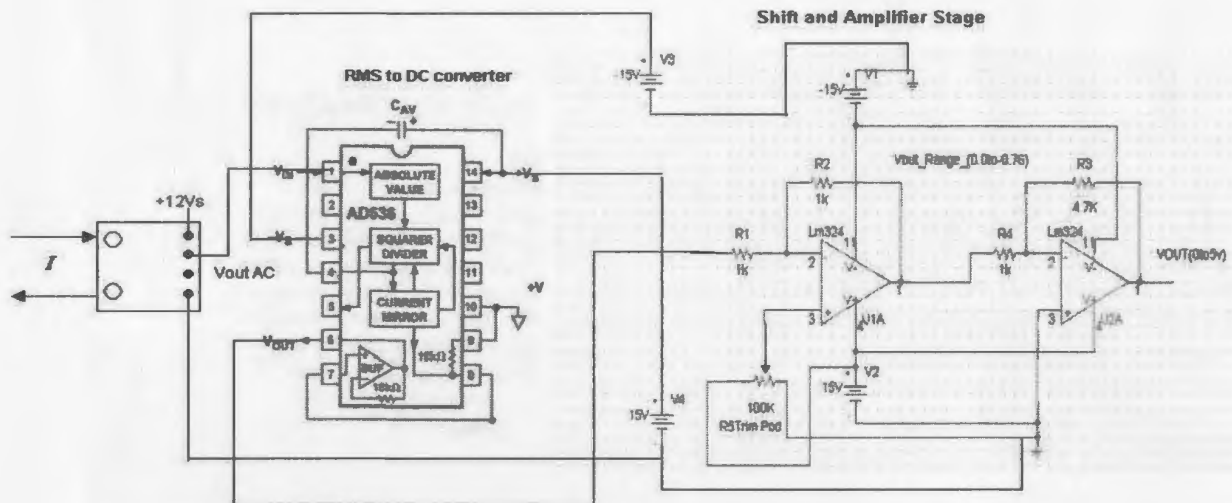


Figure 5.11 Current sensor with AD636 and amplifier and shift stage

5.4.3 Vibration Sensor instrumentation

The datasheet of accelerometer ACH-01 provides a typical interface circuit to retrieve the signal. The circuit consists of a high frequency filter, operating at ± 15 volts DC. After connecting the output of transducer from the test bench setup to oscilloscope, the vibration signal was available centered at 0-volt. The signal was required to be shifted to a positive offset so that the negative half of the AC signal can also be sampled by the SBC. A shift stage is used to offset the signal to +2.14 volt level to provide maximum peak to peak resolution. This offset is set back to zero when the signal is sampled for the FFT computation. Figure 5.12 gives the illustration of the interface circuit with shift stage.

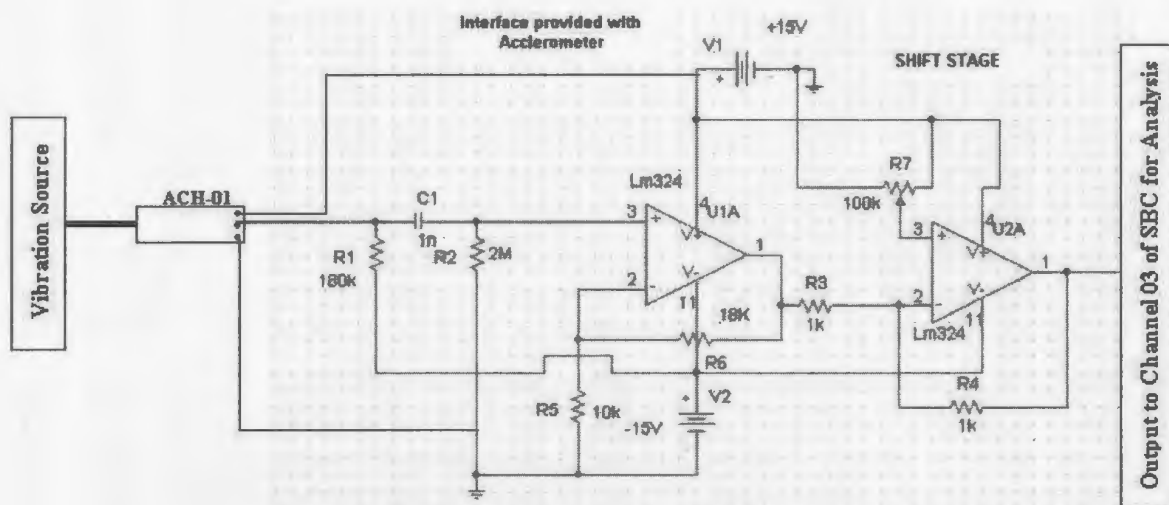


Figure 5.12 Vibration interface circuit for ACH-01 with Shift stage

After the implementation of above-mentioned circuits the instrumentation board was developed, which is shown in Figure 5.13.

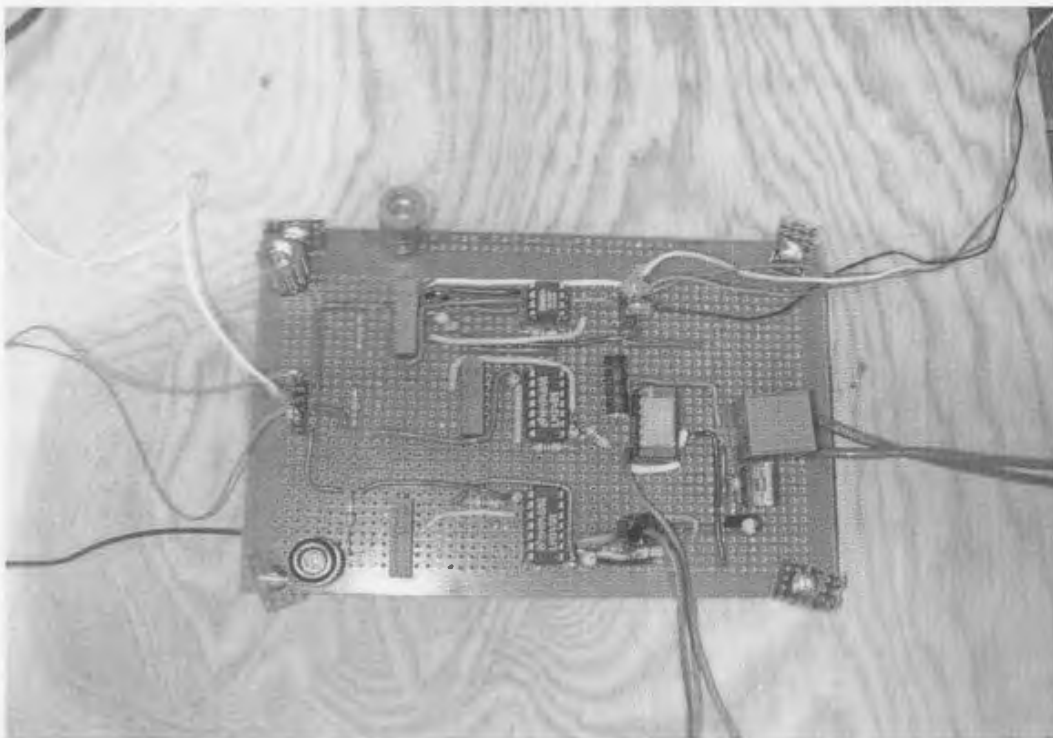


Figure 5.13 Instrumentation Board

5.6 Signal Calibration

Signal calibration is required for the monitoring algorithm. After designing and building the circuit, the most important task is to interpret the system. The input values have to be known before interpretation of the data set and analysis. The values of current are determined by configuring an ampere meter in series with the current variation setup. The input from the bridge circuit for strain measurements is determined by using the voltmeter between pin 2 and 3 for the instrumentation amplifier (INA-128). The corresponding output can be observed on the oscilloscope. The point to be noted is that the bending on the beam has to be applied in one direction for calibration purposes. Once a relation between the input and output is established, the strain in both directions of the bend can be manipulated in the routine. In the following the calibration equations and graphs are presented which are obtained from the data sets presented in Appendix 3. For current calibration, the data was recorded as input to sensor using ampere meter. It was plotted as input current to the sensor versus the output DC voltage. However, when plotting the data, the input current is plotted on y-axis as a function of output voltage. The graph is presented along with the equation in Figure 5.14. This graph is plotted using MATLAB and equation is obtained using the curve-fitting tool. The 5th order equation fits the best to the curve presented by the data set, which signifies that it is a non-linear plot. Some discrepancies in the plot can be seen where it does not fit properly and are adjusted in the monitoring routine implementation.

$$Y (\text{current}) = 0.112 x^5 - 1.656 x^4 + 9.432 x^3 - 25.72 x^2 + 34.05 x - 16.28 \quad (5.3)$$

x = output voltage from current circuit

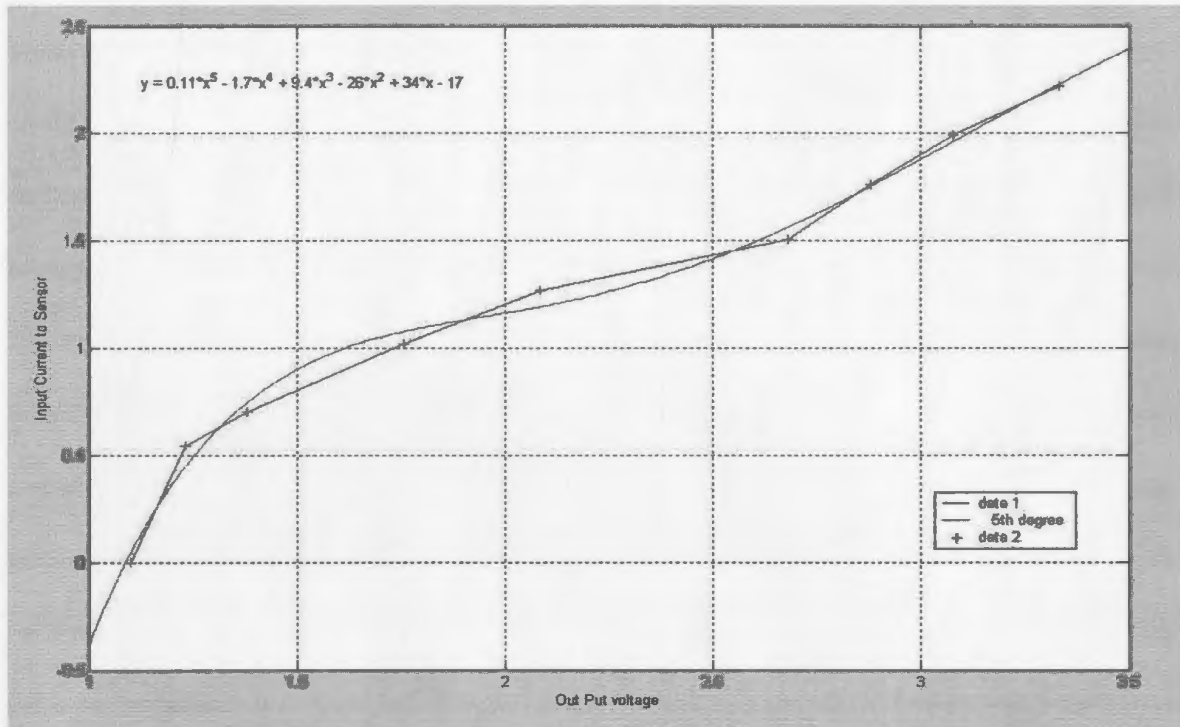


Figure 5.14 Current calibration graph Curve fitting using MATLAB from dataset

The calibration of strain is done in a similar way. The input from the bridge is measured against the output of the interface circuit. The circuit is calibrated to give an output voltage of 1.7 volts for an inherent change in resistance of 9 mili-ohm as suggested by CM design in chapter 4 (equation 4.2). Since the task is to determine the amount of strain, the strain is plotted as a function of the output voltage sensed from the interface circuit. Plotting the data points in MATLAB and fitting the curve using the curve-fitting tool determined the calibration equation provided in the following:

$$Y (\text{strain}) = 0.0064 x'^3 - 0.052 x'^2 + 0.14 x' - 0.11 \quad (5.4)$$

x' = output voltage form strain circuit

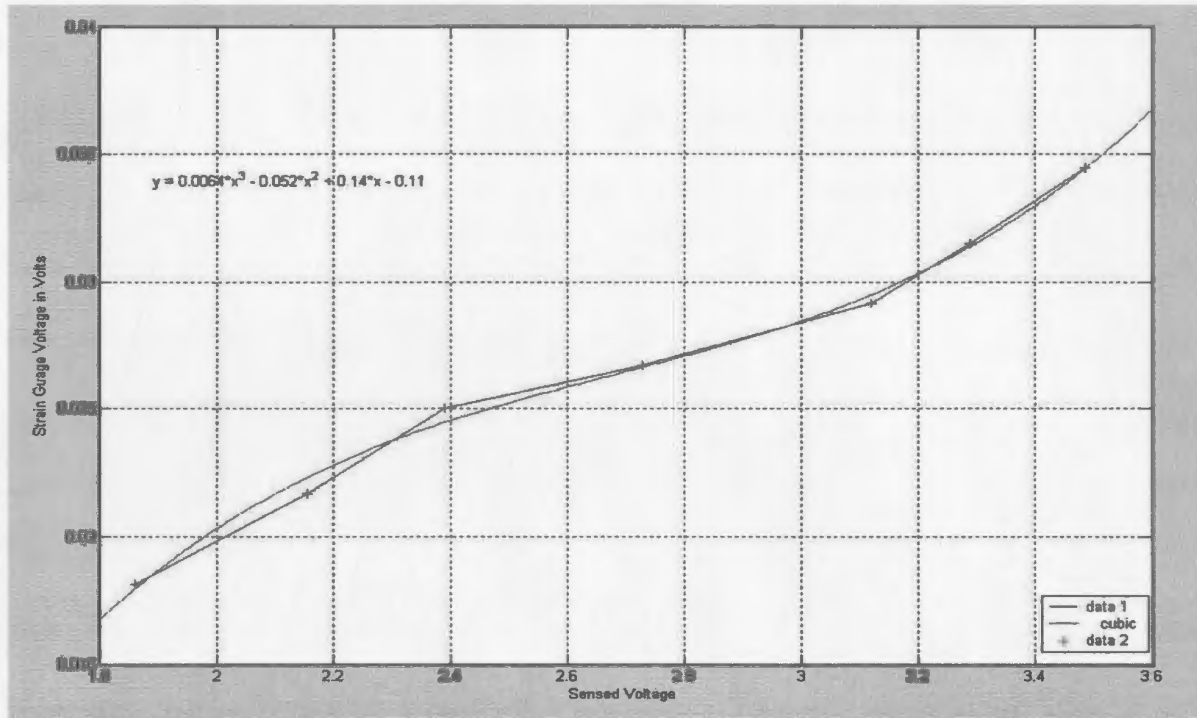


Figure 5.15 Strain calibration graph and Curve fitting using MATLAB from data set

The graph signifies a 3rd order equation. The strain gauge is usually a linear device; however, the shift and amplifying stages have made the circuit nonlinear, which is depicted in the graph in Figure 5.15.

The calibration required for vibration signal is the DC-offset required to interpret the full AC signal. The signal is offset by 2.1 volts and is offset back in the monitoring routine for FFT computation. The monitoring routine and FFT algorithm are discussed in the next section.

5.7 Monitoring Scheme and Results

After calibrating the circuits using data set plots and fitting curves, the last task left is to sample the voltages using analog channels of SBC for analysis and monitoring. The Pico Flash SBC comes with Borland C++ compiler for embedded application as discussed previously in section 5.3. A monitoring routine has to be designed in order to monitor all three parameters. Separate analog channels are selected for signal inputs listed as under:

- Channel 00 – Current samples
- Channel 01 – Strain samples
- Channel 02 – Vibration samples

Time-efficient scheme has to be devised so that if a fault occurs the condition monitoring system should be able to identify the fault and shut the system down by sending an interrupt to the system's main PLC. A flow chart for the scheme designed for monitoring is shown in figure 5.16.

The sampling and analysis for current and strain are not time consuming and are done without any delay, but the FFT computation is of concern. FFT computation if done using complex mathematics would require N^2 complex multiplication and $N(N-1)$ additions using equation 4.6 (Oppenheim Schafer and Buck 1999). The total time required for computation of 256 frequency harmonics is more than one minute for one iteration. Moreover, this processor does not fulfill the computational capability required to compute complex multiplications.

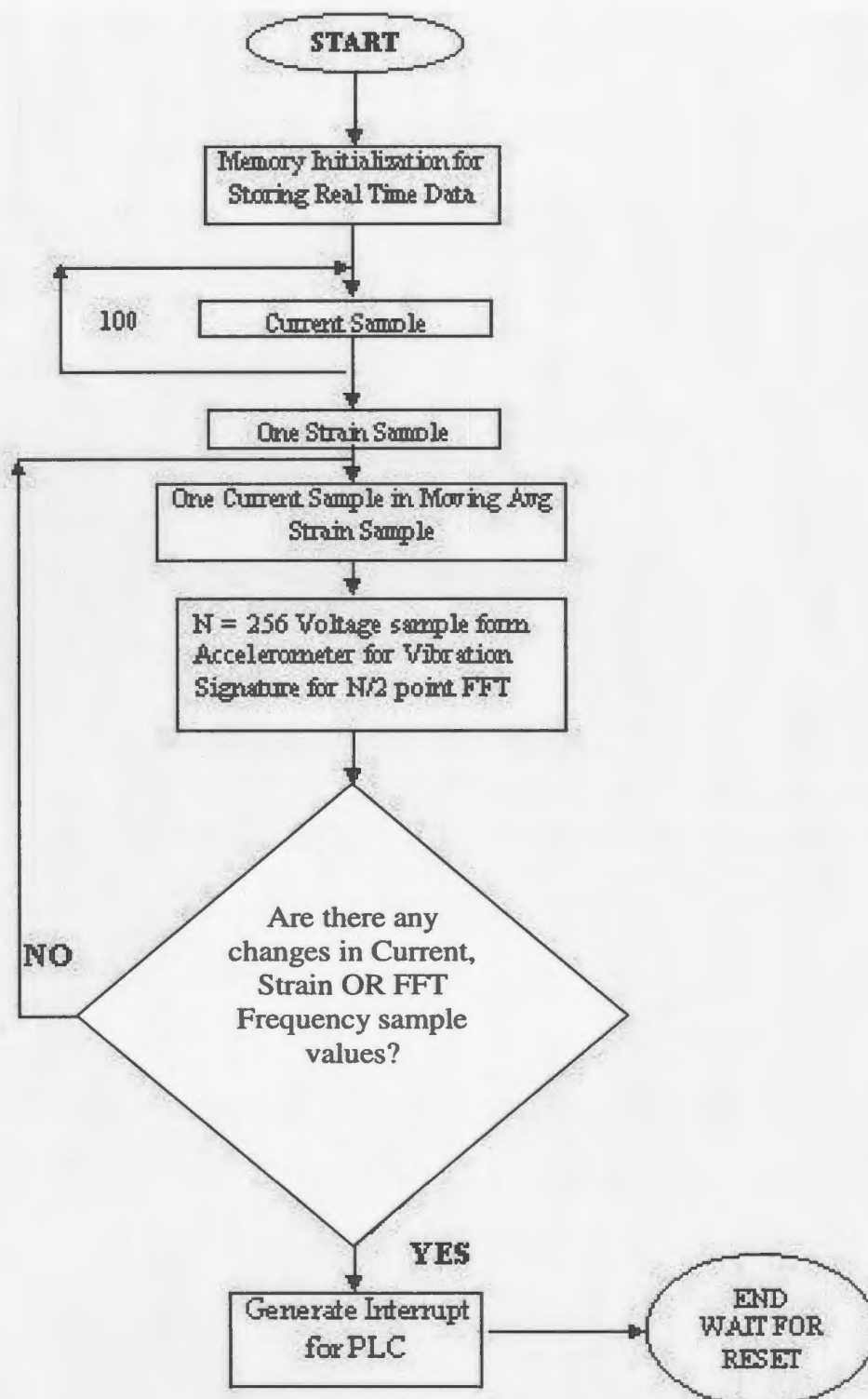


Figure 5.16 CM Routine- The Flow chart representation

A smarter and more efficient routine is required to do the required task. In the following the methodology adopted is discussed in detail.

5.7.1 Smart FFT Computation routine – Decimation in Time Algorithm

A number of smart FFT routines are available in the literature to compute Discrete Fourier Transform (DFT) of a signal. The decimation in time algorithm which is commonly known as butterfly algorithm is adopted due to its efficiency in time as well as in memory usage. The explanation and understanding of this algorithm is provided in any standard Digital Signal Processing (DSP) book however the implementation differs when it comes to embedded applications. Explanation here is based upon the work of (Oppenheim, Schaffer & Buck 1999).

Decimation in time works on the principle of decomposition of sequence of time samples $x[n]$ into successively smaller subsequences. The number of subdivisions depends on the length sequence. For convenience, the number of samples taken for this process are powers of 2. So samples can be $2^8, 2^{10}$ corresponding to the N-points of FFT. Since N will always be an even integer, $X[n]$ will be computed by separating samples sequence $x[n]$ into two $N/2$ -point sequences consisting of even numbered and odd numbered samples of the original sequence. If equation (4.6) is considered here once again with $n\omega = k$

$$X[k] = \sum_{n=0}^{N-1} x[n] e^{-jkn\frac{2\pi}{N}} \quad (5.5)$$

If W is defined as; $e^{\frac{2\pi j}{N}}$ then the above equation can be rewritten for $k = 0, 1 \dots N-1$ as

$$X[k] = \sum_{n=0}^{N-1} x[n] W_N^{nk} \quad (5.6)$$

If this sequence of samples is subdivided in two sequence of even and odd samples, denoted $n = 2r$ for even and $n=2r+1$ for odd, the following expression can be considered:

$$\begin{aligned} X[k] &= \sum_{r=0}^{N/2-1} x[2r] W_N^{2rk} + \sum_{r=0}^{N/2-1} x[2r+1] W_N^{(2r+1)k} \\ &= \sum_{r=0}^{N/2-1} x[2r] (W_N^2)^{rk} + W_N^k \sum_{r=0}^{N/2-1} x[2r+1] (W_N^2)^{rk} \end{aligned} \quad (5.7)$$

Now $W_N^2 = W_{N/2}$ (Oppenheim Schafer & Buck, 1999)

Equation (5.7) can be rewritten as under;

$$X[k] = \sum_{r=0}^{N/2-1} x[2r] W_{N/2}^{rk} + W_N^k \sum_{r=0}^{N/2-1} x[2r+1] W_{N/2}^{rk} \quad (5.8)$$

This can be rewritten with $G[k]$ and $H[k]$ as under:

$$X[k] = G[k] + W_N^k H[k] \quad k = 0, 1 \dots N-1$$

Every sum in equation (5.8) is known as $N/2$ point DFT, the first sum being the DFT of the even numbered samples and second will be the DFT of odd numbered samples of the original sequence. Despite the range of 'k' mentioned above, each sum is computed only $(\frac{N}{2})-1$ times, since $G[k]$ and $H[k]$ are each periodic in k with period of $N/2$. This tells us that the useful portion of magnitude spectrum will be in the first $(N/2)-1$ frequency points only. For a complete period $(-\pi$ to $\pi)$ the two sequences are combined together as mentioned in equation (5.8) to yield N -point DFT $X[k]$. But this process of sub-division does not stop here. Equation (5.8) illustrates the process of decomposition of original

sequence into two sequences of length $N/2$. Now if $N/2$ is even, which it will be as N is as N is a power of 2, then each $N/2$ DFT in equation (5.8) can be computed by subdividing each $N/2$ sequence into further 2 sequences and hence computing an $N/4$ point DFT which will then yield a $N/2$ DFT. This derivation is provided in Appendix 4. The example of 8-point DFT computation for an assumed data sample as considered in Oppenheim, Schafer and Buck (1999) is shown in Figure 5.17 (b). The complete computation can be reduced to a computation of 2-point DFT as shown in figure 5.17 (a).

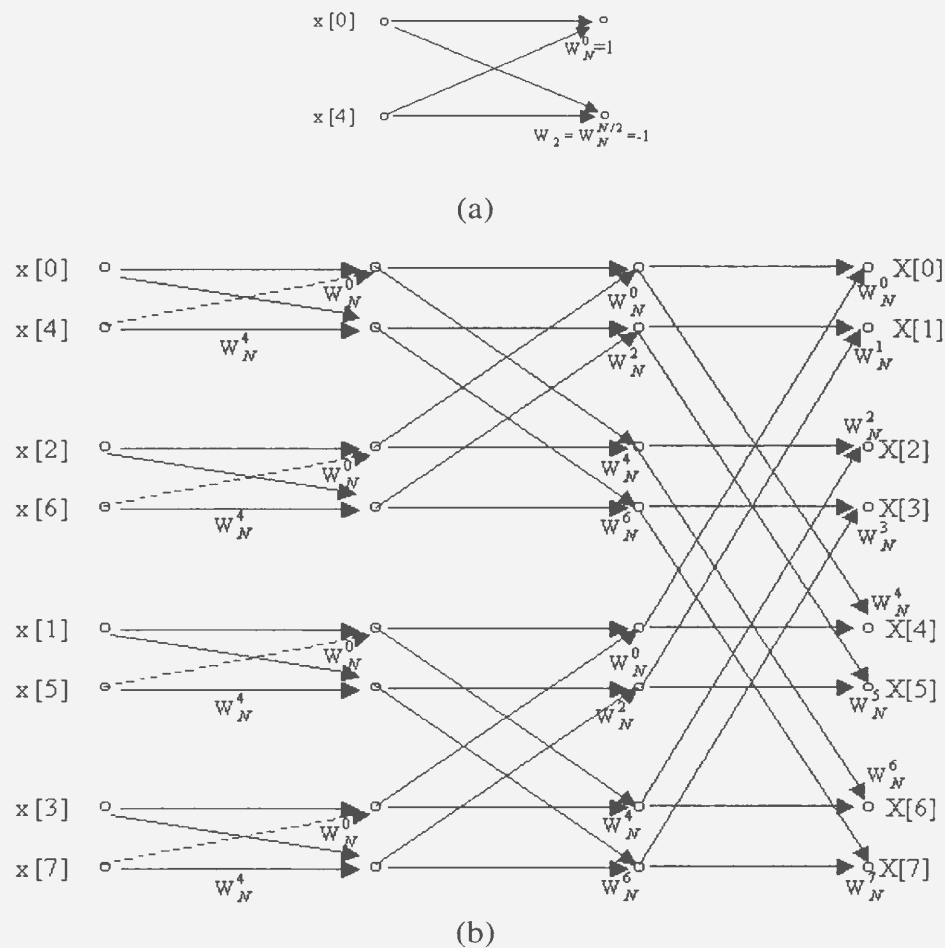


Figure 5.17 (a) 2-point DFT Flow Graph (b) Flow of complete Decimation in Time of an 8-point DFT computation

An interesting by product of this routine as mentioned in Oppenheim, Schafer and Buck (1999) is the storage and sorting of the data. It can be seen from figure 5.17(b) that in order for FFT coefficients to be computed the data have to be sorted in bit reversed order. Taking a closer look at Figure 5.17 (a) if $x[0]$ and $x[4]$ are said to be $x[p]$ and $x[q]$ at a given computation stage $m-1$, then the computation of $X[p]$ and $X[q]$ at stage m will only require $x[p]$ and $x[q]$. Thus only one complex array of N storage registers is physically needed to implement the complete computation. This kind of computation scheme is referred to as an in-place computation (Oppenheim, Schafer and buck, 1999).

This in-place computation is implemented by Danielson & Lanczos and is mentioned by Press et. al. (1992). The routine is adopted from this source, which is provided as a subroutine in the code presented in Appendix 1. However the sample storage has to be implemented before passing out the real samples to the routine with in the code. Routine takes as input an array twice the length of the real sample array length and requires that the real data be mapped at even numbers (0,2, ... N) with N being a power of 2. The odd numbered array elements are filled by floating 0.0 as complex component of real samples. This is done keeping in view that when the routine will return the frequency components, they will be arranged in the similar order. The F_0 will be stored in $data[0]$ and $data[1]$ which will be the average of the magnitude value of positive part of spectrum (0- π). The negative portion of the spectrum will be stored in increasing magnitude with real parts of the first harmonics in $data[2N-3]$ and $data[2N-2]$. The point to be noted that $data[N+3]$ and $[N+4]$ will be containing the real and imaginary parts of one aliased point in the spectrum. The complete mapping includes the mapping of real data array of length

N on an array of length, double the size (2N). After FFT computation the resultant array of real and imaginary components of frequency (2N) is mapped on the input sample array of length 2N and the magnitude of frequency components are computed using equation (4.8) and are mapped on another array of length N using real and imaginary frequency components. This mapping is done on all iterations of routine for new samples and is shown in Figure 5.18.

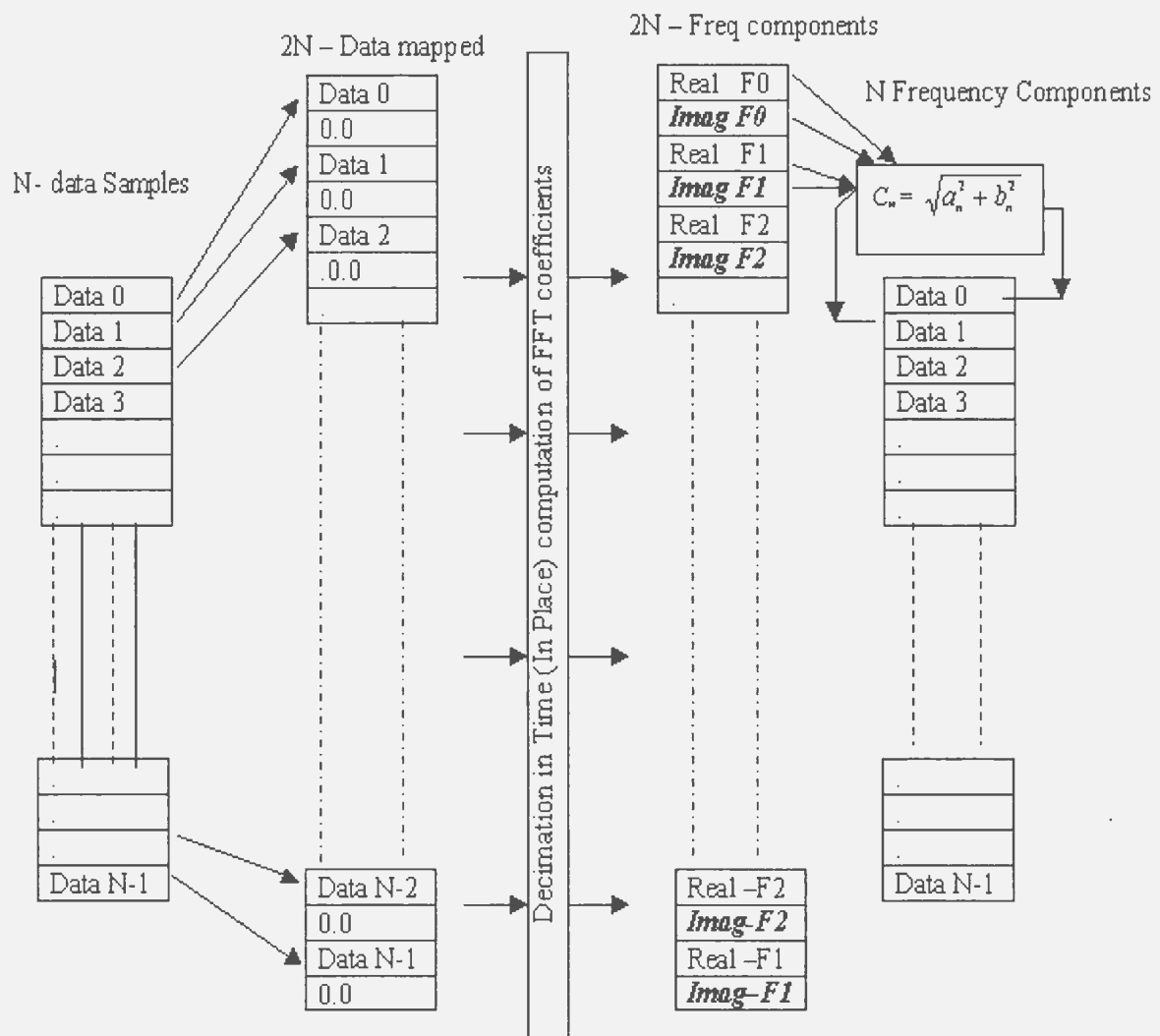


Figure 5.18 Mapping process implemented in the computation of Frequency coefficients

5.7.2 Results of FFT computation and Frequency Spectrum

The results and the look of the output screen are presented in Appendix 5. However the first 20 harmonics are plotted for 5 different samples of data for 4 different speeds of motor giving different levels of vibration in Figure 5.19.

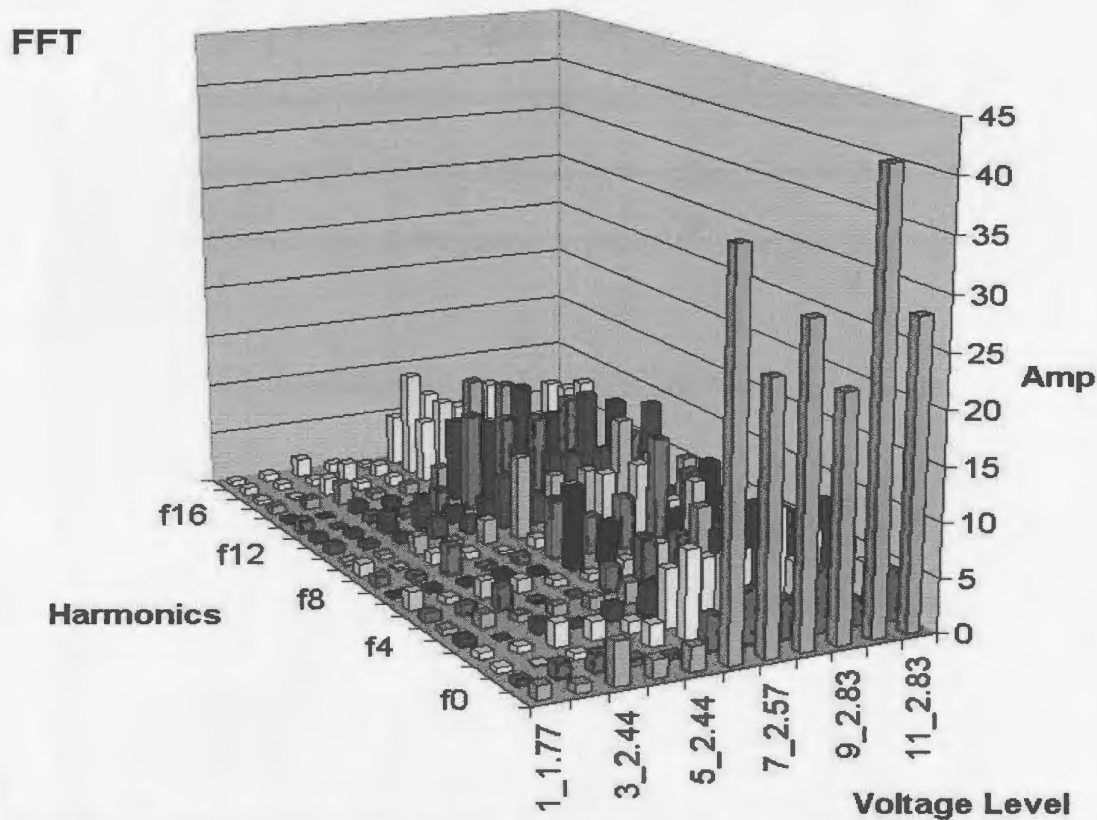


Figure 5.19 FFT Spectrum for 20 Harmonics for five iterations at different vibration levels

The resolution of FFT spectrum can be obtained by observing and finding out the sampling rate of the data. The sampling rate for the adopted strategy was determined by a

series of observations and is 9.58 ms, with $\omega_s = \frac{2\pi}{NT}$ giving the first harmonic F_1 at 2.5

Hz and rest at similar intervals. The sequence continues as under:

$X(n\omega_s)$ for $n = 0, 1 \dots N-1$

$n=1; F_1=2.5 \text{ Hz}$

$n=2; F_2 = 2(2.5) = 5\text{Hz}$

$n=3; F_3 = 2(2.5) = 7.5\text{Hz}$

Keeping in view the Nyquist criteria we have sampling frequency of 104.38 Hz that will give us the useful range for signal reconstruction up to 50Hz only. The reason for selecting this frequency is to confirm the accuracy of the current methodology and routine. The normal working conditions of the motor will give the vibration levels of a known limit. This limit is put as a check in the routine. Here, only F_0 , which is computed in Data 0 after using equation (4.8), is considered for comparison purposes. The value is F_0 contains the average value of magnitude of all frequency harmonics in the spectrum and changes with change in vibration level. However later on specific harmonics can also be specified that would represent the frequency related to a specific rotating parts.

5.8 Summary

The chapter has discussed in detail the design, implementation and results of the implementation of condition monitoring system. The development of the instrumentation board was the most important step in this process, design details for which are mentioned in this and previous chapter. The Single Board Computer has provided with a good computational capability for FFT. The typical outputs observed on the hyper-terminal connection with SBC are shown in Appendix 5.

Chapter 6

Conclusions and Recommendations

6.1 Introduction

After presenting the details of the research in previous chapters, this chapter will summarize the major conclusions arrived through this study. This chapter also lists the recommendations and future scope of study with regards to reliability analysis and condition monitoring. It appears that room of improvement is there with regards to condition monitoring system. The suggested condition monitoring system will need certain refinements as outlined in the subsequent sections.

6.2 Conclusion of Research

This research was comprised of set of objectives for reliability and condition monitoring, the conclusions are given accordingly:

- The reliability analysis of AOC-15/50 provides the results similar to those predicted by other researchers for different wind turbine systems. Analysis has

shown that wind turbine systems are prone to failure due to unpredictable environmental load.

- The life of wind turbine components will depend upon the environmental conditions and operational load, a reduction in component life is observed if the wind turbine is located in a harsh environment such as Newfoundland and Labrador.
- The unavailability of failure data related to wind engineering systems is a serious concern. This compels to adopt data from other sources, which introduce uncertainty in results. Therefore it is important to develop public access database for wind engineering data.
- Based on available data, Yaw bearing and Tip Breaks came forth as the vulnerable components for AOC-15/50. The Markov and Fault tree analysis also showed a less than 50% availability of the system.
- Twice a-year maintenance can improve the overall reliability of the system in spite of once per year as conducted by the manufacturer now.
- The condition-monitoring system is designed for AOC-15/50 considering the results of reliability analysis performed. It is probable that change in reliability (or failure) data may lead to a different design of condition monitoring system.
- The monitoring to three parameters namely strain, current and vibration is suggested in the condition monitoring system design and is implemented and tested in lab.

- The strain and current sensors have performed excellent on the test-bench setup. The performance may differ with varying condition of temperature when mounted on AOC-15/50.
- The current sensor exhibits voltage drift. It is due to two reasons: it is a Hall effect sensor, which is characterized by a voltage drift, secondly the load resistors are temperature sensitive, which continuously affect the conductivity resulting in frequent changes in current readings.
- Sensor for vibration monitoring and analysis works fine, however the speed of processor may become a concern if a larger number of samples are required.
- The Single Board Computer (SBC) is capable to handle more sophisticated situation such as more number of parameters and computations.

6.3 Recommendations for improvement

Following recommendations are suggested to improve the system reliability and condition monitoring system: -

- Precise wind turbine reliability parts data is required for reliable results of analysis. The data and results from previous studies should be published in public domain.
- For reliability analysis the subdivision of system into different components was limited to basic components in this research. However if failure data is available for all different components with in a designated component, the results can be more accurate.

- Condition monitoring systems needed to be tested in field before mounting on AOC-15/50.
- The condition monitoring system proposed can be expanded to communicate via TCP/IP with the capabilities of SBC. This provides an opportunity for a central monitoring setup using LAN or wireless network connections using the same single board computer enabling remoter access.
- An improved current sensor can alleviate the problem of voltage drift and hence elevate the sensing capability for current.
- Four simultaneous mounting setups are required for strain monitoring with 90-degree angles around the ball bearing ring. It is recommended that it should be carried out at the manufacturing time of AOC-15/50.
- Vibration analysis and monitoring is performed by comparing the average value of spectrum magnitude. However if it is required to specify a frequency component with every rotating part. A different manipulation strategy will be required to accomplish this.
- An anti-aliasing analog pre-filter of the value of $\text{sampling frequency}/2$ is required in order to provide accurate sampling with no aliasing. Currently a low pass filter of 10k Hz is used in the interface of ACH-01 which is the specified maximum operating frequency of accelerometer.
- The range and resolution have to be kept in mind with regards to FFT computation. A smaller sampling time will lead to a larger frequency capture range, however the resolution, which pertain to the first frequency component and then the successive values of components will increase. This may cause to lose

the frequency information of the intermediate components. As an example in present case the frequency information for 2.5Hz and onward is available with a difference of 2.5 Hz between each harmonic. If the magnitude information for the 4Hz component is needed, a different sampling rate will be required and hence will change range of spectrum. For this reason more then one sampling setup may be required for sampling at different sampling time for different frequency component.

- Keeping in view a compelling requirement to manipulate a complete frequency spectrum up to 1 kHz, a high-speed Single Board Computer with a similar Intel architecture, programming and LAN capabilities is required. Better computational capabilities will enhance system performance considerably.

References

- American Society of Civil Engineering [ASCE] (1991). Guidelines for Electrical and Transmission Line Structural Loading. *ASME Manuals and Reports on Engineering Practices No.74. Published by ASME. NY*
- Rademakers, L.W.M.M, Verbruggen, T.W and Braam, H. (2004). Condition Monitoring for Lowering Maintenance costs of Offshore Wind Turbines. *Proceedings of International Conference on Noise and Vibration Engineering. Belgium. pp 3943-3952.*
- Billinton, R. and Karki, R. (2001). Maintaining supply reliability of Small isolated power systems using Renewable Energy. *IEE proceedings on Generation, Transmission and Distribution. Vol- 148, n 6, pp 530 – 534.*
- Bond, L.J. and Clayton, B.R. (1989). Non-destructive Testing and Condition Monitoring of Wind turbine Blades. *Journal of Wind Engineering. Vol –13, n 1, pp 19-29.*
- Byers, E. F and Snyder, R.D (1969). Engineering Mechanics of Deformable Bodies. *Intext Educational Publishers.*
- Caselitz, P. and Giebhardt, J. (1999). Advance Condition Monitoring for Wind Energy Converters. *Proceedings of European Wind Engineering Conference (EWEC), Nizza.*
- Caselitz, P. and Giebhardt, J. (2003). Fault prediction Techniques For Offshore Wind Farms Maintenance and Repair Strategies. *Proceeding of EWEC, Madrid, Spain.*
- Caselitz, P. and Giebhardt, J. (2003). Advanced Maintenance and Repair for Offshore Wind Farms using Fault Prediction Techniques. *Proceedings of EWEC 2002, Berlin.*
- Ebeling, C. E. (1997). An Introduction to Reliability and Maintainability Engineering. *McGraw Hill Inc.*

- Fashny, Kamal El, Chouinard, Luc E and McClure, G. (1998). Reliability Analysis of a Telecommunication Tower. *Canadian Journal of Civil Engineering*. Vol-26, pp 1-12.
Copy righted by NRC – Canada.
- Horing, B. (2003). Condition Monitoring for Offshore Wind Parks. *Journal of Power Technology of Germany*. Vol- 83, n 6, pp 58- 65.
- Hann, F., Kensche, C. W., Paynter, R.J.H, Dutton, A.G., Kildegaard, C. and Kosgaard, J. (2002). Design Fatigue Test and NDE of a Sectional Wind Turbine Rotor Blade. *Journal of Thermoplastic Composite Materials*. Vol –15, pp 267 – 277.
- Johnson, G.J. (2004). Wind Energy Systems, *Electronic Addition*.
<http://www.eece.ksu.edu/~gjohnson/>
- Jonkman, J., Dam, J.V., Davis, D. and Forsyth, T. (2003). Investigation of IEC safety Standard for Small Wind Turbine Design through Modeling and Testing. *Proceedings of ASME Symposium 2003*.
- Jacobs, N. and Johansen, T. (2003). Report on Examples of Fatigue Life time and Reliability Evaluation of Larger Wind Turbine Components. *Riso National Laboratory, Roskilde, Denmark*.
- Klein, William E. and Lali, Vincent R. (1990) Model –OA wind turbine Generator: Failure Mode and Effect Analysis. *Ninth ASME Wind Energy Symposium, USA*. Vol – 9, pp 191 – 199.
- Lees, F.P. (1996). Loss Prevention in Process Industries, Hazard Identification, Assessment and Control. *Reed Educational and Professional Publishing 96*.

- Li, B., Yen, M., Tipsuwan, Y. and Hung, J.C. (2000). Neural Network-Based Motor Rolling Bearing Fault Diagnosis. *IEEE Transactions on Industrial Electronics*. Vol-47, n 5, pp 1060 – 1069.
- Manwall, J. F., McGowan, J.G. and Rogers, A.L. (2002). Wind Energy Explained, Theory Design and Application. *John Wiley Sons Ltd*.
- Michos, D., Dialynas, E. and Vionis, P. (2002). Reliability and Safety Assessment of Wind Turbine Control and Protection System. *Journal of Wind Engineering*, Vol –26, n 6, pp359 – 369.
- Morrow, H.W. (1999). Static and Strength of Material. *Prentice Hall Publications*.
- Non-Electric Part Reliability Database (1995). *Published by 'Reliability Analysis Center', NY, USA*
- Oppenheim, Alan V., Schafer, Ronald W. and Buck, John R. (1999). Discrete Time Signal Processing. *Prentice Hall Publications*.
- Parametric Study for Larger Wind Turbine Blades (2002). Report presented for: *Sandia National Laboratories. RI, USA*
- Peterson, S. M., Thomsen, K. and Dawin, A.S. (1992). Measurement of Wind Conditions and Loads on a Wind Turbine in Inhomogeneous and Complex Terrain. *Proceedings of American Society of Mechanical Engineers Symposium (ASME'92)*. Vol-12, pp 89-96.
- Popa, L.M. and Boleda, I. (2003). Condition Monitoring of Wind generators. *Proceedings of IEEE 38th Annual Industry Application Conference, UT, USA*, pp 1839 – 1846.

Power Performance Test Report for the AOC 15/50 Wind Turbine, Test B (2003). Report presented by: *National Wind Technology Center and National Renewable Energy Laboratories. CA, USA*

Press, W.H., Teukolsky, S.A, Vetterling, W.T. and Flannery, B.P. (1992). Numerical Recipes in C: The Art of Scientific Computing, Second Edition. *Cambridge University Press.*

Rao, B.K.N. (1996). Handbook of Condition Monitoring. *Published by Elsevier Advanced Technologies.*

Sayas, F. Castro and Allan, R.N. (1996). Generation availability of Wind Farms. *IEEE Proceedings Journal*, Vol- 143, n 5, pp 507-518.

Safety and Function Test Report for the Atlantic Orient 15/50 Wind Turbine (2003). Report presented by: *National Wind Technology Center and National Renewable Energy Laboratories.*

Sedra, Adel. S. & Smith, Kenneth, C. (1998). Micro-Electronic Circuits – 4th Edition. *Oxford University Press.*

Seebregts, A.J., Rademakers, L. W. M.M. and Horn, B.A van Der (1995). Reliability Analysis in Wind Turbine Engineering. *Journal of Microelectronic Reliability*, Vol- 35, n 9-10, pp 1285 – 1307.

Trutt, F.C., Sottle, J. and Kohler, J. L. (2002). Condition Monitoring of Induction Motor Stator windings using Electrically excited Vibrations. *Transactions of 37th Annual Industry Application Society Conference. PA, USA.* pp 2301-2305.

Ugokwe, E. C. (1992). Offline 1774 PLC Reliability Case Study. *Transactions of Industry Application Society Annual Meeting. TX,USA.* Vol-2, pp 1969 – 1977.

- Veer, P.S. (1990). Fatigue and Reliability of Wind Turbine Components, *Proceedings of Wind Power, 90. USA.* pp 176-183.
- Veer, P. S. (1990). Estimating the Reliability of Wind Turbine Blades. *Proceedings of 9th Wind Energy Symposium.* pp 153.
- Veer, P.S and Winterstein, S.R. (1998). Application of measured loads on Wind Turbine fatigue and Reliability Analysis. *Journal of Solar Energy Engineering, Transactions of ASME.* Vol –120, n 4, pp 233-239.
- Viplay, B. (2002). Report on 2MW Wind Turbine Rotor Development. *Report Presented by NEG Micon Rotor Ltd. Surrey, UK.*
- Verbruggen, T.W. (2003). Wind turbine Operation and Maintenance based on Condition Monitoring. *Final Report presented in co-operation with Lagerwey and Wind Master, Siemens Netherlands and SKF.*
- Vittal, S. and Teboul, M. (2004). Performance and Reliability Analysis of Wind Turbine using Monte Carlo based methods based on System Transport Theory. *Proceedings of American Institute of Aeronautics and Astronautics conference.*
- Wang, Y.F. and Kootsookos, P. J. (1998). Modeling of Low Shaft Speed Bearing Faults for Condition Monitoring. *Journal of Mechanical System and Signal Processing.* Vol-12, n 3, pp 415-426.
- Wilson, R. A. (1990). Implementation and optimization of Mechanical Braking and Safety Systems. *Journal of Wind Engineering.* Vol-14, n 4, pp 231- 242.
- Winterstein, S.R. and Lange, C. H. (1995). Load Models for fatigue reliability from Limited Data. *Journal of Wind Energy.* Vol –16. pp 73 – 81.

Appendix 1

Condition Monitoring Routine – C++ Code

```

#include <stdlib.h>
#include <stdio.h>
#include <conio.h>
#include <math.h>

#include "pio_drvr.h"

# define CPV 819.0      // CONVERSION FACTOR from digital to analog
# define N 256          // NUMBER OF PRIMARY SAMPLES (window width)

# define SWAP(a,b) tempr=(a);(a)=(b);(b)=tempr

void fourl(float data[], unsigned long nn, int isign);

int main(void)
{
    // InitIO();          //Board Initialization;

    // Variables for Current Data
    float c_bf [20],sum_bf=0.00;    // Current Buffer ---
    int a,ad0,ad1,i,j,dummy,flag1,flag=0;
    float diff_c, s,Eq,AvG1,AvG2,AvG3,AvG4,AvG5=5.00;

    // Variables for Strain data

    int v_l,dum;

    // Strain measurment - Memory initialization.(only for Strain)

    float strain,ch_st,Eq_st,stR_t4,stR_t3,stR_t2,stR_t1,stR_t0=0.00;
    float stress, bend_moment, Load, N_Load;
    long double y_modulus = 193*pow(10,9);    // YOUNG's MODULUS FOR STEEL 316

    // Variables for Vibration and FFT data
    int sign =1;

    float* samps;
    float samples[N];
    float sam_data[2*N];    // array with REAL and imaginary storage capability

```

```

float result[N];           // FFT cofficents returned in a separate array Just to be safe
float avg;

int ind;                   // sample index
int d_samp;                // Digital value from ADC

// MONITORING ALOGORITHEM.....
do {

/*****CURRENT SAMPLING AND CALIBRATIION SECTIOHN OF ROUTINE*****/

if(flag== 0)               // OUTER IF flag
{
    // FIRST TIME
    // Initial LOOP for Acquiring Steady state value of Current

    for (dummy =0;dummy<100;dummy++)
    {
        if(flag1 ==0)      // INNER IF      flag1
        {
            sum_bf=0.0;
            for(i=0;i<=19;i++)
            {
                ad0= GetAD(0);
                c_bf[i] = ad0/CPV;
                ad0=0;
                flag1==1;
            }
        }

        if(flag1==1)
        {
            for (int xy=0;xy<=18;xy++)
            c_bf[xy] = c_bf[xy+1]; // swap for Moving average initially

            ad0=GetAD(0);
            c_bf[19]= ad0/CPV;
        }
        // Summing up initital array for average
        for(int ab=0;ab<+19;ab++)
            sum_bf+=c_bf[ab];

        s = sum_bf/19;

        printf("\n Average Sample Value= %5.5g", s);

        AvG1=AvG2;

```

```

AvG2=AvG3;
AvG3=AvG4;
AvG4=AvG5;

```

```
Eq = 0.1129*pow(s,5)-1.6561*pow(s,4)+ 9.432*pow(s,3)-25.724*pow(s,2)+34.053*s-16.298;
```

```

if(s > 1.1 && s <= 1.240){           // Calibration Adjustments with regards to equatoin
Eq = Eq + 0.1;
}

if(s > 1.240 && s <= 1.380){
Eq = Eq-0.05;
}

if(s > 1.380 && s <= 1.757){
Eq = Eq + 0.0;
}

if(s > 1.757 && s <= 2.086 ){
Eq = Eq + 0.05;
}

if(s > 2.086 && s <= 3.030){
Eq = Eq-0.1;
}

if(s > 3.030 && s <= 4.9){
Eq = Eq-.2;
}

printf("\n Acquiring Steady State Value; Current Value= %5.5g", Eq);
AvG5 = Eq;

}           // End FOR --- Dummy for Initial Current Values

```

```
// Initial Strain Values
```

```
// Recording the First Value of Starin To Eleminate the First Change in RECORDED Value
```

```
ad1 = GetAD(1);
```

```
v_1 = ad1/CPV;
```

```
// Out put voltage from Circuit in Volts.. !
```

```
// calibratin Eq for Starin
```

```
Eq_st = 0.0064123*pow(v_1,3)- 0.051591*pow(v_1,2)+ 0.14428*v_1 - 0.1132;
```

```
// Recording the first value of starin
```

```

stR_t0 = fabs(Eq_st);

    flag=1;
} // END first IF

//***** REPETITIVE LOOP ALL TIMES *****

if(flag==1)
{
    sum_bf=0.0;
    for(j=0;j<=18;j++)
        c_bf[j]= c_bf[j+1]; //swaping for moving average calculatoin

    ad0=GetAD(0);
    c_bf[19]=ad0/CPV; // New sample as the last element of array!!!

    for(a=0;a<=19;a++)
    {
        sum_bf+=c_bf[a];
    }

    } // END Second IF

// One complete sample of Voltage depending upon the I/P current to sensor.
s = sum_bf/a;

printf("\n *****CURRENT MEASURMENT*****");
printf("\n Voltage Sample = %f ", s);

AvG1=AvG2;
AvG2=AvG3;
AvG3=AvG4;
AvG4=AvG5;

// Input the sample value in the Calibration Equaiton to get the Actual Value of Current.
// A Fifth (5th) Order Equation in this case will server the purpose.

Eq = 0.1129*pow(s,5)-1.6561*pow(s,4)+ 9.432*pow(s,3)-25.724*pow(s,2)+34.053*s-16.298;

    if (s <= 1.1000){
printf("\n ...Sensor Error- Check the D/C offset value for proper Calibration....");
    }

    if(s > 1.1 && s <= 1.240){ // Calibration Adjustments with regards to equatoin
Eq = Eq + 0.1;
    }

```

```

    if(s > 1.240 && s <= 1.380){
        Eq = Eq-0.05;
    }

    if(s > 1.380 && s <= 1.757){
        Eq = Eq + 0.0;
    }

    if(s > 1.757 && s <= 2.086 ){
        Eq = Eq + 0.05;
    }

    if(s > 2.086 && s <= 3.030){
        Eq = Eq-0.1;
    }

    if(s > 3.030 && s <= 4.9){
        Eq = Eq-.2;
    }

    if (s > 4.99){
        printf("\n ...Sensor Error- I/P OUT OF SENSOR's RANGE....");
    }

    AvG5= Eq;          // Storing the Calibrated value in most recent Memory.
    printf("\n Comparison of THREE PREVIOUS Values of Current ");
    printf("\n Avrge(t-4)= %5.5g A: Avrge(t-3)= %5.5g A: Avrge(t-2)= %5.5g A : Avrge(t-1)=
    %5.5g A : Avrge(t)= %5.5g A \n\n",AvG1,AvG2,AvG3,AvG4,AvG5);

    diff_c = fabs(AvG1- AvG5); // Differential Current in the Moving Average

    if (diff_c > 0.4)    // TERMINATING CONDITION FOR CURRENT
    break;

    /*****STRAIN SAMPLING AND CALIBRATION SECTION OF ROUTINE*****/

    ad1 = GetAD(1);
    v_1 = ad1/CPV;          // Out put voltage from Circuit in Volts
    Eq_st = 0.0064123*pow(v_1,3)- 0.051591*pow(v_1,2)+ 0.14428*v_1 - 0.1132; // calibratin Eq

    stR_t4 = stR_t3;
    stR_t3 = stR_t2;
    stR_t2 = stR_t1;
    stR_t1 = stR_t0;

    stR_t0 = fabs(Eq_st);          // Absoulte value of Calibration Eq

```

```
// ABSOLUTE CHANGE IN RESISTANCE CALCULATED from current and previous value.
```

```
ch_st = fabs(stR_t0 - stR_t1) ;
```

```
strain = ch_st/(2*120);           // strain in IN/IN units
strain = strain / 39.36;         // Conversion into m/m units;
```

```
stress = strain * y_modulus;     // Stress on Bearing
```

```
// DIMENSION OF BEARING from Kaydon Website and AOC15/50 Specs
```

```
bend_moment = (stress * 0.0806)/0.254;
```

```
printf("\n ***** STRAIN and LOADING MEASUREMENTS*****\n");
printf(" \n....Comparisons of 5 Previous Values of strain .... \n");
printf("Str(t-4) = %5.5g ; Str(t-3) = %5.5g ;Str(t-2) = %5.5g ;Str(t-1) = %5.5g Str(t) = %5.5g ;
\n", stR_t4,stR_t3,stR_t2,stR_t1,stR_t0);
```

```
v_l = 0;
if(ch_st!=0.00)    // TERMINATING CONDITION FOR STRAIN
break ;
```

```
/******VIBRATION ANALYSIS PORTION OF ROUTINE*****/
```

```
printf("\n***** Samples for Vibration*****\n");
```

```
for (ind =0; ind< N; ind++){
d_samp= GetAD(2);           // sampling data
samples[ind] = (d_samp/CPV)- 2.1450;    // conversion and storing.
printf("\t %5.3g", samples[ind]);
}
```

```
for(int a=0;a < N; a++){
```

```
// Filling up alternative space with Imaginary comp of every sample = 0.0
```

```
sam_data[2*a] = samples[a];
sam_data[(2*a)+1] = 0.0;    //
}
```

```
samps = sam_data;
```

```
four1(samps-1,N,sign); // call FFT routine
```

```

    // calculating the magnitude ;   MAG = SQRT(REAL* REAL + IMAG*IMAG)

printf("\n\n FFT cofficents Ready for printing\n");

for (int z=0; z<256;z++)
{

result[z] = sqrt(sam_data[2*z]*sam_data[2*z] + sam_data[2*z+1]*sam_data[2*z+1]);
printf("\t %5.3g ", result[z]);
}

    avg = result[0];

// TERMINATING CONDITION FOR VIBRATION AVERAGE OF MAGNITUDE

    if(avg > 15.00)
        break;

// END of WHILE LOOP for KEY BOARD FOR MANUAL TERMINATOIN

}while(!kbhit());

printf("\n SENDING INTRRUPT TO PLC ");

for (long int ab=0; ab<100000;ab++)
SetIOPt(1);


ClrIOPt(1);

printf("\n Waiting for RESET \n");

//getch();

    return 0;
}

/*****
// Routine adopted from “Numerical recipes in C++, Oxford Univ Press, 1992”

void four1(float data[], unsigned long nn, int isign)
{
    unsigned long n,mmax,m,j,istep;
    int i;

```

```

double wtemp,wr,wpr,wpi,wi,theta; //Double precision for the trigonometric recurrences.
float tempr,tempi;
n=nn << 1;
j=1;
    for (i=1;i<n;i+=2) {          //This is the bit-reversal section of the routine.
        if (j > i) {
            SWAP(data[j],data[i]);      //Exchange the two complex numbers.
            SWAP(data[j+1],data[i+1]);
        }
        m=nn;
        while (m >= 2 && j > m) {
            j -= m;
            m >>= 1;
        }
        j += m;
    }
//Here begins the Danielson-Lanczos section of the routine.
mmax=2;
    while (n > mmax) { //Outer loop executed log2 nn times.
        istep=mmax << 1;
        theta=isign*(6.28318530717959/mmax); //Initialize the trigonometric recurrence.
        wtemp=sin(0.5*theta);
        wpr = -2.0*wtemp*wtemp;
        wpi=sin(theta);
        wr=1.0;
        wi=0.0;
        for (m=1;m<mmax;m+=2) {    //Here are the two nested inner loops.
            for (i=m;i<=n;i+=istep) {
                j=i+mmax;
                //This is the Danielson-Lanczos formula:

                tempr=wr*data[j]-wi*data[j+1];
                tempi=wr*data[j+1]+wi*data[j];
                data[j]=data[i]-tempr;
                data[j+1]=data[i+1]-tempi;
                data[i] += tempr;
                data[i+1] += tempi;

            }

            wr=(wtemp=wr)*wpr-wi*wpi+wr;    // Trigonometric recurrence.
            wi=wi*wpr+wtemp*wpi+wi;
        }

        mmax=istep;
    }
}
}
/*****/

```


Appendix 2

Vibration Signatures at Different Input Voltage

The vibration signatures with different input voltages are indicative of different speed and vibration levels. The different levels observed and tested are presented as under: -

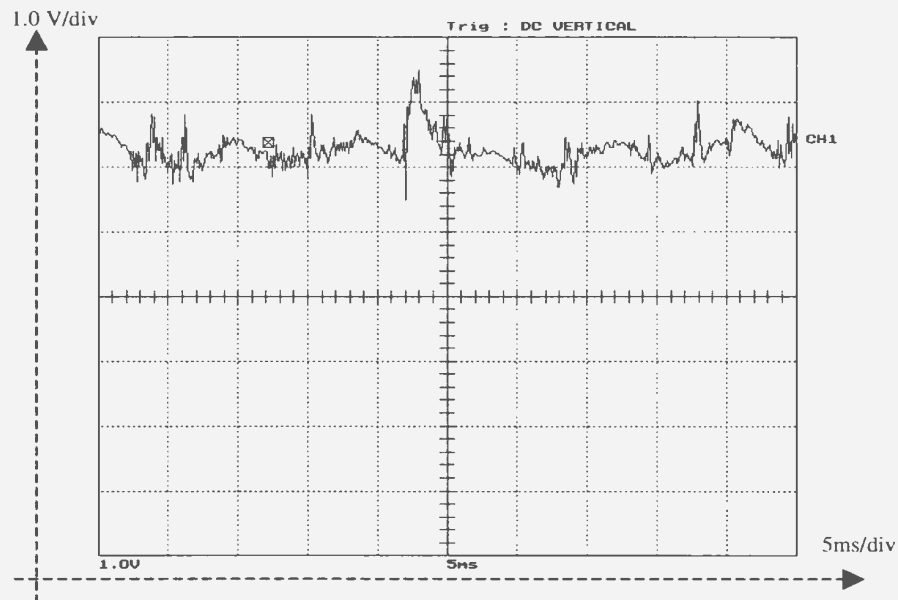


Figure A2.1 Vibration Signature at input voltage of 2.24 volts

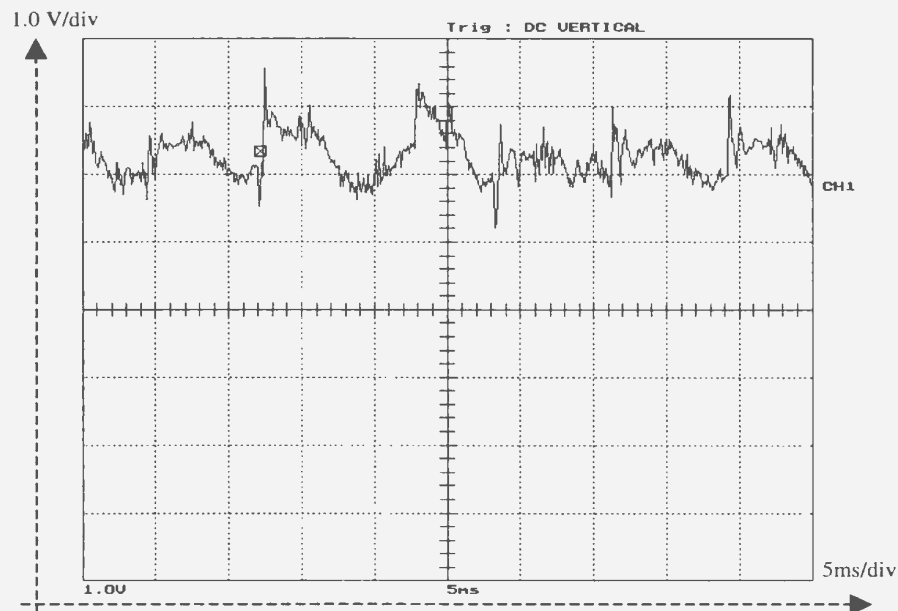


Figure A2.2 Vibration Signature at input voltage of 2.57 volts

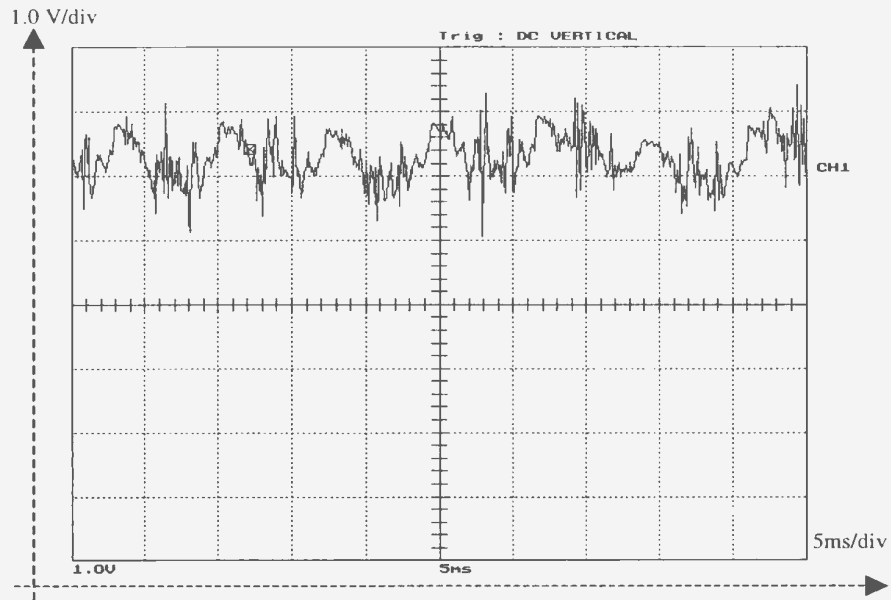


Figure A2.3 Vibration Signature at input voltage of 2.84 volts

Appendix 3

Data Sets – Observations used in Current and Strain Calibration

The data set recorded for observation for performing calibration of current and Strain circuits is presented in following along with the MATLAB code used to plot them: -

Table A3.1 Data set for Current Calibration

Input Current (Amperes)	Output Voltage (DC-volts)
0.0	1.10
0.544	1.23
0.703	1.38
1.022	1.76
1.267	2.09
1.507	2.68
1.766	2.89
1.99	3.08
2.22	3.34

Current_Calibrate.m

```
-----
% Current Sensor Instrumentation circuit calibration Model

Cur_ip = [0.0 0.544 0.703 1.022 1.267 1.507 1.766 1.99 2.220];
Volt_opl = [1.10 1.230 1.380 1.757 2.086 2.682 2.879 3.080 3.334];

plot(Volt_opl, Cur_ip, 'b-', Volt_opl, Cur_ip, 'r+')
grid
ylabel('Input Current to Sensor')
xlabel('Out Put voltage')

% The fitting gives a 5th Order Fit to be accurate.
%  $y = p_1x^4 + p_2x^3 + p_3x^2 + p_4x^1 + p_5$ 

%Coefficients:
%  $y = p_1x^5 + p_2x^4 + p_3x^3 + p_4x^2 + p_5x^1 + p_6$ 

%Coefficients:
p1 = 0.11249;
```

```

p2 = -1.6561;
p3 = 9.4312;
p4 = -25.724;
p5 = 34.053;
p6 = -16.598;

```

```

y = p1*x^5 + p2*x^4 + p3*x^3 + p4*x^2 + p5*x^1 + p6

```

Similarly data set was recorded for strain calibration. Strain was applied at the lose end of the cantilever beam and the input strain was recorded by a voltmeter on the input pins of instrumentation amplifier INA-128. The output was recorded from the strain instrumentation circuit. The data set is presented in the following table: -

Table A3.2 Data Set for Strain Calibration

Input Strain (10^{-3}V)	Output (DC-Volts)
18.12	1.86
21.67	2.15
25.00	2.39
26.73	2.73
29.17	3.12
31.51	3.29
34.50	3.49

Strain_Calibrate.m

Straing guage Calibration

```

Vin_mVs=[18.12e-3 21.67e-3 25.00e-3 26.73e-3 29.17e-3 31.51e-3 34.5e-3];
Vout = [1.86 2.155 2.389 2.729 3.119 3.289 3.486];

plot(Vout,Vin_mVs,'b-',Vout,Vin_mVs,'r+')
grid
xlabel('Sensed Voltage ')
ylabel('Strain Guage Voltage in Milli Volts')

```

```
% y = p1*x^3 + p2*x^2 + p3*x^1 + p4
%
% Coefficients:
p1 = 0.0064123;
p2 = -0.051591;
p3 = 0.14428;
p4 = -0.1132;
```

```
y = p1*x^3 + p2*x^2 + p3*x^1 + p4
```

Appendix 4

Further subdivision of Sample Array to Compute FFT

As per discussion in Chapter 5 the sequence of N samples is divided in two sequences of length N/2 and the relation is provided in equation (5.8) for N/2 DFT computations. However the process of subdivision will not stop unless the whole sample length is divided and sub divided again and again in two point DFTs. The subdivision of N/2 sequence in to further two sub sequences as adopted from Oppenheim, Schafer, and Buck(1999) is stated as under :

$$X[k] = \sum_{r=0}^{N/2-1} x[2r] W_{N/2}^{rk} + W_N^k \sum_{r=0}^{N/2-1} x[2r+1] W_{N/2}^{rk} \quad (5.8)$$

Which can be rewritten with G [k] and H [k] as under:

$$X[k] = G[k] + W_N^k H[k] \quad k = 0, 1 \dots N-1$$

The sub-division of G[k] into further even and odd sub-sequence will follow as under:

$$\text{Now } G[k] = \sum_{r=0}^{(N/2)-1} g[r] W_{N/2}^{rk} = \sum_{l=0}^{(N/4)-1} g[2l] W_{N/2}^{2lk} + \sum_{l=0}^{(N/4)-1} g[2l+1] W_{N/2}^{(2l+1)k} \quad (A4.1)$$

$$= \sum_{l=0}^{(N/4)-1} g[2l] W_{N/4}^{lk} + W_{N/2}^k \sum_{l=0}^{(N/4)-1} g[2l+1] W_{N/4}^{lk} \quad (A4.2)$$

Similarly H[k] can be subdivided as under:-

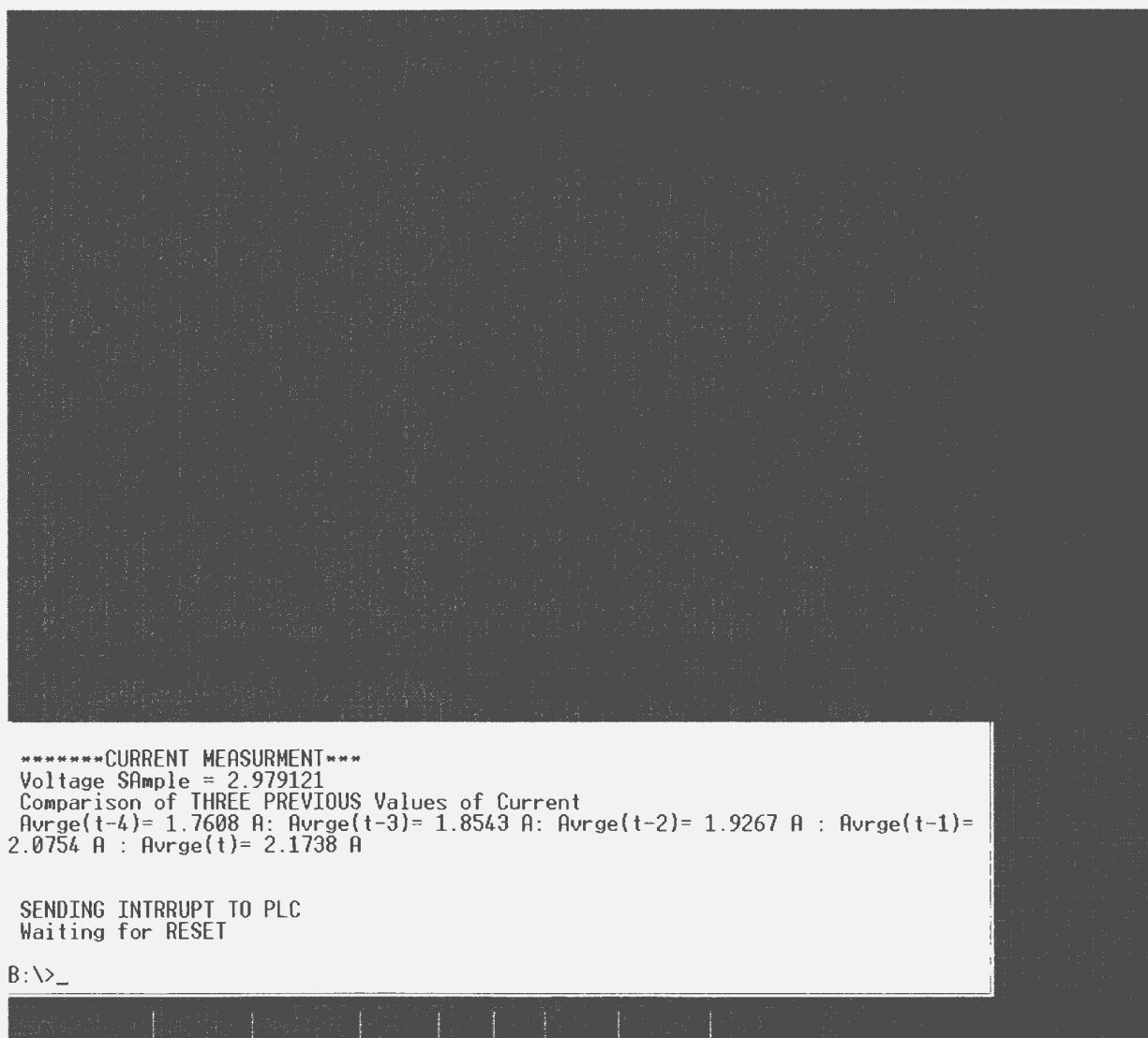
$$H[k] = \sum_{l=0}^{(N/4)-1} h[2l] W_{N/4}^{lk} + W_{N/2}^k \sum_{l=0}^{(N/4)-1} h[2l+1] W_{N/4}^{lk} \quad (A4.3)$$

The N/2 point DFT can be obtained by combining the N/4 point DFTs of above sequences g[2l] and g[2l + 1].

Appendix 5

Output Screen for SBC connection through Hyper-terminal

The board was programmed through a Hyper-terminal connection with the serial port of Laptop. Ideally the output screen will not matter as the routine will be running in the memory in real time, however here to give a better understanding it is necessary.



```
*****CURRENT MEASURMENT***  
Voltage Sample = 2.979121  
Comparison of THREE PREVIOUS Values of Current  
Avrge(t-4)= 1.7608 A: Avrge(t-3)= 1.8543 A: Avrge(t-2)= 1.9267 A : Avrge(t-1)=  
2.0754 A : Avrge(t)= 2.1738 A  
  
SENDING INTRRUPT TO PLC  
Waiting for RESET  
B:\>_
```

Figure A5.1 Typical Out put Screen

Appendix 2
 Output Screen for SBC connection through Hyper-terminal
 The board was programmed through a Hyper-terminal connection with the serial port of
 Laptop. Ideally the output screen will not appear as the routine will be running in the
 memory in real time, however here to give a better understanding it is necessary.

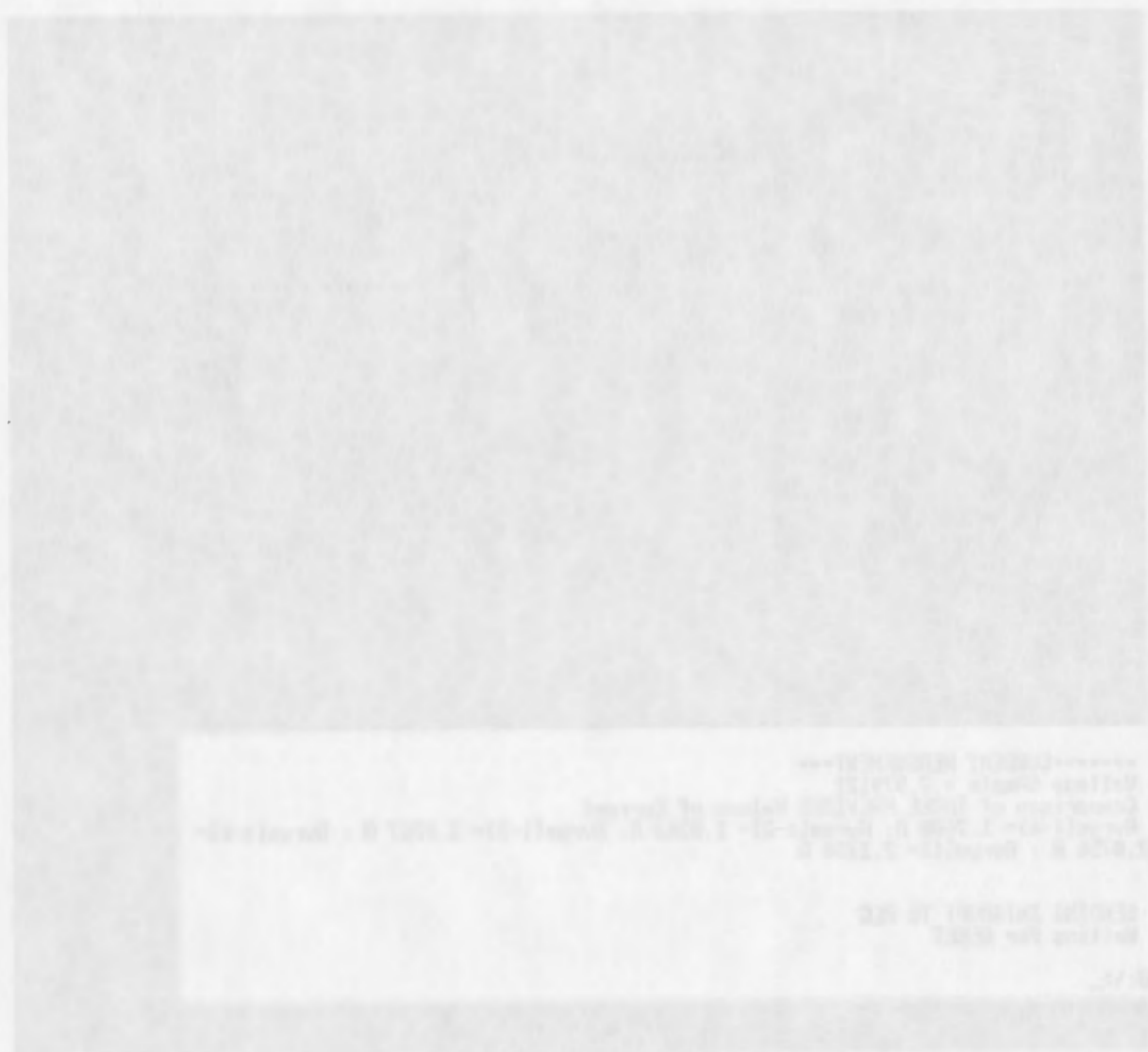


Figure A2.1 Typical On port Screen

